NORTHWESTERN UNIVERSITY

Sum Frequency Generation Spectroscopy of Interactions at Model Biointerfaces

A DISSERTATION

SUBMITTED TO THE GRADUATE SCHOOL
IN PARTIAL FULFILLMENT OF THE REQUIREMENTS

for the degree

DOCTOR OF PHILOSOPHY

Field of Chemistry

By

Laura Lynne Olenick

EVANSTON, ILLINOIS

December 2017

© Copyright by Laura Olenick 2017

All Rights Reserved

Abstract

Sum Frequency Generation Spectroscopy of Interactions at Model Biointerfaces

Laura Olenick

The expanding use of nanomaterials in consumer products challenges scientists to understand the impact of these materials before their inevitable release into the environment. In the same way that the widespread use of DDT and asbestos has caused unforeseen negative impacts on both the environment and on human health, the increasing incorporation of nanotechnology in our daily lives has the potential to significantly alter ecosystems unless a deeper knowledge of these materials is developed. The Center for Sustainable Nanotechnology (CSN) has accepted this challenge and aims to develop an understanding of the interactions of nanomaterials with the environment in order to predict and control these interactions.

As a part of the effort of the CSN, the work presented in this thesis explores the nano-biointerface primarily using Sum Frequency Generation (SFG) spectroscopy, a technique which is well-suited for targeting and observing molecular changes at interfaces. An exploration of SFG spectroscopy of supported lipid bilayers (SLBs), used as model cell membranes, finds that SFG signals from SLBs heavily depend on the transition temperature of the component lipids and the experimental temperature. This result points towards the future use of SFG spectroscopy to discover bilayer phase changes due to interactions with nanomaterials. In addition, this study highlights the strengths of a broadband SFG system over a scanning SFG system. SFG spectroscopy is utilized along with a suite of other techniques in order to examine the formation of a lipid corona around a nanomaterial. In determining that the lipid corona forms around a nanoparticle of either gold or nanodiamond core composition with the positively charged ligand, poly(allylamine hydrochloride) (PAH), and that the creation of contact ion pairs plays a role, this

research lays the foundation for future multidisciplinary studies on the nano-biointerface. Additional research on the interactions of PAH with lipid monolayers on oil droplets illustrates two main pathways of interaction which are dependent on the concentrations of PAH and NaCl, showing that controlling solution conditions is just one lever to use in the control of nanomaterial interactions. From understanding a spectroscopic technique used in an uncommon way under challenging conditions, to using this technique to understand a complex biochemical interaction at the nano-biointerface, to discovering a potential way to control these interactions, this thesis demonstrates how spectroscopy, coupled with complementary techniques under the direction of talented scientists, can effectively explain important biophysical phenomena.

_____

Professor Franz M. Geiger

Research Advisor

Acknowledgments

First, I would like to thank my advisor, Professor Franz Geiger. His passion for science and his adoration of sum frequency generation spectroscopy have made working with lasers bearable. His understanding of the importance of professional development activities coupled with his encouragement to take advantage of these opportunities is outstanding. As someone with industrial career aspirations, this encouragement was greatly appreciated. I would also like to thank him for the many external research opportunities that I was afforded on my research projects. Thanks also to my committee members, Professor Teri Odom and Professor Emily Weiss for their advice over the course of my academic career. I aspire to be as organized and focused in my future career. Special thanks to Professor George Schatz for joining my committee for this dissertation. I appreciate his time and effort throughout this process.

I would also like to thank my previous manager, Dr. Jonathan Goff at Gelest, Inc. Without his dedication to understanding effective management styles, I would not have built the confidence to return to graduate school. Under his direction, I revived my interest in chemistry and decided to pursue my dream of obtaining a PhD in chemistry. Thanks also to my previous graduate school advisor, Professor Lynden Archer, for teaching me perseverance in scientific research. Many thanks as well to my undergraduate research advisor, Professor Rebecca Conry, for noticing how much I loved laboratory research and encouraging me to pursue a career in chemistry.

Of course, this project would not have been possible without the Center for Sustainable Nanotechnology. Collaborating with Professors Robert Hamers, Christy Haynes, Joel Pedersen, Cathy Murphy, Rebecca Klaper, Galya Orr, Rigoberto Hernandez, Howard Fairbrother, Qiang Cui, Vivian Feng, Hong-fei Wang, Sylvie Roke, as well as their many graduate students and post-docs, was an invaluable experience in project management and communication within a distributed

center. These effective collaborations led to the research presented in this thesis. Special thanks to Dr. Miriam Krause and Dr. Michael Schwartz for their relentless dedication to the students of the center and for being kind, patient and attentive to student input. To the many others within the center, it was great getting to know all of you during both the in-person meetings and the innumerable online meetings.

Sincerest thanks to the entire Geiger group. Jen, Steph, Dave, Carly, Mona, Sarah, Juli, Mary Alice, Jess, Hilary, Alicia, Merve, Danielle, Mavis, Paul, Ariana, Johnny, Tian, Naomi and Dawning. In my entire graduate school career, I have never seen a more welcoming and supportive group. The countless times you all stopped what you were doing to help tune the OPA, find lost signal, or troubleshoot a temperamental laser system, demonstrate your truly selfless sense of teamwork. Working with all of you has been the highlight of my graduate school experience here at Northwestern.

Heartfelt thanks my entire family, especially my grandmother Dolores Malinky, my mother Renea Malinky, my father Joseph Olenick, my brother Thomas Olenick, my husband Brenton Cox, and the newest member of my family, my son, Benjamin Cox. Without my mother's unflinchingly optimistic belief in my abilities and my husband's masterful handling of my regular graduate school crises, I would never have been able to make it through this gauntlet. Benjamin has certainly not made life easier, but has managed to put life back into perspective. I have a truly amazing and patient family, who has waited many, many years for me to finally say that I am done with graduate school. I am truly grateful to all of you.

To my husband, Brent

TABLE OF CONTENTS

List of Figures

Chapter 1

Sum Frequency Generation Spectroscopy in Biointerface Science

1.1 Nanomaterials in the Environment

The ubiquitous use of nanomaterials and their inevitable environmental dispersal fuels the investigation into the interactions of these materials with biological systems. Science has learned from mistakes made in the use and dispersal of chlorofluorocarbons (CFCs), asbestos, and DDT. We, as scientists, do not wish to make these mistakes again. The research presented in this thesis is a part of the knowledge that we are developing in the Center for Sustainable Nanotechnology (CSN) to understand, predict, control, and prevent the potentially negative biological effects of nanomaterials from adversely impacting our world.[1]

Despite the acceleration in the number of products containing nanomaterials entering our daily lives, our understanding of their fate and transport in environmental and biological systems is limited. Nanomaterials are a class of materials characterized by a size between 1 and 100 nm in at least one dimension. These novel materials are present in a variety of everyday products, such as towels, lubricants, and even chocolate, to name a few.[2] Nanomaterials are used to help rebuild bones,[3] to store energy,[4] to protect skin from the sun,[5] to produce intense color in TV displays,[6] and to deliver drugs.[7] Prevalence in consumer goods is so ubiquitous that most nanomaterials in consumer goods are synthesized in multi-ton quantities, according to "The Global Market for Nanomaterials 2010-2027" report produced by Research and Markets and reported by Cision PR Newswire.[8] With the massive amount of nanomaterials produced and their wide availability to the general public, these materials will inevitably be released into the environment at some point during their production, use, and disposal particularly since these materials are poorly regulated. Currently, no regulations exist which state that companies must report nanomaterials in the list of ingredients on any product, including food. In most cases, companies must report the ingredients that the product contains, but not the size regime of those ingredients. This lack of regulation is in

stark contrast to the massive global Nanotechnology market. Global revenue from nanotechnology based products has grown from $339 billion in 2010 to $1 trillion in 2013.[9] The US government has invested nearly $24 billion in the National Nanotechnology Initiative (NNI) since fiscal year 2001.[10] The NNI includes 20 US government agencies and departments that work together to understand the nanoscale and share this knowledge with industry and academia for social benefit, resulting in a massive market for nanomaterials that continues to grow.[10]

In January 2014, a report was released by the United States Government Accountability Office (GAO) which revealed that despite ten years of discussion, little is known about the environmental impacts of nanotechnology on health and safety concerns regarding nanotechnology, and current information on this topic involves only a relatively small subset of the materials on the market.[11] Predicting the environmental impact of new materials is essential in preventing hazardous environmental toxins from entering the environment. Furthermore, prediction and prevention is less costly than remediation. To avoid large scale remediation efforts, such as those underway at Superfund sites, knowledge is vital. In 2012, a National Science Foundation (NSF) workshop about the interaction between nanoparticles and the environment concluded that more fundamental research is necessary to ensure the sustainability of the development and distribution of nanomaterials. [12]

1.2 The NSF Center for Sustainable Nanotechnology

To fill this knowledge gap, the NSF has funded the Center for Sustainable Nanotechnology (CSN) as part of its Centers for Chemical Innovation program. The CSN is a research collective composed of twelve universities and national labs dispersed around the country which draws on the varied expertise of the scientists involved to accomplish one goal: to develop guidelines to facilitate the development of sustainable nanotechnology by understanding the fundamental

molecular interactions between engineered nanomaterials and model biointerfaces, from lipid bilayers to single- and multicellular organisms such as bacteria and water fleas.[12]

Figure 1.1. The twelve universities and institutions which compose the NSF-funded Center for Sustainable Nanotechnology.

With this goal in mind, the Center researches the fundamental chemistry of engineered nanomaterials to better understand the toxic effects of these materials on the environment in order to better predict and control their impact. Ideally, the CSN will be able to use the knowledge of the properties of various nanomaterials in order to predict the potentially toxic effects of these

materials, and suggest ways in which to counteract this toxicity. Ongoing international collaborations in Switzerland (with Professors Sylvie Roke and Francesco Stellaci) and Germany (with Professor Karen Lienkamp) enhance the global impact and relevance of this work. The varied research within the CSN spans organismal biology, molecular cell biology, genetics, organic chemistry, inorganic chemistry, physical chemistry, materials science, and computational chemistry. This thesis research is part of the CSN. Ultimately, the CSN benefits from a multi-disciplinary approach and seeks to achieve its goal by uniting the focus of highly skilled experts tackling this complex and challenging global problem.

1.3 Lipid Bilayers as Model Cell Membranes

One of the CSN's primary research areas is the cell membrane. The cell membrane functions as the first layer of protection against hazards in the surrounding medium, maintaining a boundary between intracellular and extracellular environments. In eukaryotes, this membrane is composed primarily of a phospholipid bilayer which allows for the entrance, exit, or rejection of foreign material. The cell itself contains a complex matrix of proteins, lipids, DNA, RNA and various molecules which allow the cell to operate as needed.

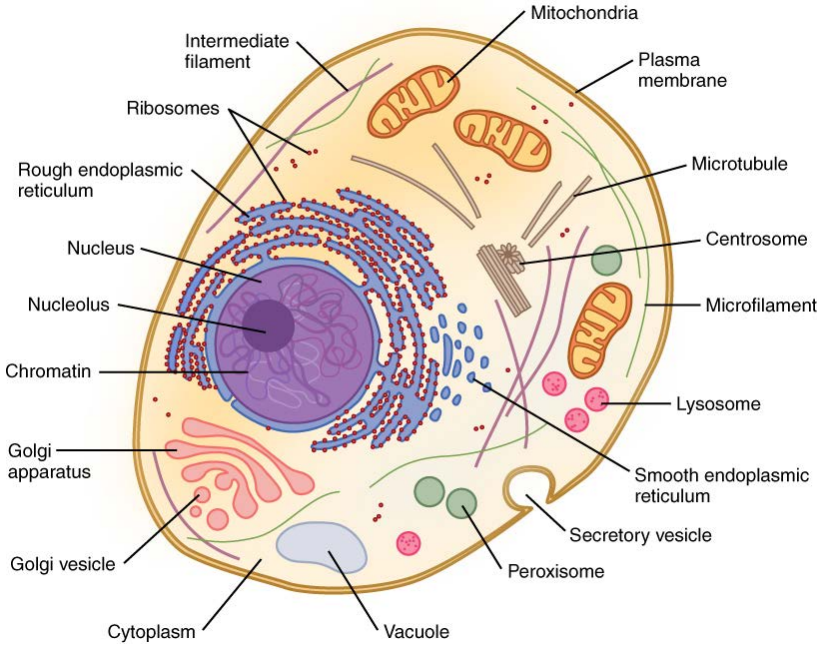

Figure 1.2. Animal cell. Figure from https://cnx.org/contents/FPtK1zmh@8.25:fEI3C8Ot@10/Preface and used under the Creative Commons Attribution 4.0 International License.

Depending on the focus of the cell research, this level of complexity can cause difficulty in interpreting experimental results. With varied molecular sizes, structures and functions embedded within the dense network of the cytoskeleton, parsing out the molecular mechanisms occurring at the cellular level becomes troublesome. This difficulty is particularly hard to address when studying the fundamentals of the interactions between the lipid membrane and the materials within the surrounding environment.

One method for accurately determining fundamental mechanisms in complex systems is to study a simplified model system that represents the relevant components of the complex system. In the case of a cell membrane, a lipid bilayer that is composed of the types of lipids that are predominant in the bilayer of interest is a reasonable model system.[13-14] Here, the bilayer of interest is a eukaryotic cell membrane which principally contains phosphatidylcholine lipids.

Eukaryotic cells are present in all animals and as such serve as excellent probes to research the effects of nanomaterials in biological systems. In this work, bilayers composed of a majority of zwitterionic phosphatidylcholine lipids are used as model systems for studying the eukaryotic cell membranes of interest.

Lipid bilayers serve as fitting model systems for cell membranes[13-15] and have been studied by scientists for use in medical implants,[16] toxicity assays,[17-18] drug delivery,[19] cell signaling,[20] cell adhesion,[21-22] and biosensors.[23-24] The cell membrane acts as a barrier between the cell and the surrounding environment, and is composed of a phospholipid bilayer interspersed with many types of proteins. The fluid mosaic model, first put forth by Singer and Nicolson in 1972, introduced the idea that the bilayer could be thought of as a fluid, with proteins moving easily within the free-flowing bilayer.[25-26] Studies since have refined that model to portray the bilayer as a structured material anchored to the cytoskeleton of the cell with transmembrane proteins and with areas containing lipid rafts which promote structural support within specific regions of the membrane.[27-28]

1.4 Studying the Nano-Biointerface

The lipid bilayer is a major component of the biointerface. The biointerface refers to the boundary between biological cells and the outside environment. Understanding the way in which foreign materials impact this intersection between the cell and the external world is important as this interaction impacts the future health of the cell. In much of this thesis, the foreign materials of interest are nanomaterials. In this case, the interface is referred to as the nano-biointerface. Two factors are important to consider when studying the nano-biointerface: the nanomaterial surface and the biological surface. Each of these surfaces is complex. The nanomaterial surface can be affected by the biological medium encountered prior to the biological interface. As a result,

the material may gain or lose ligands, ions, or other coatings, or it may increase in size due to agglomeration or decrease in size due to dissolution. The biological interface is also dynamically changing, as it can bend and flow around or away from foreign objects it encounters. The membrane can also change charge state, size, rigidity, and local composition to dynamically react to external stimuli. All of these dynamic transformations depend on the conditions of the interactions such as ionic strength, pH, temperature, pressure, etc. Therefore, investigating molecular interactions at biointerfaces *in situ* and in real time is crucial for understanding the environmental impact of nanomaterials, yet *in situ* measurements are challenging to obtain.[29]

In fact, few techniques are capable of accessing the detailed, molecular level information needed to understand the nano-bio interface.[30-31] With advances in electronics, coatings, medical devices and precision applications of new materials, understanding molecular interactions at interfaces *in situ* is crucial for the further development of, and for controlling the environmental impact of, these materials. [29] Biointerfaces, in particular, have historically been difficult to study using spectroscopy, typically requiring samples to be in an aqueous solution with other components such as a buffer. It can be difficult to perform spectroscopy under aqueous solution conditions and receive easily interpretable spectra from these experiments. Scanning Electron Microscopy (SEM),[32] Transmission Electron Microscopy (TEM),[33] and X-ray Photoelectron Spectroscopy (XPS)[34] are often used to observe this size regime, but these techniques typically use ultra-high vacuum (UHV) conditions which vastly differ from conditions existing in a cellular environment. Cryo-TEM can be used to observe the interface after a liquid sample preparation, but the cryogenic temperatures freeze the interactions in place.[35] Thus, cryo-TEM is difficult to use to study dynamically changing events in real time. Atomic Force Microscopy (AFM) is an effective technique for studying the phase of lipid bilayers,[36] as well as the presence or absence of

nanomaterials[37] but the method is not chemically specific and subject to scanning artifacts.[38] Fluorescence imaging is also useful for observing changes in the lipid bilayer in real time,[39] but this technique uses external labels that may significantly affect experimental results. The influence of labels was clearly illustrated by Anglin and Conboy with a study on the kinetics of lipid flip-flop without labels, compared to the kinetics reported for labeled lipids.[40] This discovery led to a shift in understanding of bilayer function, with lipid flip-flop taking place orders of magnitude faster than originally thought. Electrophysiology experiments can also be useful,[41] but do not give structural information. Moreover, the free-standing bilayer used in such studies is often only stable for a few hours, limiting potential experimental parameters.[42] Also, the study of interactions at biointerfaces can be difficult because these interactions occur at fast timescales.

SFG spectroscopy is particularly well-suited for studying biointerfaces because it is an inherently interface-specific technique. SFG spectroscopy allows the study of ultrafast dynamics at interfaces, since these experiments can be conducted at fast timescales.[43] Many complex interactions occur at buried interfaces that are challenging to access without obstruction from the bulk.[44] The necessity for observations at these timescales, and the selectivity for buied interfaces drives the need for laser spectroscopy as a tool in the study of biointerfaces.

Sum Frequency Generation (SFG) spectroscopy is a coherent, vibrational spectroscopy[45] that has been used extensively to study the surface orientation of adsorbed molecules from various solutions onto substrates of interest, which in this thesis includes IR-grade fused silica and CaF_2.[46-49] SFG is not allowed in centrosymmetric media,[45-46] therefore, studies of interfaces where symmetry is inherently broken often utilize SFG spectroscopy. As a label-free, non-destructive, chemically specific method,[45-46] SFG spectroscopy reveals information about the order and orientation of lipids in a supported lipid bilayer.[50] The use of SFG spectroscopy as a tool to study

biointerfaces, including lipid monolayer orientation at the air-water interface,[51-52] monolayer relaxation,[53] the structure of lipid bilayers in response to temperature,[54] and the kinetics of lipid exchange between membrane leaflets,[55-57] continues to grow. Investigation into lipid bilayer structure and function also has benefitted from the use of SFG spectroscopy. This technique has been used to study lipid flip-flop,[40, 57] lipid orientation, incorporation of materials into a lipid membrane,[58] lipid domain formations,[59] and lipid transition temperatures.[54] Many of these studies, however, used various deuterated lipids in either one or both leaflets of the bilayer in order to yield an SFG signal,[50, 60] or a monolayer is studied in place of a bilayer.[53, 61-63] These studies also frequently used deuterated water as a solvent to simplify spectral interpretation, especially in the CH stretching region, which overlaps slightly with the OH stretch continuum.[64-65] The work in this thesis employs lipid bilayers, avoids use of deuterated lipids, and primarily uses H_2O, not D_2O, for a more biologically relevant exploration of the nano-bio interface. More detailed information on SFG spectroscopy can be found in Chapter 2.

1.5 Conclusion

Determining the root causes of bioadverse responses of a biointerface with engineered nanomaterials is the key step toward predicting and controlling these interactions. With this knowledge, scientists can foresee complications in disposal and unintended dispersal of novel nanomaterials before large-scale production of them has begun. In-depth research will provide the understanding necessary to alter or avoid detrimental properties of the nanomaterials, while conserving their industrial functionality.

The nonlinear optical technique of sum frequency generation (SFG) spectroscopy is an important tool in the study of short timescale molecular dynamics and kinetics of non-centrosymmetric media such as interfaces. As will be described in Chapter 2, SFG spectroscopy

is particularly powerful when combined with complementary analytical techniques in the study of the nano-biointerface. Based on the current rate of advances in nanotechnology and nanomaterials in consumer products, SFG spectroscopy will certainly be an essential tool for probing the interactions of these materials at biologically relevant interfaces. The research detailed in this thesis will serve as an important step towards using SFG spectroscopy to its fullest extent to probe the fundamental dynamics of interactions at biointerfaces with the ultimate goal of gaining a deeper understanding of our impact on our environment.

1.6 Scope and Organization of Thesis

Chapter 1 provides the introduction to the field.

Chapter 2 describes the technique of SFG spectroscopy, and highlights the particular advantages and disadvantages of this techniques in the study of phenomena at the nano-biointerface. This chapter demonstrates that the nonlinear optical response of interfaces where symmetry is naturally broken can be analyzed in order to understand the order and orientation of the molecules at the interface.

Chapter 3 explores lipid bilayers through SFG spectroscopy. This chapter reveals the differences in the SFG spectra of two groups of phosphatidylcholine-containing lipids: those that have a transition temperature below the experimental temperature and those that have a transition temperature above the experimental temperature. Chapter 3 also explores the effect on the SFG spectrum of varying the experimental temperature on one specific lipid bilayer composed of 1,2-dimyristoyl-*sn*-glycero-3-phosphocholine (DMPC) and 1,2-dimyristoyl-*sn*-glycero-3-phospho-(1'-rac-glycerol) (sodium salt) (DMPG) lipids.

Chapter 4 makes use of SFG spectroscopy and complementary techniques to describe the formation of a lipid corona surrounding a nanomaterial coated with the cationic polymer,

poly(allylamine hydrochloride) (PAH) in response to interactions with a supported lipid bilayer. Through highly collaborative research within the CSN, this lipid corona effect is chronicled using atomic force microscopy (AFM), transmission electron microscopy (TEM), biological toxicity assays, fluorescence microscopy, and fluorescence recovery after photobleaching (FRAP).

Chapter 5 takes a step back to probe the interactions of the cationic polymer, PAH, and a monolayer of PC-lipids, in order to better understand the lipid corona mechanism without the influence of a nanomaterial core or a solid support. The research presented in this chapter utilizes sum frequency scattering (SFS) spectroscopy to study the interaction of a monolayer of DMPC lipids on the surface of an oil droplet with varying concentrations of PAH under varying salt conditions.

Chapter 6 concludes the thesis by reiterating the main findings and discussing routes of inquiry into how to build upon this research using SFG, SFS, and fluorescence microscopy. The future work proposed in this chapter will assist future researchers in the CSN, and elsewhere, to progress from understanding the interactions at the nano-biointerface, to controlling these interactions based upon the properties of the nanomaterials.

Chapter 2

Sum Frequency Generation Spectroscopy: An important surface sensitive technique

Portions of this chapter are part of the following pending manuscripts:

Olenick, L.L.; Troiano, J. M.; Vartanian, A.; Melby, E. S.; Mensch, A. C.; Zhang, L.; Qui, T.; Bozich, J.; Lohse, S.; Zhang, X.; Kuech, T. R.; Millevolte, A.; Gunsolus, I.; McGeachy, A. C.; Dogangun, M.; Hu, D.; Walter, S. R.; Mohaimani, A.; Schmoldt, A.; Torelli, M. D.; Hurley, K. R.; Dalluge, J.; Chong, G.; Feng, Z. V.; Haynes, C. L.; Hamers, R. J.; Pedersen, J. A.; Cui, Q.; Hernandez, R.; Klaper, R.; Orr, G.; Murphy, C. J.; Geiger, F. M., Lipid Corona Formation from Nanoparticle Interactions with Bilayers and Membrane-Specific Biological Outcomes. **2017.** *In Revision.*

Olenick, L. L.; Troiano, J. M.; Smolentsev, N; Ohno, P. E.; Roke, S.; Geiger, F. M., Sum Frequency Scattering Spectroscopy of the Interactions of Cationic Polymers and Phospholipid Monolayers on Oil Nanodroplets. **2017.** *In Prep.*

Portions of this chapter have been reproduced from the following paper with permission from the Royal Society for Chemistry:

Olenick, L. L.; Chase, H. M.; Fu, L.; Zhang, Y.; McGeachy, A. C.; Dogangun, M.; Walter, S. R.; Wang, H.-f.; Geiger, F. M., Single-Component Supported Lipid Bilayers Probed Using Broadband Nonlinear Optics. *Physical Chemistry Chemical Physics* **2017**.

2.1 Sum Frequency Generation Background

Nonlinear optical spectroscopy uses the nonlinear interaction of light with matter to study the properties of a system.[1-4] The study of nonlinear optical processes has been a subject of attention in physics and chemistry since the late 1800s when Friederich Carl Awin Pockels discovered the Pockels effect, and John Kerr documented the Kerr effect.[5] Nonlinear optics as it is known today began with the observation of second harmonic generation (SHG) by Franken et al. in 1961 at the University of Michigan.[1, 6] After Nicolaas Bloembergen received a preprint of the paper by Franken et al., he realized the importance of this discovery and developed the theory of sum frequency generation (SFG) and SHG spectroscopy in the early 1960's at Harvard University.[7-10] Recognized by the scientific community for his ground-breaking work, Bloembergen shared the Nobel Prize in Physics in 1981 with Arthur Leonard Schawlow for their work in laser spectroscopy along with Kai M. Seigbahn for his work in electron microscopy.[11]

Under the guidance of Bloembergen, Yuen-Ron Shen received his PhD in Applied Physics in 1963.[12] Shen used his background in nonlinear optics to publish the first SFG spectrum in 1986 at the University of California, Berkeley.[13] In a 1986 communication in *Physical Review B*, Shen and colleagues, X. D. Zhu and Hajo Suhr, probed the interface between coumarin 504 dye and fused silica under nitrogen, and showed that using an input beam in the IR frequency range of molecular vibrations, one can indeed record resonantly-enhanced SFG signals from the vibrational modes of molecules at an interface.[13]

2.2 Sum Frequency Generation Spectroscopy Theory[1-3]

Much of this section follows the SFG tutorial developed by Alex Lambert, Paul Davies, and David Neivandt.

The SFG process consists of two input oscillating fields that overlap in time and space on a sample and combine to form a signal oscillating at the sum of the two input frequencies. In the case where one beam is on resonance with molecular vibrational modes, the technique is termed vibrational SFG spectroscopy, with $\omega_{SFG} = \omega_{IR} + \omega_{VIS}$. In SFG, the interaction between the two input beams and the sample results in no net transfer of energy or momentum, and no change in state of the sample.[4]

Energy level diagrams are one way to visually represent the interactions of the two input beams for vibrational SFG spectroscopy, as shown in Figure 2.1. In Figure 2.1 A, it is important to note that while the solid lines represent the ground state and the IR-excited vibrational state of the molecule, the dashed line does not represent an actual excited state of the molecule, but instead represents a virtual state, at least for standard SFG spectroscopy.

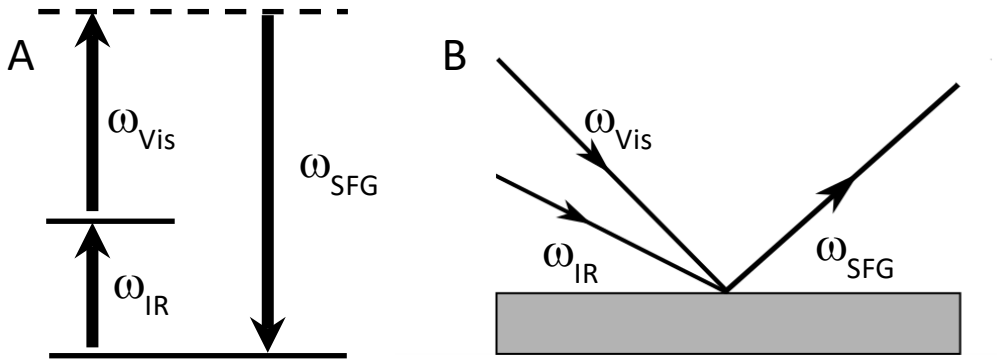

Figure 2.1. (A) Energy level diagram for vibrational SFG spectroscopy. (B) Schematic of visible and IR beams producing an observable SFG signal.

Nonlinear processes occur when the response of a medium to an applied oscillating electromagnetic field, termed the susceptibility, χ , is no longer linear, producing higher-order

terms such as the second-order susceptibility, $\chi^{(2)}$. To understand $\chi^{(2)}$, we begin with the dipole moment, μ, produced in response to an applied field, E:[9]

$$\boldsymbol{\mu} = \boldsymbol{\mu}^0 + \alpha \boldsymbol{E} \tag{1}$$

where α is the molecular polarizability and μ^0 is the static dipole of the system. From the macroscopic perspective of an actual experimental setup, this can be written in terms of the polarization, P, or the dipole moment per unit volume:

$$\boldsymbol{P} = P^0 + \varepsilon_0 \chi^{(1)} \boldsymbol{E} \tag{2}$$

$\chi^{(1)}$ is a susceptibility tensor equal to the number of molecules, N, multiplied by the polarizability, α, averaged over all of the orientations of the molecules in the material, divided by the vacuum permittivity, ε_0:

$$\chi^{(1)} = N\langle\alpha\rangle/\varepsilon_0 \tag{3}$$

This view is appropriate for low intensity light. When high intensity laser light is used, however, higher terms must be included in these equations because the material response is no longer well-represented by the simple harmonic oscillator model. Expanding with a power series, the dipole moment can be represented as:

$$\boldsymbol{\mu} = \boldsymbol{\mu}^0 + \alpha \boldsymbol{E} + \beta \boldsymbol{E^2} + \gamma \boldsymbol{E^3} + \cdots \tag{4}$$

where β is the 1st order hyperpolarizability, γ is the 2nd order hyperpolarizability, and so on. Similarly, the macroscopic total polarization response is expressed as:

$$\boldsymbol{P} = \boldsymbol{P}^{(1)} + \boldsymbol{P}^{(2)} + \boldsymbol{P}^{(3)} + \cdots \tag{5}$$

And substituting the polarization equation relating P to χ yields:

$$\boldsymbol{P} = \varepsilon_0(\chi^{(1)}\boldsymbol{E} + \chi^{(2)}\boldsymbol{E}^2 + \chi^{(3)}\boldsymbol{E}^3 + \cdots) \tag{6}$$

From Equation 6, it follows that:

$$\boldsymbol{P}^{(2)} = \varepsilon_0 \chi^{(2)} \boldsymbol{E}^2 \quad (7)$$

Processes that involve only the $\chi^{(1)}$ susceptibility tensor are linear, and processes involving the $\chi^{(2)}$ susceptibility tensor and higher are nonlinear processes. Since the intensity is proportional to the square of the electric field,[14] the detected signal is linear with respect to $\chi^{(1)}$ and nonlinear with respect to $\chi^{(2)}$ and higher. $\chi^{(1)}$ is a second-rank tensor, $\chi^{(2)}$ is a third-rank tensor, $\chi^{(3)}$ is a fourth-rank tensor, and so on.[1]

In second harmonic generation (SHG), a specific case of SFG, $\omega_1 = \omega_2$, and the nonlinear polarization generates an output beam at frequency 2ω. Using Equation 7, but accounting for the sign of the applied oscillating field,

$$\boldsymbol{P}^{(2)}(t) = \varepsilon_0 \chi^{(2)} |\boldsymbol{E}(t)|^2 \quad (8)$$

Substituting Equation 8 with the equation for a single wavelength electric field squared, Equation 9, yields Equation 10.

$$|\boldsymbol{E}(t)|^2 = \boldsymbol{E}_0^2 \cos^2(\omega t) \quad (9)$$

$$\boldsymbol{P}^{(2)}(t) = \varepsilon_0 \chi^{(2)} (\frac{\boldsymbol{E}_0^2}{2})[\cos(2\omega t) + 1] \quad (10)$$

Equation 10 demonstrates that $P^{(2)}(t)$ will oscillate at 2ω. This mathematical result illustrates that, in the physical phenomenon of second harmonic generation, the SHG beam oscillates at $\omega_1 + \omega_2$ or 2ω.

Similarly, for two beams, as in the case of SFG spectroscopy, the following equation for the electric field is valid:

$$\boldsymbol{E} = \boldsymbol{E}_1 cos(\omega_1 t) + \boldsymbol{E}_2 cos(\omega_2 t) \quad (11)$$

Substitution into Equation 8 yields:

$$\boldsymbol{P}^{(2)} = \varepsilon_0 \chi^{(2)} \big(\boldsymbol{E}_1 cos(\omega_1 t) + \boldsymbol{E}_2 cos(\omega_2 t)\big)^2 \quad (12)$$

From trigonometry, Equation 12 is expanded to:

$$\boldsymbol{P}^{(2)} = \varepsilon_0 \chi^{(2)} \left[(\boldsymbol{E}_1^2 + \boldsymbol{E}_2^2) + \left(\boldsymbol{E}_1^2 cos(2\omega_1 t) + \boldsymbol{E}_2^2 cos(2\omega_2 t) \right) + \left(\boldsymbol{E}_1 \boldsymbol{E}_2 cos\left((\omega_1 - \omega_2) t \right) \right) + \left(\boldsymbol{E}_1 \boldsymbol{E}_2 cos\left((\omega_1 + \omega_2) t \right) \right) \right] \quad (13)$$

The fourth term in the brackets in Equation 13 corresponds to SFG and illustrates that the frequency of the SFG wave oscillates at $\omega_1 + \omega_2$, or ω_{SFG}. Equation 13 shows that signals at other frequencies occur as well, for instance the difference of ω_1 and ω_2. For vibrational SFG spectroscopy, ω_1 and ω_2 are defined as follows:

$$\omega_1 \equiv \omega_{IR} \quad (14)$$

$$\omega_2 \equiv \omega_{Vis} \quad (15)$$

When the time dependence of this process is ignored, Equation 16 results in Equation 17:

$$\omega_{SFG} = \omega_{IR} + \omega_{Vis} \quad (16)$$

$$\boldsymbol{P}_{SFG}^{(2)} = \varepsilon_0 \chi^{(2)} \boldsymbol{E}_{Vis} \boldsymbol{E}_{IR} \quad (17)$$

Because an induced polarization will radiate an electric field linearly proportional to its magnitude, and the intensity of light is proportional to the electric field squared,[14] the intensity of light, I, depends upon $\left| P^{(2)} \right|^2$, and the following equation is valid in the limit of the assumptions of linear response functions, where I_{SFG} is the intensity of the SFG signal, $I_{\omega_{IR}}$ is the intensity of the IR light, and $I_{\omega_{Vis}}$ is the intensity of the visible light:

$$I_{SFG} \propto \left| \chi^{(2)} \right|^2 I_{\omega_{IR}} I_{\omega_{Vis}} \quad (18)$$

Since $\chi^{(2)}$ is the macroscopic average of the molecular hyperpolarizabilities of the molecules at the interface, the next step is to link the macroscopic $\chi^{(2)}$ to the molecular frame of

the individual molecules producing the nonlinear response using rotational matrices.[3] Beginning with Equation 18, but expanding to the laboratory frame yields:

$$\chi_{ijk}^{(2)} = \frac{N}{\varepsilon_0}\sum_{\alpha\beta\gamma}\langle R(\psi)R(\theta)R(\varphi)\beta_{\alpha\beta\gamma}\rangle \quad (19)$$

where i, j, k are indices representing the three dimensions of the laboratory frame and α, β, γ are indices representing the three dimensions of the molecular frame. In converting between the laboratory frame and the molecular frame, Euler angles must be used, which are represented above as ψ, θ, φ. Rotational matrices, designated above as R, for each of these Euler angles do the work of moving between these two coordinate systems.[3, 15]

The molecular response can be estimated using perturbation theory under the electric dipole approximation, giving:

$$\beta_{\alpha\beta\gamma} = \frac{1}{2\hbar}\left(\frac{M_{\alpha\beta}A_{\gamma}}{\omega_{Vis}-\omega_{IR}-i\Gamma}\right) \quad (20)$$

Equation 20 is the basis for the selection rules for SFG spectroscopy, since $M_{\alpha\beta}$ is the Raman transition moment and A_{γ} is the IR transition moment. $\hbar$ is simply Planck's constant, h, divided by 2π and Γ^{-1} refers to relaxation time of the vibrational mode of interest.[3] The second order susceptibility, which is the susceptibility relevant to SFG spectroscopy, depends on the number of molecules per unit volume, the molecular orientation distribution, and on a mode being both Raman and IR active.

A necessary point to address here is that $\chi^{(2)}$ has both resonant, $\chi_R^{(2)}$, and non-resonant, $\chi_{NR}^{(2)}$, components:

$$\chi^{(2)} = \chi_R^{(2)} + \chi_{NR}^{(2)} \quad (21)$$

Therefore, the intensity of the SFG light measured by the detector is dependent on both resonant and non-resonant contributions as well as their phases, ε and δ, respectively.

$$I_{SFG} \propto \left|\chi_R^{(2)}\right|^2 + \left|\chi_{NR}^{(2)}\right|^2 + 2\left|\chi_R^{(2)}\right|\left|\chi_{NR}^{(2)}\right| cos[\varepsilon - \delta] \quad (22)$$

Note that this dependence is important in the interpretation of work performed under aqueous buffer conditions described in subsequent chapters of this thesis. The signal from the OH stretches in the water can be strong enough to contribute to signal in the CH stretching region causing interference effects which can complicate peak assignments.

Within the electric dipole approximation, SFG is only allowed in non-centrosymmetric media. This selection rule is best explained using mathematics and accurately treating the polarization and the electric field as vectors. If a sample is centrosymmetric, it has inversion symmetry. Therefore, if Equation 22 is generalized over x, y, z space, the result is Equation 23.

$$\boldsymbol{P}^{(2)}(x,y,z) = \chi^{(2)}|\boldsymbol{E}(x,y,z)|^2 \quad (23)$$

If the inversion operation is used on Equation 23, the result is Equation 24, which simplifies to Equation 25:

$$\boldsymbol{P}^{(2)}(-x,-y,-z) = -\boldsymbol{P}^{(2)}(x,y,z) = \chi^{(2)}|\boldsymbol{E}(-x,-y,-z)|^2 = \chi^{(2)}|\boldsymbol{E}(x,y,z)|^2 \quad (24)$$

$$\chi^{(2)}|\boldsymbol{E}(x,y,z)|^2 = -\chi^{(2)}|\boldsymbol{E}(x,y,z)|^2 \quad (25)$$

This equation can only be true if $\chi^{(2)} = 0$. Therefore, the SFG process is forbidden in centrosymetric media, where there exists an inversion symmetry operation. The necessity for non-centrosymmetric media is why SFG is an interface-specific technique. Symmetry breaks at an interface because of induced polarization effects and constrained molecular motion at the interface.

With regards to the overall orientation of a molecule at interfaces, standard SFG spectroscopy can only give the tilt angle in relation to the surface normal. Determination of the absolute orientation of the molecule was accomplished using SHG by Kemnitz et al. in 1986 with a publication that explains the experimental setup necessary for the measurements of the phase of

$\chi^{(2)}$ and β (where β is the molecular second order polarizability).[16] For example, in the simplified equation relating one of the allowed $\chi^{(2)}$ terms to β, namely the ZZZ component:

$$\chi^{(2)}_{ZZZ} = N\beta_{ZZZ}\langle\cos^3\theta\rangle_{OR} \quad (26)$$

$\langle\cos^3\theta\rangle_{OR}$ refers to the orientational angle averaged over all the molecules at the interface sampled by the beam spot and N is the number of molecules. If the sign of $\chi^{(2)}$ is measured and the sign of β is known from calculation, the absolute molecular orientation is determined from the sign of θ, since N is the number of molecules at the surface, per area of the beam spot in cm^2, which is a positive number.[17] SFG spectroscopy can also be used to study the molecular orientation of adsorbates. A study by Ward et al. showed that dodeconal in an aqueous solution adsorbs onto a nonpolar substrate and orient with the OH group towards the aqueous phase and the hydrophobic region towards the nonpolar substrate, a finding that is consistent with chemical intuition.[18]

SFG spectroscopy does have certain limitations. Because of the non-centrosymmetric requirement, the specificity of SFG spectroscopy for the interface limits which materials can be studied with this technique.[9] Dilute colloidal solutions and other highly dispersed systems are not feasible yet for SFG research,[9] though some colloidal systems can be studied using sum frequency scattering (SFS) spectroscopy, as will be discussed in later chapters of this thesis. Occasionally, the dependence of SFG signals on modes that are both IR and Raman active can severely reduce the number of vibrational modes that can be studied.[9] The intensity of an SFG active mode may be low because of its low IR or Raman activity, or because of its orientation. Moreover, the tunability of currently available laser systems limits the type of vibrational modes that can be probed by SFG. With current table-top techniques, it is in principle possible to use SFG to probe vibrational modes down to 250 cm^{-1}.[19] In order to detect vibrational modes below 250 cm^{-1} using

SFG, advances are needed in the practical matters of filters and detectors,[19] and light sources, including free electron lasers. In addition, increasing the intensity of the input beams to overcome low SFG activity has only been moderately successful. After a certain threshold intensity is reached, the sample may be damaged by the laser power.[9] Therefore, careful power studies of each sample must be completed prior to analyzing SFG spectra. These power studies ensure that the sample is not being damaged by the laser during the experiment.

Other disadvantages of SFG spectroscopy arise from difficulty in data analysis. SFG spectroscopy is not sensitive to the number of randomly oriented molecules at the surface, so it is difficult to determine surface coverage of non-oriented molecules compared to oriented molecules.[9] Interpretation of SFG spectroscopic data can sometimes require in-depth knowledge of the system, and specific analysis requires knowledge of terms such as the hyperpolarizability of the molecules of interest. Often, these terms are unknown and analysis must be carried out without this information, or by approximation. The analysis can be complicated by the fact that, with certain materials, the electric dipole approximation can break down and the centrosymmetric bulk can contribute to χ_{NR} through the electric quadrupole.[20-22] This can happen because, although the electric quadrupole term is much weaker, there are many more molecules in the bulk that can contribute to this term. The same applies to charged systems, where third-order responses can be important.[23-27]

Another consideration in SFG spectroscopy stems from the fact that the technique does not affect the sample. No net change occurs in the state of the sample that is interacting with the input beams to produce the output signal, leading to a constraint on the refractive index, *n*, of the media.[4] In SFG spectroscopy, there exists a phase matching condition. This phase matching condition exists because SFG spectroscopy is a coherent process. Thus, if SFG is generated at different

points in a dispersive media, the SFG beams generated will be out of phase, thereby allowing for destructive interference.[1] This destructive interference reduces the signal and introduces random noise into the experiment. In order for the SFG waves to be in phase at all points in the region of overlap of ω_1 and ω_2, the refractive index of the media with respect to the propagation of the SFG waves must equal the refractive index of the input beams. Since the refractive index of a material changes with respect to the frequency of the propagating wave, the phase matching condition is rarely met. Therefore, the experimentally detected SFG signal will always be subject to some amount of random noise.

2.3 Sum Frequency Generation Spectroscopy of Lipid Bilayers

Besides atomic force microscopy (AFM),[28-30] electrophysiology,[31-32] quartz crystal microbalance (QCM) measurements,[33-34] fluorescence imaging,[35] interferometric scattering microscopy[36] or surface plasmon resonance (SPR),[37] nonlinear optical probes have been used extensively to successfully provide new molecular information on lipid flip-flop[38-40] within bilayers, phase transitions,[41] the positions of peptides[42-44] and proteins[45-46] within membranes, domain formations,[47] transition temperatures (T_m),[48] membrane potentials,[17, 49-51] and interactions with molecules,[52-53] proteins,[54-56] DNA,[57] polysaccharides,[58] and engineered nanomaterials.[49, 59-63] Breaking of centrosymmetry is a key requirement that makes second-order nonlinear optical methods interface-selective.[64]

SFG spectroscopy can reveal important information about these boundaries. Roke et al. investigated the phase response of a monolayer membrane to the surface coverage of the lipid.[65] Using SFG spectroscopy, Roke et al. were able to follow molecular dynamics they attributed to the long chain hydrocarbon portion of the model lipid "uncurling" in response to compression by the greater surface coverage of the lipids.[65] Liu and Conboy studied the "flip-flop" of lipid bilayers

through the complete deuteration of one of the leaflets in the bilayer.[48, 66] The deuterated leaflet initially introduced asymmetry at the interface and therefore caused a high intensity SFG signal in the CH stretching region. Using a nanosecond Nd:Yag laser and input beams of 532 cm^{-1} and 1064 cm^{-1}, Liu and Conboy were able to monitor the SFG signal decay caused by interleaflet "flip-flop" at various temperatures in order to understand the kinetics of lipid movement in lipid bilayers.[48, 66] Chen and coworkers reported that the rate of lipid flip-flop was linearly dependent on the concentration of the cytotoxic polymer, polyethylenimine (PEI). They also showed that branched PEI had a much greater effect on lipid flip-flop rate than linear PEI and suggested the faster rate was due to the higher charge density of the branched polymer.[67] In researching lipid monolayers, Tahara and coworkers demonstrated that pH at the lipid/water interface differs from the pH in the bulk, and depends on the charge of the lipids.[68] Tan et al. revealed that if the length of an interacting peptide is shorter than the distance between the interface and the support for a lipid bilayer, lipid accumulation can occur in what they term a "hydrophobic-mismatching interaction."[69]

In addition to the studies which focus on lipid movement and order within a bilayer, several scientists explored complicated questions in biochemistry using SFG spectroscopy. In fact, Luo and coworkers demonstrated that SFG spectroscopy can be used to determine the secondary structure of antimicrobial peptides at the lipid bilayer/water interface.[70-71] Protein secondary structure is a notoriously difficult problem in biochemistry. Using the complementary techniques of SFG spectroscopy and attenuated total reflectance Fourier transform infrared spectroscopy (ATR-FTIR), Chen and coworkers studied a model ion channel getting mechanism by following a change in alamethicin orientation in a SLB in response to pH changes.[45] Chen and coworkers also found that alamethicin orientation within the lipid bilayer depended on the solution

concentration.[72] Probing interfaces in emulsions and adsorbate-solid interfaces is also critical for understanding the function of various additives in food and other materials.[9] Studies like these help to explain the forces and reactions that occur at these difficult-to-reach interfaces, which are observable with SFG spectroscopy.

Frequently, bilayer studies by vibrational sum frequency generation (SFG)[73-74] spectroscopy in particular have employed asymmetric membranes, which vary in their number density of deuterated lipids in either one or both leaflets of the bilayer so as to yield considerable SFG signal intensities.[75-77] Sum frequency scattering (SFS) spectroscopy is an additional way to probe lipids at interfaces of solvent-suspended droplets.[78-79] Other approaches successfully employ hybrid bilayer membranes[80-81] or a lipid monolayer[55, 65, 82-90] in lieu of a lipid bilayer. Yet, while lipid monolayers at the air/water interface produce strong SFG signal intensities, they carry sizeable dipole potentials,[91] which are negligible in lipid bilayers due to symmetry considerations. SFG studies of lipid bilayers also frequently rely on deuterated water as a solvent to aid in spectral interpretation, especially in the C–H stretching region,[92-93] from where molecular information about the lipid tails and their head groups can be obtained. In addition, much research has been carried out using SLBs formed using a Langmuir−Blodgett trough,[94-98] which is an expensive instrument. Research presented in this thesis generally utilizes fully hydrogenated lipids, under aqueous buffer conditions, at physiological pH, at room temperature to form supported lipid bilayers using the vesicle fusion technique.

2.4 General Experimental Details

2.4.1 Broadband SFG Spectroscopy Experimental Approach

The hybrid broadband scanning approach pioneered by Esenturk and Walker was used in the SFG spectroscopy studies described in this thesis, unless otherwise stated.[99] The broadband

system collects signal that spans a larger range of wavelengths in a single acquisition than the more conventionally used scanning systems. The scanning system can probe a larger range of wavelengths overall than the broadband system, but does so in a series of acquisitions in a step-wise fashion with many acquisitions. In the hybrid approach, multiple acquisitions are recorded at various IR center frequencies and summed to yield the final SFG spectrum. This method of combining a scanning SFG system and a broadband SFG system makes use of the advantages of both: a large wavelength range in just a few short acquisitions. Examples of the few IR center frequencies obtained on the broadband system which are summed to create the SFG spectrum are illustrated in Fig. 2.2 A.

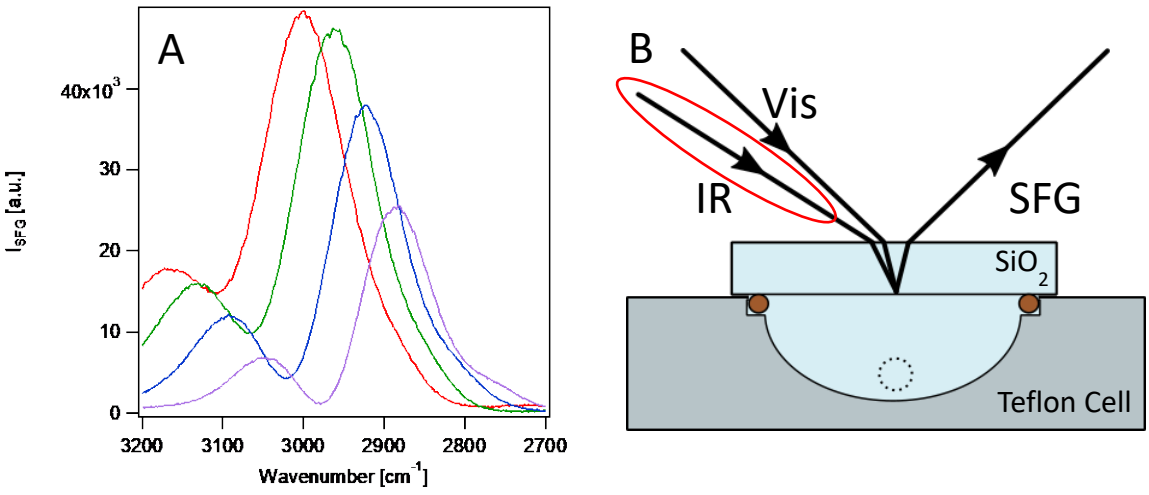

Figure 2.2. (A) *ssp*-polarized SFG spectra of a gold film on the surface of an IR grade fused-silica window recorded in near total internal reflection at various tuned IR frequencies across the CH stretching region. **(B)** A schematic of the sample cell used in the SFG experiments discussed in this thesis. The IR beam is highlighted to illustrate that the frequency of this beam is changing to yield the various SFG spectra shown in A.

2.4.2 Description of Broadband SFG Laser System

A description of the laser system used in this work has been previously published.[27, 49, 100-102] The SFG experiments were performed using a regeneratively amplified Ti:Sapphire system that produced 800 nm light in femtosecond (~120 fs) pulses (Spitfire Pro, Spectra Physics, 1 kHz

repetition rate, 2.5 mJ/pulse, complete with Mai Tai and Empower). The 800 nm light was sent through a 50/50 beam splitter (Spectra-Physics, 10RQ00UB.4), with half of the beam pumped into an optical parametric amplifier (Spectra Physics, OPA-800CF, difference frequency mixing option) to produce an IR beam in the CH stretching frequency region (~3.4 μm, 140 cm^{-1} fwhm) which passed through an IR filter (Newport Corporation, 2702-0271) before four gold mirrors (Edmund Optics, 45606) directed the beam through a BaF_2 IR focusing lens (ISP optics, BF-PX-200) and onto the sample at an angle 60° from the surface normal. The residual 800 nm light that passed through the 50/50 beam splitter was directed by 4 gold mirrors (Edmund Optics, 45606) before it passed through two variable density filters (ThorLabs, NDC-50C-4), one additional gold mirror, a home built delay stage with two 3mm thick gold mirrors (CVI, PW1-1025C) on a translational stage (ThorLabs, PT1), three additional gold mirrors and finally through an iris (ThorLabs, ID12), a narrow band pass filter (CVI, Melles Griot, F1.1-800.0-UNBLK-1.00), a half waveplate (Karl Lambrecht Corp., MWPAA2-12-700-1000), and a plano-convex focusing lens, to overlap in time and space with the IR beam on the sample at a 45° angle from the surface normal. Once the IR and visible beams overlapped and produced the SFG signal, the SFG light was recollimated using an achromatic lens, a polarizer (ThorLabs, Glan polarizer, GL15), a half waveplate (Karl Lambrecht Corp., MWPAA2-12-400-700), two gold mirrors, a short pass filter (Edmund Optics, 45646), a long pass filter (Edmund Optics, 600 nm, 66054), a plano-convex focusing lens, and a notch filter (Kaiser Optical Systems, Inc., holographic notch-plus filter, HNPF-800.0-1.0) until finally detected with a charged coupled device (CCD) camera (Roper Scientific, 1340 × 100 pixels) cooled by liquid nitrogen and combined with 0.5 m spectrograph (Spectra Pro 500i Acton Research). Each SFG spectrum was background-subtracted, calibrated to the 2850 cm^{-1} and 3060 cm^{-1} peaks of polystyrene (International Crystal Laboratories,

polystyrene calibration film, 76 μm, 0009-8181), and normalized to the non-resonant sum frequency signal of a gold-coated silica window plus one.

All SFG data reported here were collected using near total internal reflection and either the *ssp*-polarization combination or the *ppp*-polarization combination. In the naming convention for these polarization combinations, the first letter refers to the polarization of the SFG beam, the second refers to the polarization of the visible beam, and the third refers to the polarization of the IR beam. The *ssp*-polarization combination probes the components of the vibrational modes that are perpendicular to the surface.[103]

2.4.3 General Description of Sample Preparation

Detailed below are specific experimental parameters relevant to the individual experiments for each chapter. To form the supported lipid bilayer in the SFG experiments, the lipids were first mixed in the appropriate molar ratios from stock solutions in chloroform and then dried under a flow of nitrogen. The lipids were rehydrated in a 10 mM Tris buffer solution at pH 7.4, 5 mM $CaCl_2$ and either no, 1, 10 or 100 mM added NaCl before extrusion. Extruding the lipid solution before use with a 0.05 μm polycarbonate membrane filter ensured the production of small, unilamellar vesicles.[104-105] For SFG experiments, after the cell was equilibrated with 10 mM Tris, pH 7.4 buffer solution at the desired experimental NaCl concentration, the extruded lipids were injected into a custom-built Teflon flow cell and the lipid bilayer formed on the surface of a clean silica window using the vesicle fusion method. [29, 106] To clean the silica window, the window was placed in NoChromix® solution for between one and fourteen hours, rinsed with Millipore water, and dried under a stream of nitrogen. Immediately before use, the window was plasma cleaned (Harrick Plasma Cleaner, PDC-32G) for twelve minutes on the “high” setting. An SFG spectrum

of the bare silica window was recorded to ensure no CH stretches were present before buffer and lipid injection.

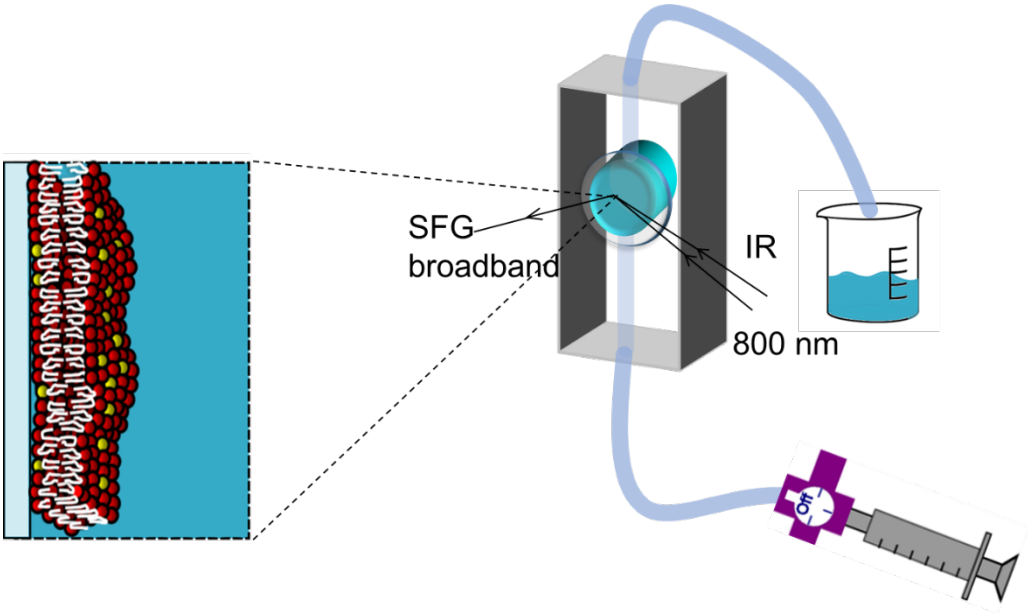

Figure 2.3. Schematic of the custom-built Teflon flow cell and experimental setup for bilayer, bilayer nanoparticle and bilayer polymer experiments.

2.5 Experimental Details for Chapter 3

2.5.1 Lipid Choice

The lipids chosen in this study all contain the PC headgroup. The zwitterionic choline headgroup is of particular importance because the PC class of lipids comprises more than 50% of the phospholipids in a majority of eukaryotic membranes.[107] Bovine pulmonary artery endothelial cells are composed of close to 20% DPPC and 20% POPC.[108] DPPC can also be found in pulmonary surfactant.[109] Degradation and the synthesis of PC lipids have been shown to play a role in cancer growth as well as apoptosis.[110-111] PC lipids are also important components in cell signaling pathways[112] and as lipid secondary messengers.[107] Moreover, estimates currently stand that approximately 15% of all bacterial species also have the ability to synthesize PC lipids.[113]

2.5.2 Flow Cell

The flow cell used in our SFG experiments has been described in detail previously.[49] For our experiments, a custom-made Teflon flow-cell with a reservoir volume of approximately 3 mL was used. For experiments which required changing the temperature, this Teflon flow-cell was heated via two low-density cartridge heaters (Omega Engineering, LDC00014) connected to a Eurotherm temperature controller. The temperature was monitored and controlled through the use of a Type K thermocouple (Omega Engineering, DH-1-20-K-12). All solutions were introduced into the cell via an approximately 8"-long PTFE tube (1/16") connected with Swagelok fittings. A 1"-diameter IR-grade fused silica window (ISP Optics) was placed on top of a Viton O-ring (Chemglass) such that a leak-tight seal was formed. The temperature-dependent experiments were carried out using the same buffer composition as the one used for the room temperature studies.

2.5.3 Bilayer Formation

To form the supported lipid bilayers, the lipids were first mixed in the appropriate molar ratios from stock solutions in chloroform, dried under a flow of nitrogen, and rehydrated in a 10 mM Tris buffer solution at pH 7.4, 100 mM NaCl, and 5 mM $CaCl_2$. The lipids were extruded using a mini-extruder kit (Avanti Polar Lipids). Extruding the lipid solution before use with a 0.05 μm polycarbonate membrane filter ensured the production of small, unilamellar vesicles.[114] 4 mL of a 0.5 mg/mL vesicle containing solution (vesicles, 100 mM NaCl, 10 mM Tris buffer, 5 mM $CaCl_2$, pH 7.4) was injected into a custom built Teflon flow cell[60] and the lipid bilayer was formed on the surface of the silica window using the vesicle fusion method.[106, 115] The bilayer was rinsed with 30 mL calcium-free buffer solution (100 mM NaCl, 10 mM Tris, pH 7.4) at a flow rate between 1 and 2 mL/min to ensure removal of excess vesicles in solution. Unless otherwise stated,

bilayer formation and rinse occurs at room temperature. This volume is more than 10 times the volume of the flow cell. SFG spectra of the lipid bilayers were recorded after this rinse.

2.5.4 Scanning and Broadband Sum Frequency Generation Spectrometers

The laser systems and configurations for the scanning and the broadband SFG experiments have been described previously.[27, 60, 102, 116-117] Briefly, the scanning SFG spectrometer is a commercial (EKSPLA) system located at Pacific Northwest National Laboratory (PNNL) operating at a repetition rate of 10 Hz and producing infrared pulses of 30 psec duration that are overlapped at the sample with a psec upconverter at 532 nm (spectral resolution of ~6cm^{-1}). The broadband system (Spectra Physics/Newport) is located at Northwestern University and operates at a 1 kHz repetition rate, producing 100 fsec infrared pulses near 3 μm (140 cm^{-1} bandwidth at FWHM) that are overlapped at the sample with a psec upconverter at 800 nm (spectral resolution ~10 cm^{-1}). Both spectrometers were used on lipid bilayers formed, as described above, on IR-grade fused silica windows (ISP Optics, QI-W-25-3, 3mm thick, 1" in diameter). Angles of incidence are 60° and 45° for the infrared and upconverter, respectively, at Northwestern University, and 55° and 65° for the infrared and upconverter, respectively, at PNNL. The differences in the incident angles shall not cause differences in the ssp spectral lineshapes for the same sample surface.[118]

SFG spectra are collected using the *ssp* polarization combination unless otherwise indicated; the abbreviation represents *s*-polarized SFG, *s*-polarized 800 nm visible light, and *p*-polarized IR light. This polarization combination probes the components of the vibrational modes that are oriented perpendicular to the membrane. The laser spot at the sample is approximately 30 μm in diameter at Northwestern University and ~300 μm at PNNL. Unless stated otherwise, each SFG spectrum recorded using the broadband system is composed of an average of 5 acquisitions each integrated over 4 minutes, background-subtracted, calibrated to the 2850 cm^{-1} and 3060 cm^{-}

[1] peaks of a polystyrene film, and normalized to the nonresonant sum frequency response of a gold-coated silica window plus one so as to account for the distribution of IR energy across the sampled frequency region. The averaged, normalized spectra are recorded at three different IR-center frequencies and summed as described in detail elsewhere.[99]

2.5.5 Fluorescence Microscopy

Fluorescence images were taken using a Leica Spinning Disk Microscope (Leica DMI6000 equipped with Yokogawa CSU-X1 Spinning Disk) with a 63X oil immersion objective (63X HC PL APO 1.4NA Oil) and a Photometrics Evolve 512 Delta (16 μm pixel size, 20 MHz digitizer, 512x512 chip camera with a back thinned EMCCD Sensor) driven by Metamorph. Fluorescence imaging was carried out with the Green ET525/50M emission filter and 488 nm 50 mW laser at 20% power. Images were recorded of bilayers formed pure DLPC, DMPC, and DSPC, doped with a 0.01 mol % TopFluor® PC. Bilayers were formed using the vesicle fusion method, in the same manner and in the same flow cell used for the SFG experiments. The window was then removed and placed in a dish containing aqueous buffer solution and a clear cover slip on the bottom. The window was positioned onto the cover slip using three small pillars of silicone grease located on the edges of the window. The bilayer was then imaged through the cover slip and aqueous buffer layer.

Fluorescence recovery after photo bleaching (FRAP) measurements were recorded on the Leica Spinning Disk microscope described above. Laser manipulation for photobleaching was performed with an iLas[2] attachment from Roper Scientific mounted on the Leica Spinning Disk. Bleaching was performed with the 488 nm laser at 10 % power. Photobleaching was carried out using the iLAS software as follows: a bleach region was drawn in the field of view, either circular or rectangular, and ranged from 65 x 10^{-2} μm^2 to 120 μm^2 depending on sample image; the laser

power was set to 10% and 5 repetitions over the defined bleach region were performed. Bleach settings were determined as those which are required to achieve at least a 60% loss of fluorescence intensity. Pre- and post-bleach imaging was performed as above. Sample preparation was the same as for fluorescence imaging, except DLPC, DMPC, and DSPC, were doped with a 0.1 mol % TopFluor® PC. Diffusion coefficients discussed are averages of a minimum of 5 measurements and analyzed using the simFRAP plugin for ImageJ.[119] Errors reported are 2 σ standard deviations. More detailed information is available in the Supporting Information of Olenick et al.[120]

2.6 Experimental Details for Chapter 4

2.6.1 Materials, nanoparticle synthesis, bilayer preparation, and characterization

The synthesis, functionalization, and characterization of the nanoparticles and bilayers studied here have been described previously by researchers within the CSN.[49, 121] The details for the procedures pertaining to the nanomaterials were optimized by Dr. Samuel Lohse, Dr. Ariane Vartanian, and Xi Zhang from the Murphy group along with Dr. Marco Torelli from the Hamers group. Bilayer preparation and optimization processes were developed by this author and fellow graduate students at Northwestern: Merve Doğangün, Alicia McGeachy, and previous graduate student Dr. Stephanie Walter along with collaborators from the Pedersen group, Dr. Thomas Kuech and Dr. Eric Melby.

2.6.1.A Nanoparticle synthesis, bilayer preparation, and characterization (in collaboration with the Murphy and Hamers groups)

In collaboration with Dr. Ariane Vartanian, Dr. Samuel Lohse, Xi Zhang, and Dr. Marco Torelli, the 15-nm gold and diamond nanoparticles were prepared and wrapped in PAH ligand following a previously described procedure.[122] For gold particles, 1 L of 0.8 mM $HAuCl_4$ was heated to a rolling boil, followed by addition of 16 mL of 5% (w/v) sodium citrate. The deep red

solution was stirred and boiled for 30 minutes to yield citrate-capped particles. The particles were centrifuged at 8000*g* for 40 minutes, and the combined pellets were redispersed in 1 L of 1 mM NaCl and stirred overnight with 50 mL of PAH solution (10 $mg \cdot mL^{-1}$ of 15,000 $g \cdot mol^{-1}$ PAH (Sigma-Aldrich) in 1 mM NaCl). The PAH-wrapped particles were purified by either tangential flow filtration (MWCO 50K) or centrifugation.

Fellow graduate student Marco Torelli obtained diamond nanoparticles (DNPs) from Microdiamant (Smithfield, PA). Synthetic diamond was synthesized by high-temperature high-pressure (HPHT) synthesis and subsequently milled and sized to achieve 15 nm diameter. The particles were oxidized by reflux in a mixture of 3:1 sulfuric and nitric acid overnight, isolated by centrifugation, refluxed again overnight in a fresh acid mixture, washed by centrifugation, and finally resuspended in NanoPure water until reaching a circumneutral pH. PAH functionalization was carried out in a manner similar to that for Au nanoparticles, by mixing concentrated diamond nanoparticle stock (~1 $mg \cdot mL^{-1}$ by gravimetric analysis) with 1 $mg \cdot mL^{-1}$ PAH in 1 mM NaCl, sonicating overnight. The particles were then cleaned by dialysis (50 Da MWCO, Spectrum Labs) through at least 12 L of water. Functionalized particle sizes and wrapping were confirmed by transmission electron microscopy (TEM), dynamic light scattering (DLS) and laser Doppler microelectrophoresis as described in the Supporting Information of Troiano et al.[49]

Tian Qiu of the Haynes group determined the amount of unbound PAH polymer in PAH-AuNPs purified by double centrifugation by following a fluorescence assay reported before using amine-reacting fluorescamine.[123] Briefly, a buffer composed of 10 mM HEPES and 100 mM NaCl adjusted to pH 7.4 was used instead of water to dissolve free PAH polymers to obtain calibration curves, and the same buffer was used to disperse PAH-AuNPs prior to centrifugation to obtain supernatant that contained free PAH ligand. After the sample was mixed with borate buffer and

fluorescamine, the solution was incubated at room temperature for 15 minutes, followed by fluorescence readout with excitation/emission wavelengths of 425/480 nm. In the data analysis of the calibration curves, second-order polynomial fitting was used instead of linear fitting to better fit the data points ($R^2 > 0.99$). Average of ten technical replicates from two material replicates were used to calculate the final concentration of free PAH ligand.

The nonlinear optical, QCM-D, and NMR procedures to study lipid bilayer-nanoparticle interactions have been described earlier work by CSN researchers in Bozich et al.[122] Nonlinear optical experiments were carried out at Northwestern with help from fellow graduate students Dr. Julianne Troiano, Merve Doğangün, and Alicia McGeachy. Dr. Thomas Kuech and Dr. Eric Melby in the Pedersen laboratory carried out the QCM-D experiments. NMR experiments were performed by Dr. Ariane Vartanian from the Murphy group. Solutions used in these experiments contained 0.01 M Tris and 0.1 M NaCl, were adjusted to pH 7.4, and were prepared in ultrapure water (18.2 MΩ·cm). Experiments using free PAH ligands were conducted with poly(allylamine hydrochloride), (Sigma-Aldrich, average M_r ~15,000 g·mol^{-1}) dissolved in ultrapure water and diluted to the desired concentration without further purification. After forming a supported lipid bilayer on the surface of fused silica windows as described previously[49] and rinsing with $CaCl_2$-free buffer to remove excess vesicles, the desired solution was injected into the flow cell, allowed to interact with the bilayer for 20 min, an SFG spectrum (not shown) was collected then the bilayer was rinsed with our buffer solution and the rinsed SFG spectrum was collected. All spectra shown in this chapter are those collected after rinsing the surface.

2.6.1.B Materials

Buffer solution refers to a 0.01 M tris(hydroxymethyl)aminomethane (Tris) (Sigma-Aldrich, 99.8%), 0.1 M NaCl (VWR, 99.0%), pH 7.4 aqueous solution. Tris and NaCl were used

as received. 1,2-dimyristoyl-*sn*-glycero-3-phosphocholine (DMPC); 1,2-dioleoyl-*sn*-glycero-3-phosphocholine (DOPC); 1,2-dimyristoyl-*sn*-glycero-3-phospho-(1'-*rac*-glycerol) (DMPG); and 1,2-dioleoyl-3-trimethylammonium-propane (DOTAP) were purchased from Avanti Polar Lipids, Inc. and used without further purification.

2.6.1.C Lipid Vesicle Preparation

Lipid vesicles were prepared via the vesicle fusion method[29, 106] as outlined in Supporting Information for Troiano et al.[122] The vesicle preparation was optimized in collaboration with the Pedersen lab.

2.6.1.D Lipid Vesicle Characterization

Size and ζ-potentials of the lipid vesicles were determined using dynamic light scattering (DLS) and laser Doppler micro-electrophoresis using a Zetasizer Nano ZS according to Supporting Information of Troiano et al.[122] The vesicle characterization method was developed in collaboration with the Pedersen, Murphy, and Hamers laboratories.

2.6.1.E Gold Nanoparticle Characterization (in collaboration with the Murphy group)

AuNPs were characterized by UV-Vis absorption spectroscopy, transmission electron microscopy (TEM), DLS and laser-Doppler micro-electrophoresis explained in the Supporting Information for Troiano et al.[122] and carried out by Dr. Ariane Vartanian and Dr. Samuel Lohse from the Murphy group.

2.6.2 Single molecule trajectories (in collaboration with the Orr and Pedersen groups)

Supported lipid bilayers were formed within 35/22 mm #1.5 glass bottom dishes (Willco Wells) by Dr. Julianne Troiano and Dr. Eric Melby. Dishes were rinsed with ultrapure water (18 MΩ·cm; MilliQ Advantage A10, Millipore), dried with N_2, and cleaned in a UV/Ozone chamber (PSD Pro Series, Novascan) for 20 min. Cleaned dishes were equilibrated with a solution

containing 0.1 M NaCl buffered to pH 7.4 with 0.010 M Tris for at least 1 h. Suspensions of small unilamellar vesicles SUVs (0.0625 mg·mL^{-1} 9:1 DMPC/DMPG with 0.0001 mol% fluorescent Atto 647N DOPE (Atto-Tec; λ_{ex} = 642 nm; λ_{em} = 667 nm) in the same buffered solution used to equilibrate the dishes) were introduced to the dish. After bilayer formation, the solution in the dish was exchanged five times with 2 mL aliquots of the buffered solution.

Single molecule fluorescence imaging of supported lipid bilayers was conducted before and after introduction of 1 nM PAH-AuNPs. Imaging was conducted on an Olympus IX71 inverted microscope with a UPlanSApo 100× 1.4 NA oil-immersion objective. Fluorescence emission was acquired with an Andor iXon Ultra EMCCD operated at 6.9 Hz. The excitation source was a 643 nm pumped laser (CL-2000, Crystal Laser). A series of at least 500 frames was collected at three spots (250 × 250 pixels, 40 × 40 μm) before and after 1 nM PAH-AuNP addition, and this was repeated on three different supported lipid bilayers. MATLAB (R2015a, MathWorks) was used by Dehong Hu to determine the trajectories of individual lipid molecules and lateral lipid diffusion coefficients. Individual fluorescent molecules were identified as unique, diffraction limited points with the expected fluorescence intensity of single dye molecules, as predetermined by spin-coating the dye molecules on a glass coverslip and imaging them using the same settings. These points were tracked from one frame to the next to reconstruct the trajectories of individual lipid molecules. The lateral diffusion coefficient, D_L, was determined from the mean squared displacement, *MSD*, and the time between frames, *t*, using the relation $MSD = 4D_L t$.

2.6.3 Computer Simulations (in collaboration with the Hernandez and Cui groups)

To understand how the lipid corona is formed around gold nanoparticles wrapped with the positively charged PAH, graduate student Gene Chong in the Hernandez group used molecular dynamics simulations with the POL-MARTINI coarse-grained force field.[124-125] The gold

nanoparticle was constructed as a 4 nm-diameter sphere with fcc lattice structure, where all beads were treated as the C1 type (the most hydrophobic in the MARTINI force field) with 4.7 Å as the van der Waals radius; a similar model for the gold nanoparticle had been employed successfully in previous coarse-grained molecular dynamics simulations of functionalized nanoparticles and their interactions with lipid membranes.[126] All beads beyond 1.8 nm from the center of the nanoparticle were assigned with a negative charge of -1, qualitatively mimicking the effect of surface passivation by citric acids. The force field of PAH was established by combining the carbon backbones of polystyrene[127] and the top bead of the lysine side chain from MARTINI.[124] Two PAH models containing 160 and 200 monomers, respectively, were constructed, since exploratory simulations indicated that these chain lengths led to a significant degree of surface coverage of the nanoparticle once it was wrapped by the PAH polymer. All monomers were assumed to be positively charged, which likely led to an overestimated charge of PAH.[128] The interfacial electrostatic potential of the nanoparticle in salt solution was about +100 mV at the van der Waals surface of the PAH polymer that wraps the gold nanoparticle, thus the ζ-potential was expected to be substantially lower, in the range of 50 mV, which can be compared to the experimental measured value of +30 mV.[129] Thus, the current model is appropriate for exploring the qualitative nature of the lipid corona. The calibration of the coarse-grained model using an all-atom representation of the PAH interacting with the gold nanoparticle is described in Supplementary Information of Olenick et al.[130]

To study the organization of lipids near the PAH-wrapped gold nanoparticle, self-assembly simulations were carried out by Dr. Leili Zhang in the Cui group by randomly placing lipids around a gold nanoparticle wrapped with a PAH chain that contains 160 or 200 monomers. The solution contained 423 copies of DMPC molecules and 47 copies of DMPG molecules, and 0.02 M NaCl

solution with MARTINI polarizable water model. The dimension of the simulation box was $15\times15\times15$ nm^3. The time step of the simulations was 20 fs. Electrostatic interactions were treated with the particle mesh Ewald (PME) method,[131] with a Fourier spacing of 0.12 nm. Van der Waals interactions were treated by the shift scheme, with a cut-off distance of 1.2 nm and the switching function turned on at 0.9 nm. Isothermal-isobaric (NpT) simulations were carried out at 300 K and 1.0 bar using the Berendsen thermostat and pressure coupling (compressibility of 3×10^{-5} 1/bar),[132] calculations were repeated using the semi-isotropic pressure coupling and the qualitative results remain the same. The system was subject to 20,000 steps of steepest descendant energy minimization before 1 ns of NVT equilibration and 400 ns of production simulations. Several independent simulations were carried out to ensure the robustness of the qualitative trends.

2.6.4 Biological studies (in collaboration with the Haynes, Feng, and Klaper groups)

As described in detail in the Supplementary Information in Olenick et al.,[130] graduate students in the Haynes group and undergraduate students in the Feng group suspended *Shewanella oneidensis* cells in a HEPES buffer (2 mM HEPES and 25 mM NaCl at pH 7.40) and then exposed them to 0.5 mg·L^{-1} PAH-AuNPs for 10 minutes, fixed with 2.5% glutaldehyde in 0.1 M cacodylate buffer, dehydrated in a graded ethanol series, and embedded in an epoxy resin. The thin-sectioned resin sample (~60-nm-thick) was stained with uranyl acetate and lead citrate prior to TEM imaging on a Tecnai T12 electron microscope operating at 120 kV.

Standard Pacific Bioscience IsoSeq cDNA synthesis and library preparation were performed by graduate students in the Klaper group with the addition of adding PacBio barcodes during cDNA synthesis. cDNA was synthesized using the SMARTer PCR cDNA Synthesis Kit (ClonTech) and amplified by PCR. All barcoded cDNAs were pooled equally by mass. Following BluePippin (Sage Science) size selection, pooled amplified cDNA was divided into four size bins:

1-2 kB, 2-3kb, 3-6kb. Size selected cDNA was further PCR amplified, enzymatically repaired, and ligated to a PacBio adapter to form the SMRTbell Template. Templates were annealed to sequencing primer, bound to polymerase, and then bound to PacBio Mag – Beads and SMRTcell sequenced.

Data was primarily analyzed through barcoded use of the Pacific Biosciences IsoSeq pipeline, in which asymmetric barcodes were employed where the reverse barcode was of ClonTech design. Execution of IsoSeq was performed through SMRTanalysis version 2.3, where only isoforms possessing at least 2 full passes around the SMRTbell adapters were permitted to pass the initial consensus sequencing correction step (e.g. CCS1 or Reads-of-Insert). The resulting isoforms were then submitted to the ICE and Quiver algorithms to produce polished, high-quality isoforms clustered into putative gene families. IsoSeq, by method design, relies in a strategy of size-fractioning genes into three size-bins: 1-2 kb, 2-3 kb, and 3+ kb. The resulting sets of genes were aligned against a composite transcriptomic reference composed of D. magna, D. pulex, C. elegans, and D. melagnogaster via BLASTX; these alignment results were used to construct a Daphnia reference consisting of per-size-bin, per-cluster gene identifiers. This reference was then relationally joined with per-isoform barcoding results to generate lists of annotated genes expressed within each experimental sample.

2.7 Experimental Details for Chapter 5

2.7.1 Selection of Materials

We selected PAH for these polymer–lipid membrane interaction studies due to its canonical importance in this area of research, ranging from supported lipid bilayer studies,[49] to cancer cell imaging[133] and organismal toxicity[121] to its use as a common wrapping for nanomaterials.[134] DMPC was used in the present study because it has also been widely studied and

contains the phosphatidylcholine (PC) headgroup, which is prevalent in the membranes of eukaryotes.[107-111] In order to probe PAH-DMPC membrane interactions, we used a membrane model system composed of phospholipid monolayers coating the surfaces of oil nanodroplets.[135] Since oil droplets are hydrophobic in nature, the phospholipid orients itself with the hydrophilic portion in the aqueous phase. The polycations introduced into the system then interact with the headgroups of the monolayer, much as they would with the headgroups in a lipid bilayer. We caution that a key difference from lipid bilayer membranes is the sizeable dipole potential of lipid monolayers.[91] Yet, the oil droplets studied here possess controllable molecular interfacial properties[135] and have been previously used to study lipid structure and orientation as well as the interactions of the oil droplets with ions.[136] When compared to lipid monolayers formed in a Langmuir trough, one advantage is that the current approach requires smaller sample volumes.[135]

2.7.2 Chemicals

PAH was purchased from Sigma Aldrich (283215, ~17.5 kDa) and used without further purification. DMPC was purchased in powder form (>99%, Avanti Polar Lipids), stored at -20°C until use, and used without further purification. Sodium chloride ($\geq$ 99%, Sigma Aldrich), d_{34}-hexadecane (98%, Cambridge Isotope Laboratories), and D_2O (99.8%, Armar Chemicals) were used as received.

2.7.3 Oil Droplet Preparation

In order to prepare nanoscale oil droplets (nanodroplets), powdered DMPC was hydrated in D_2O in a 2 mL glass vial at a concentration of 2 mM for CH SFS experiments and 1 mM for PO SFS experiments for 30 minutes at approximately 40°C, ensuring that the hydration occurred above the transition temperature of the lipids (24 °C for DMPC).[137] Deuterated hexadecane (1 vol %) was then added to the hydrated DMPC suspension. The lipid-oil suspension in D_2O was

sonicated for periods of five minutes at an intensity setting of 40% on the ultrasonic bath (35 kHz, 400 W, Bandelin sonorex digiplus) until a DLS size measurement indicated a polydispersity index (PDI) below 0.25 and a diameter between 100 and 200 nm. Once the sample met these criteria and the solution was milky white and homogeneous, the sample was used for no more than one week, stored in the refrigerator, and stability was verified with DLS before each SFS measurement.

For SFS experiments in the CH stretching region, PAH solutions were made from PAH stock solutions composed of 41 mM PAH in 1 mM NaCl in D_2O. For SFS experiments in the PO stretching region, PAH solutions were made from PAH stock solutions composed of 2.3 mM PAH in D_2O. Aliquots of PAH stock solutions were added to the lipid-oil droplet solutions via micropipette to reach the desired concentrations. Solutions were mixed thoroughly with the pipette tip and then allowed to sit at room temperature for 15 to 20 minutes prior to SFS experiments. For SFS measurements, 60 μL of the nanodroplet solution was placed into a cuvette composed of a fused silica window with a slight interior indentation (Hellma Analytics, 106-0.20–40, Germany) and a detachable CaF_2 window (CeNing Optics, 1.3 mm thick, 60-40S/D, L/2). Care was taken not to trap air bubbles within the sample during preparation of the cuvette. The CaF_2 window was oriented towards the incoming IR and visible beams, and the quartz window was oriented towards the detector.

2.7.4 SFS system

Vibrational SFS spectra were recorded using our previously described approach.[138-140] Briefly, an 800 nm regeneratively amplified 1 kHz Ti:sapphire system (Spitfire Pro, Spectra physics) was used to pump a HE-TOPAS-C (Light Conversion) optical parametric amplifier to generate IR pulses. The visible beam was split off directly from the amplifier and spectrally shaped with a home-built pulse shaper for a spectral resolution of 10 cm^{-1}. The angle between the 10 μJ

visible (VIS) beam (800 nm, FWHM 10 cm^{-1}) and the 6 μJ IR beam (9700 nm or 3200 nm, FWHM 160 cm^{-1}) was 20° (as measured in air). The IR and visible beams were focused using parabolic gold mirror with effective focal length of 101.6 mm (84-625, Edmund Optics) and plano-convex lens (LA1484-B, Thorlabs) overlapped in a sample cuvette with a path length of 200 μm at incident angles of 35° and 55°, respectively. At a scattering angle of 55° with respect to 800 nm beam, the scattered SF light was collimated using a plano-convex lens (f=15 mm, Thorlabs LA1540-B) and passed through two short wave pass filters (3rd Millenium, 3RD770SP). The SF light was spectrally dispersed with a monochromator (Acton, SpectraPro 2300i) and detected with an intensified CCD camera (Princeton Instruments, PI-Max3) using a gate width of 10 ns. The acquisition time for a single spectrum was 10-20 min for PO stretch modes and 20 min for CH stretch modes. A Glan-Taylor prism (Thorlabs, GT15-B), a half-wave plate (EKSMA, 460-4215), and a polarizing beam splitter cube (CVI, PBS-800-050), and two BaF_2 wire grid polarizers (Thorlabs, WP25H-B) were used to control the polarization of the SFG, VIS, and IR beams, respectively. The SFG and VIS beams were polarized in the vertical (S) direction and the IR beam was polarized in the horizontal plane (P) with respect to the plane of incidence, leading to the polarization combination $S_{out}S_{in}P_{in}$. The recorded intensity was baseline subtracted and normalized to the SFG spectrum obtained from a gold mirror in $P_{out}P_{in}P_{in}$ polarization and in a conventional reflection geometry (with incident angles of 45° for vis and 65° for IR) that was recorded before each measurement. Droplet size was accounted for by dividing the SFS spectrum by the radius of the droplet cubed (r^3), based on DLS data, as described previously.[141] Daily changes in power were accounted for by dividing the SFS spectrum by the power (both IR and visible) multiplied by the acquisition time (in seconds).

2.7.5 Zetasizer

Dynamic Light Scattering measurements utilized a Malvern Zetasizer Nano ZS. Samples were prepared by adding 20 μL of lipid-oil droplet solution to 1 mL H_2O in a microcuvette. Each size result shown is the average of three measurements, each of which is the average of 11 data points. Standard deviation is calculated from the three replicates. All DLS data was acquired on the same samples that were used to acquire the SFS data.

2.7.6 Infrared Spectroscopy

All IR spectra were obtained using a Bruker Vertex 70 FTIR spectrometer and analyzed using OPUS 6.0 software.

Chapter 3

Single-Component Supported Lipid Bilayers Probed Using Broadband Nonlinear Optics

Portions of this chapter have been reproduced from the following paper with permission from the Royal Society for Chemistry:

Olenick, L. L.; Chase, H. M.; Fu, L.; Zhang, Y.; McGeachy, A. C.; Dogangun, M.; Walter, S. R.; Wang, H.-f.; Geiger, F. M., Single-Component Supported Lipid Bilayers Probed Using Broadband Nonlinear Optics. *Physical Chemistry Chemical Physics* **2017**.
doi 10.1039/C7CP02549A

3.1 Introduction

As pointed out in chapters 1 and 2, lipid bilayers serve as valuable models for studying processes involving biointerfaces[1-7] and Sum Frequency Generation (SFG) spectroscopy is an excellent tool to study the interactions of many materials with model lipid bilayer systems. This chapter explores the SFG spectroscopy of supported lipid bilayers (SLBs) composed of lipids with various transition temperatures under aqueous buffer conditions.

Biointerface research is complicated by the need for *in situ* observations under ambient pressure and aqueous conditions, which are accessible parameters when using SFG spectroscopy. This technique is applicable because of its inherent specificity for the interface due to the requirement that symmetry be broken for the generation of the sum frequency signal. The specificity of this technique for the interface, the chemical information contained within the spectra, and the short timescales that can be resolved using this technique illustrate the excellent pairing of SFG spectroscopy with the study of biointerfaces.

A survey of the recent literature on the SFG spectroscopy of lipid bilayers shows that the majority of the published data has been obtained using low-repetition rate (tens of Hz) scanning laser systems. The pulses produced by these spectrometers contain significantly less peak power (mW, from a few hundred μJ pulse energy per tens of psec pulse duration in the infrared) than those produced by broadband SFG spectrometers, which are based on nominally 100-femtosecond long infrared pulses, with tens of μJ pulse energy, corresponding to 100-fold increases in peak power. The considerable peak power and the kHz repetition rate of broadband SFG spectrometers therefore offer the opportunity to probe single-component lipid bilayers by SFG spectroscopy without having to impose membrane asymmetry using deuterated lipids. Unlike the recent study by Yan and co-workers,[8] who found little to no broadband SFG signal intensity from symmetric

lipid bilayers formed from purely anionic lipids (PG- and PS-terminated), this research focuses on phosphatidylcholine (PC)-terminated lipids for reasons outlined in Chapter 2.

This chapter reports on SFG spectra that were obtained using broadband and scanning SFG spectrometers in the C-H stretching region from largely single-component supported bilayers formed from zwitterionic PC-terminated lipids in contact with solutions formed from H_2O, 10 mM Tris buffer, and 100 mM NaCl. Deuterated lipids were not used in this study and D_2O was only used for spectral clarification. The membranes surveyed in this chapter are formed from six lipids spanning transition temperatures (T_m's) between -18 to +55 °C and this research finds that the signals are sufficiently large to obtain SFG spectra within a few minutes. Finally, the spectra are grouped into those produced by membranes with T_m's below the laboratory temperature and those produced by membranes with T_m's above it. This key result could be used in the future to assess bilayer phase change in response to foreign objects such as nanomaterials, using SFG spectroscopy.

3.2 Results

Fig. 3.1 demonstrates the differences in signal-to-noise ratio obtained when probing a supported lipid bilayer formed from a 9:1 mix of DMPC and DMPG lipids using the scanning and the broadband SFG spectrometers.

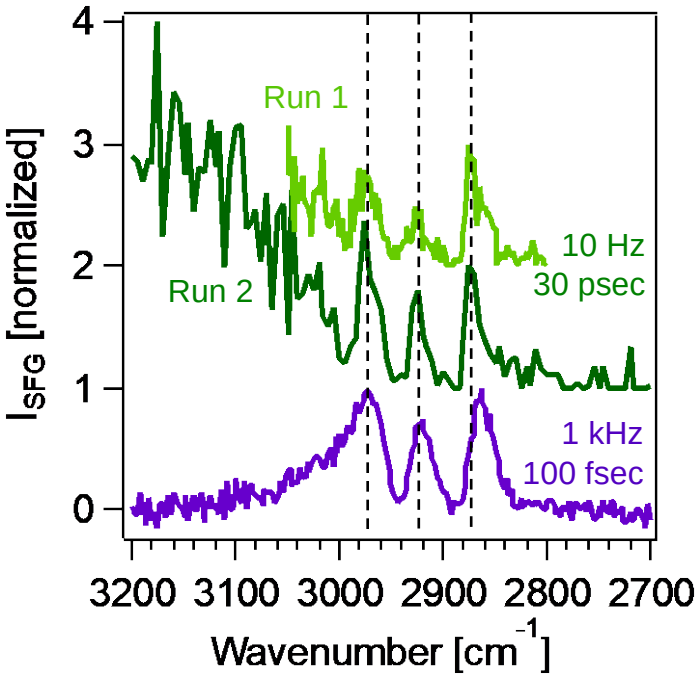

Figure 3.1. Comparison of *ssp*-polarized SFG spectra of supported lipid bilayers formed from a 9:1 mixture of DMPC/DMPG phospholipids on a fused silica window on a scanning SFG system (top, light green) at 2 cm^{-1}/s scan rate (middle, dark green) 5 cm^{-1}/s scan rate and a broadband SFG system (bottom, purple) in 100 mM NaCl, 10 mM Tris, pH 7.4 at room temperature. While the O-H spectral feature was clearly present in the scanning SFG data, this feature was not captured due to the lack of intensity at the blue edge of the IR spectral profile in the broadband SFG measurement.

All spectra were recorded using the *ssp*-polarization combination. The aqueous solution phase in these experiments was maintained at pH 7.4 using 10 mM Tris buffer, and contained 100 mM NaCl. The acquisition of the spectra took comparable amounts of time, namely ~120 minutes, using either spectrometer. Despite the increased signal-to-noise ratio in the broadband SFG data, the spectra acquired using the scanning system show substantial signal intensity towards the OH stretching continuum of water, which is not evident in the SFG spectrum recorded with the broadband system. This difference is due to the fact that the bandwidth of the broadband system did not extend out much beyond 3000 cm^{-1}, i.e. the broadband system was not tuned to sample OH

stretching modes. Nevertheless, as shown below in H_2O-D_2O exchange studies, the spectral lineshape sampled by the broadband system is subject to spectral interference from the OH stretching continuum. Therefore, special care needs to be taken when measuring and interpreting SFG spectra using the broadband system with limited spectral sampling range, as the spectral features near the edge of the range of the spectral profile of the IR pulse used in the experiment may be overlooked.

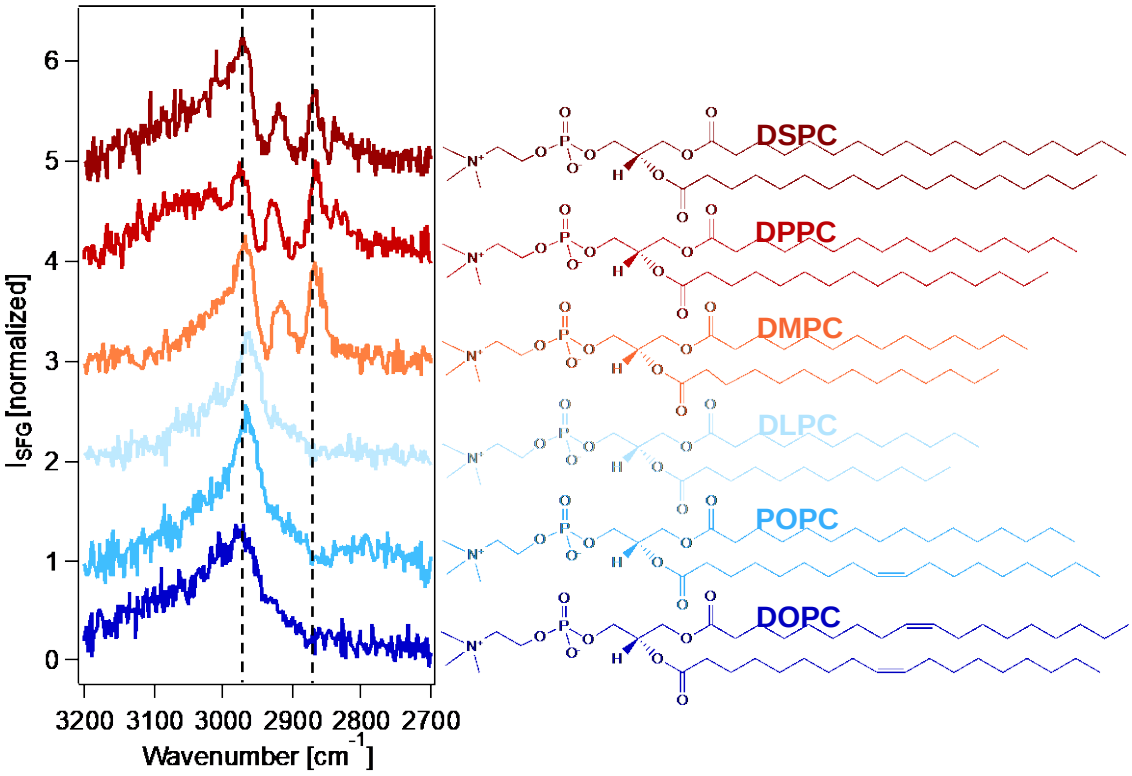

Figure 3.2. (Left) Comparison of *ssp*-polarized SFG spectra of supported lipid bilayers on fused silica windows at 100 mM NaCl, 10 mM Tris, pH 7.4. Top to bottom: DSPC, DPPC, DMPC, DLPC, POPC, DOPC. Spectra are offset for clarity. (Right) Chemical structure of phospholipids used in this study.

Fig. 3.2 shows the ssp-polarized SFG spectra observed for supported lipid bilayers formed from DOPC, POPC, DLPC, DMPC, DPPC and DSPC. The signal-to-noise ratio is sufficiently good, even at the relatively short spectral acquisition times, to discern important differences in the

spectra, even though they are produced without using deuterated lipids in one leaflet of the bilayer. This result is attributed to the asymmetry induced by the presence of the solid substrate (fused silica) on one side of the membrane and aqueous solution on the other.

In general, this chapter finds that the SFG spectra obtained from the supported lipid bilayers differ from one another depending on the T_m's of the lipids in the bilayer relative to the laboratory temperature: The T_m's of DOPC, POPC, DLPC, DMPC, DPPC and DSPC, the lipids used for these studies, are -18°C, -2°C, -2°C, 24°C, 41°C, and 55°C, respectively, while the laboratory is maintained at 21°C ± 1°C. Yet, common to all spectra is a peak at ~2980 cm^{-1}, which is subject to interference between the C-H and the O-H stretches from the aqueous phase.[9] Indeed, Fig. 3.3 shows that switching between H_2O and D_2O in the same flow cell coincides with the presence of three vs. two discernable peaks in the SFG spectra.

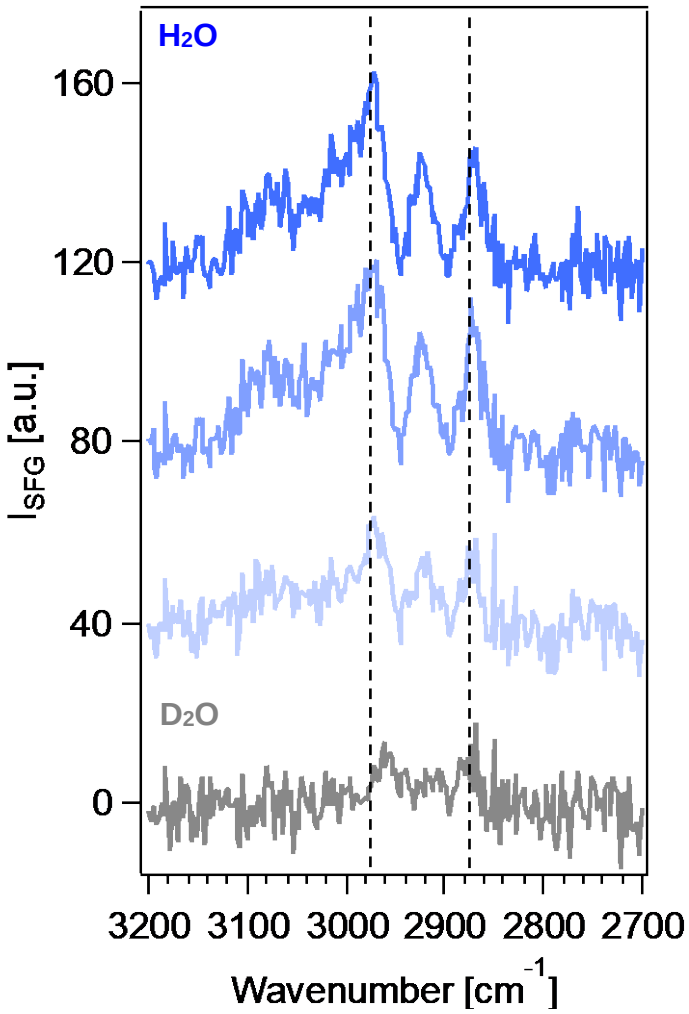

Figure 3.3. Evolution of *ssp*-polarized SFG spectra of 9:1 DMPC/DMPG bilayer during solvent exchange from 10 mM Tris, 100 mM NaCl in D_2O (gray) to 10 mM Tris, 100 mM NaCl in H_2O (blue). Spectra are offset for clarity. Each spectrum was acquired over 4 minutes and at one IR-center frequency as explained in the Experimental section of Chapter 2.

The SFG spectra of bilayers formed from DMPC collected in D_2O show spectral signatures at 2950 cm^{-1} and 2880 cm^{-1} and a shoulder at 2900 cm^{-1}. These features are in reasonable agreement with those recorded in D_2O for asymmetric bilayers containing deuterated lipids having T_m's above room temperature, be they, for instance, DMPC[10] or DSPC.[11-12] Yet, the small peak at

2850 cm^{-1} from the symmetric methylene stretches that is typically observed from asymmetric, deuterium-containing bilayers[10-12] is not observed in the symmetric bilayers studied here.

Returning to Fig. 3.2, the membranes having T_m's above the laboratory temperature exhibit SFG spectra with at least two additional peaks, one at ~2920 cm^{-1} and another at ~2880 cm^{-1}. The similarity of the SFG spectra obtained from the DMPC, DPPC, and DSPC is in good agreement with prior work on asymmetric bilayers formed from these lipids.[11] The intensity of the peak at 2880 cm^{-1} seems to be largest for DMPC, whose T_m is close to the laboratory temperature. This result also seems to be consistent with literature data: Using DSPC and DSPC-d_{83} lipid films, Liu and Conboy reported that the SFG signal intensity due to the methyl symmetric stretch at 2875 cm^{-1} undergoes a maximum intensity near the transition temperature of the lipid bilayer.[11] Comparison of bilayer formation below (21°C) and above (35 °C) the T_m (24°C) for DMPC shows qualitatively similar spectra (Fig. 3.4), at least in terms of peak positions. Yet, the overall SFG signal intensity is low, particularly with respect to the peak near 2880 cm^{-1}, when the bilayer is formed at 35 °C, or formed at room temperature and then heated to 35 °C. These findings are in good agreement with the results presented in this chapter for the series of symmetric (non-deuterated) lipid bilayers, at least within the limited number of PC lipids surveyed.

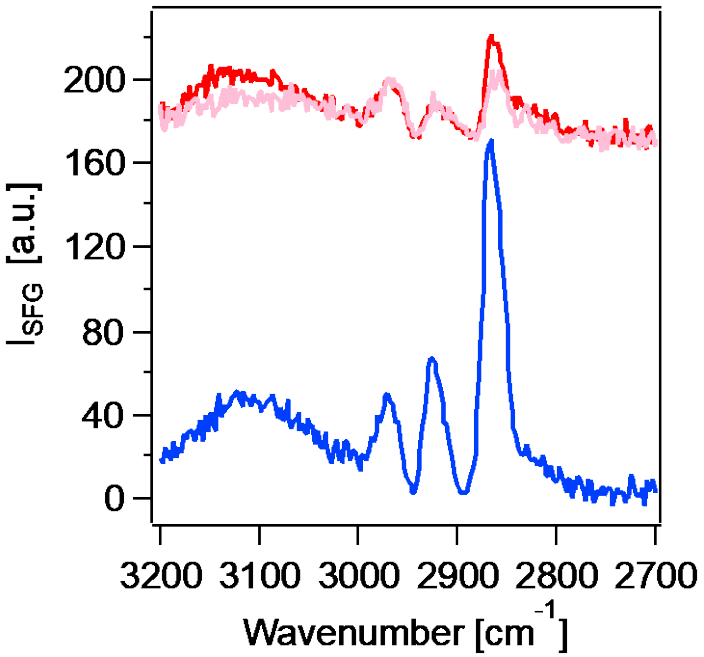

Figure 3.4. *ssp*-Polarized SFG spectra of a supported lipid bilayer formed from a 9:1 mixture of DMPC/DMPG phospholipids in 100 mM NaCl, 10 mM Tris, pH 7.4 on a fused silica window at 35°C (red) cooled to 22°C (blue) and heated again to 35°C (pink). Spectra are offset for clarity. Each spectrum was acquired at two IR-center frequencies as explained in the Experimental section of Chapter 2.

Further supporting the notion that results obtained with symmetric (non-deuterated) vs. asymmetric membranes (containing deuterated lipids) are generally in good agreement is the result of an orientation analysis carried out using the intensity ratio method.[13-17] Fig. 3.5A shows the *ssp*- and *ppp*-polarized SFG spectra recorded from supported lipid bilayers formed from a 9:1 mix of DMPC/DMPG in D_2O buffer solution. The *ssp*-polarized spectrum shows again the two peaks described earlier (Fig. 3.3). The *ppp*-polarized spectrum shows a significantly smaller SFG signal intensity from the alkyl tail terminal methyl group symmetric stretch at 2875 cm^{-1}, which, as shown from spectral fitting described in the Supporting Information of Olenick et al., yields a point estimate of approximately 0.44 ± 0.01 for the *ppp*/*ssp* amplitude ratio.[18] From this analysis, the terminal methyl groups within the lipids were determined to be tilted at an angle of 15° to 35° from

the surface normal, depending on the width of the monomodal orientation distribution used in the analysis (see Supporting Information of Olenick et al.).[18] Orientation analyses such as the one presented here should be viewed with caution if molecular orientation distributions are broad, as those will often predict a tilt angle of approximately 39° (±2), as presented by Simpson and Rowlen.[19] These results are within the standard deviation, albeit possibly somewhat larger, of the point estimate provided by Liu and Conboy,[20] who used a delta distribution function in their analysis of SFG spectra obtained from lipid bilayers made asymmetric by use of deuterated and hydrogenated lipids.

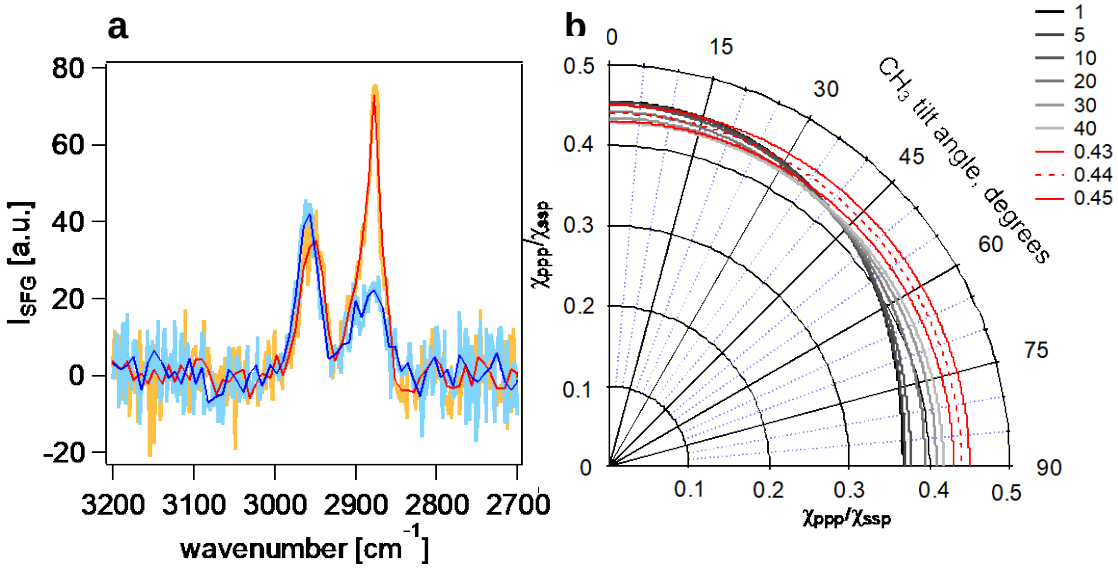

Figure 3.5. (A) *ssp* (red) and *ppp* (blue) polarized SFG spectra of a supported lipid bilayer formed from a 9:1 mixture of DMPC/DMPG phospholipids in a D_2O buffer solution used in this orientation analysis of the alkyl CH_3 group. A total of four fits were averaged to obtain a point estimate and standard error for the amplitude ratio for the 2875 cm^{-1} peak assigned as the CH_3 symmetric stretch (dashed line). (B) Ratio of χ_{ppp}/χ_{ssp} computed as a function of CH_3 tilt angle. The dashed red line indicates the point estimate amplitude ratio based on multiple fits, and the thin red lines indicate the standard error associated with this ratio. The red cone is the range of tilt angles assuming a 1° monomodal Gaussian distribution width, and the purple cone indicates the range of tilt angles when accounting for standard error through multiple peak fittings. The varying grey shade curves are theoretical monomodal Gaussian orientation distribution widths ranging from 1 to 40, which result in a range of tilt angles from 0 - 37° from the surface normal.

Given that the SFG signal intensity depends quadratically on the number of oscillators at the interface, this chapter analyzed the quality of these supported lipid bilayers using fluorescence microscopy. The images show bright spots (Fig. 3.6), which are often seen in the fluorescence images of supported lipid bilayers and are attributed either to excess vesicles[21] or to contaminants.[22] Image analysis using the ImageJ software package indicates that these regions compromise just 0.3±0.3% of the total image area for DLPC, 1.1±0.7% for DMPC, and 3.9±2.2% for DSPC. Given that the more than 97% of the remaining supported lipid bilayer shows no such features, the SFG spectra reported in this chapter are due to the supported lipid bilayer, and not the bright features seen in the fluorescence images.

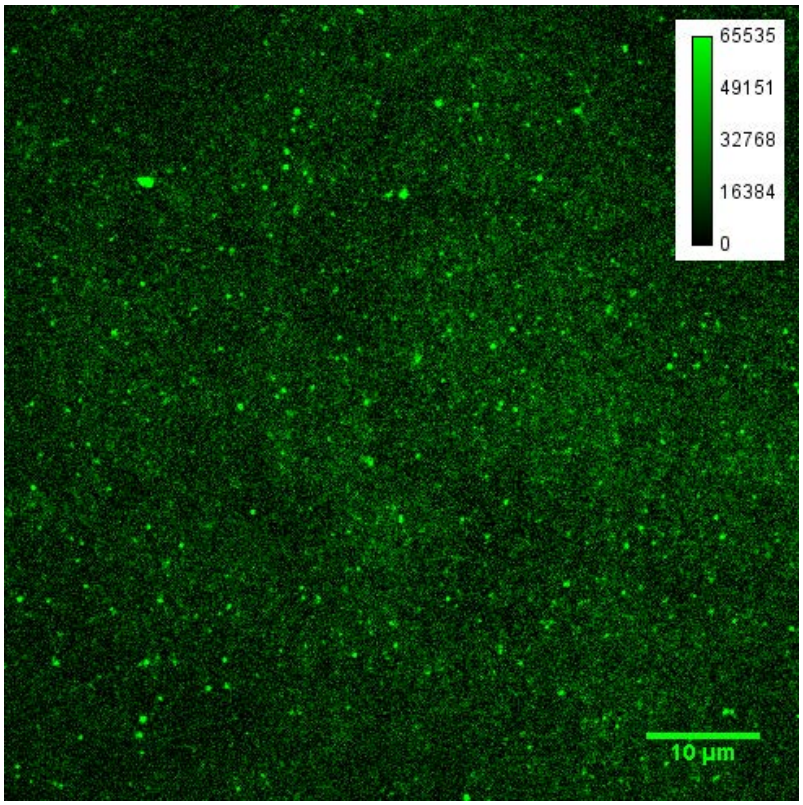

Figure 3.6. Fluorescence microscopy image of a supported lipid bilayer formed from DMPC doped with 0.01% TopFluor PC phospholipids on a fused silica window at pH 7.4, room temperature, and in 10 mM Tris buffer and 100 mM salt.

Moreover, vesicles left over after bilayer formation and rinsing are unlikely to produce the SFG signals reported here, as the SFG signals grow in slowly with time, comparable to the time it takes for the fluorescence signal to evenly cover the surface, as opposed to immediately upon vesicle addition. Further assurance for the notion that the SFG spectra reported here are from well-formed bilayers is provided by the results from room temperature (~21°C) FRAP measurements, which are in good agreement with reported literature data for DMPC,[23] DPPC,[23-24] and DSPC[25] bilayers, namely 0.82 ± 0.35 $\mu m^2/s$ for DMPC, 0.10 ± 0.06 $\mu m^2/s$ for DPPC, and 0.062 ± 0.06 $\mu m^2/s$ for DSPC. These results are consistent with bilayers either transitioning between the gel and fluid phases as in the case of DMPC or in the gel phase as in the case of DPPC and DSPC.[26-31]

3.3 Conclusion

In conclusion, the research presented here has shown that even though broadband SFG spectroscopy offers advantages over scanning systems in terms of signal-to-noise ratios when probing symmetric supported lipid bilayers formed specifically from zwitterionic lipids having PC headgroups, special care needs to be taken when spectral sampling ranges are limited when using the broadband SFG system, as the spectral features near the edge of the range of the spectral profile of the IR pulse used in the experiment may be overlooked. The results presented here validate spectroscopic and structural data from SFG experiments reported by others utilizing asymmetric bilayers in which one leaflet differs from the other in the extent of deuteration. These findings also support recently published phase modulation infrared absorption spectra of asymmetric bilayers supported on gold whose electrochemical phase behavior was only marginally influenced by the use of deuterated vs hydrogenous lipids.[32]

Differences in H_2O-D_2O exchange experiments reveal that the lineshapes of the broadband SFG spectra are significantly influenced by interference from OH oscillators in the aqueous phase, even when those oscillators are not probed by the incident infrared light in the broadband setup used in these experiments. In D_2O, i.e. in the absence of spectral interference from the OH stretches of the solvent, the alkyl chain terminal methyl group of the bilayer is found to be tilted at an angle of 15° to 35° from the surface normal, in good agreement with earlier studies, emphasizing that the impact of using deuterated or hydrogenated lipids on bilayer structure is probably small.

The approach presented here is in principle applicable to membranes formed from lipids having headgroups other than zwitterionic PC such as phosphatidylserine (PS) and phosphatidylethanolamine (PE) which play important roles in apoptosis[33-34] and protein assembly[35] respectively. Moreover, the approach allows for the facile investigation of bilayers modified with biological membrane components like cholesterol, which has been shown to affect the packing density of the surrounding SLB,[36] as well as peripheral membrane proteins like cytochrome c[37-38] or membrane channels like those formed by gramicidin.[39-41]

Chapter 4

Lipid Corona Formation from Nanoparticle Interactions with Bilayers and Membrane-Specific Biological Outcomes

Portions of this chapter are part of the following pending manuscript:

Olenick, L.L.; Troiano, J. M.; Vartanian, A.; Melby, E. S.; Mensch, A. C.; Zhang, L.; Qui, T.; Bozich, J.; Lohse, S.; Zhang, X.; Kuech, T. R.; Millevolte, A.; Gunsolus, I.; McGeachy, A. C.; Dogangun, M.; Hu, D.; Walter, S. R.; Mohaimani, A.; Schmoldt, A.; Torelli, M. D.; Hurley, K. R.; Dalluge, J.; Chong, G.; Feng, Z. V.; Haynes, C. L.; Hamers, R. J.; Pedersen, J. A.; Cui, Q.; Hernandez, R.; Klaper, R.; Orr, G.; Murphy, C. J.; Geiger, F. M., Lipid Corona Formation from Nanoparticle Interactions with Bilayers and Membrane-Specific Biological Outcomes. **2017.** *In Revision.*

4.1 Introduction

As discussed in Chapter 1 of this thesis, understanding interactions at biointerfaces using a variety of techniques is important to predict and control the fundamental interactions occurring at these surfaces in response to novel materials. Utilizing the knowledge developed in Chapter 3 with respect to sum frequency generation (SFG) spectroscopy of SLBs, this chapter takes a focused look at the mechanism of lipid corona formation using SFG spectroscopy along with many other complementary techniques. This chapter explores the evidence of the formation of a lipid corona around various nanomaterials in contact with certain lipids at the nano-biointerface. In a highly collaborative research effort within the Center for Sustainable Nanotechnology (CSN), the research presented here probes lipid corona formation using model systems which range from supported lipid bilayers (SLBs) to whole organisms, and techniques which range from nonlinear optical spectroscopy to biological toxicity assays.

The propensity of biological species to form coronas around nanoparticles[1-4] has been used for preparing engineered nanomaterials that can be distributed in biological systems with some control.[5-9] While protein coronas in particular have been studied extensively,[1-3, 5-6] our understanding of lipid coronas is just now beginning to emerge,[10-11] especially our understanding of those formed upon unintended nanoparticle contact with living cells. The protein and lipid corona formation mechanisms appear to differ substantially, as "hard" and "soft" coronas,[12] typical for the former, have not been described for the latter.[3] While pulmonary surfactants can lead to lipid corona formation,[3, 13-15] it is unclear whether the process can also occur in the more general case of lipid bilayers, which lack the considerable dipole potential carried by their monolayers counterparts.[16] For lipid corona formation from cellular bilayer membranes, some precedent exists in the budding of viruses, which do not contain the machinery to produce their own lipids, but

instead use charged patches on proteins for sheathing their RNA with a membrane scavenged from the host cell membranes.[17-18] Likewise, computer simulations indicate that coronas of certain lipids may be stable on certain particles,[19-20] but the roles of specific functionalization patterns or charge remain poorly understood.[21]

Due to the complexity of this research, exploration of the lipid corona formation requires the expertise of a variety of scientists in many laboratories around the United States. As described in the Introduction to this thesis, this complex research is ideal for the CSN. The researchers involved are from the following institutions: Northwestern University, University of Illinois Urbana-Champaign, Pacific Northwest National Laboratory, University of Wisconsin-Madison, University of Minnesota, University of Wisconsin-Milwaukee, Johns Hopkins University, and Augsburg College. Though the focus of the work presented in this thesis is the SFG studies, many of the methods used in this chapter are critically important in understanding the lipid corona. Since no one technique has been proven to reveal all of the nuances of the lipid corona formation, each of these techniques is integral to understanding these interactions at the nano-biointerface and will be discussed in this chapter.

This chapter explores whether lipid coronas can form spontaneously around negatively and positively charged nanoparticles when they interact with immobilized lipid bilayer membranes, such as those surrounding cells fixed within the extracellular matrix of a living organism. This research coordinates advanced imaging and spectroscopy with molecular dynamics simulations[22] to probe the lipid corona at an unprecedented level of detail. A wide spectrum of model systems was used ranging from supported and suspended lipid bilayers to *Shewanella oneidensis*, an important earth dwelling bacterium, and the water flea *Daphnia magna*, chosen as a well-characterized eukaryote. To test whether corona formation differs for particles having diameters

close to or larger than the bilayer thickness, spherical gold metal nanoparticles (AuNPs) with core diameters of 4 and 15 nm were examined. This type of nanomaterial was chosen because the methods to synthesize, functionalize, and characterize them are well established.[23] Complementary experiments using 15 nm-diameter nanodiamond particles reveal the generality of the interactions across some varied range of core compositions.

This study focuses largely on particles wrapped in the cationic encapsulation polyelectrolyte poly(allylamine hydrochloride) (PAH), while particles functionalized with the negatively charged molecular ligand mercaptopropionic acid (MPA) show no lipid corona formation. Some batches of PAH-AuNPs that were purified using diafiltration, were found to contain high amounts of residual free PAH polymer in the nanoparticle solution, as assessed by fluorescence.[24] This assay also showed that double centrifugation, the method used to prepare the particles used in vibrational sum frequency generation (SFG) studies, resulted in a fraction of 0.27 ± 0.04 for the free PAH mass concentration when compared to the mass concentration of AuNPs. Special attention was therefore given to the role of unbound ligands on the systems surveyed. These idealized model systems focus on particle interactions with supported and suspended lipid bilayers composed of the lipid 1,2-dimyristoyl-*sn*-glycero-3-phosphocholine (DMPC), given the direct relevance of the zwitterionic PC headgroup to biological membranes.[25-26] Additional work probed bilayers formed from DMPC mixed with 10% lipids containing negatively charged headgroups in the form of 1,2-dimyristoyl-*sn*-glycero-3-phospho-1'-rac-glycerol (DMPG). Lipids containing headgroups composed of PC and PG moieties from pulmonary surfactant monolayers have also been reported to be preferentially taken up by carboxylated carbon nanotubes in pulmonary exposure routes.[15] Other lipid combinations surveyed[27] did not show the effects discussed below.

4.2 Results and Discussion

4.2.1 Lipid tail disruption in zwitterionic lipid bilayers

Vibrational SFG spectroscopy is interface selective and provides information on the number of CH oscillators at the interface and their hyperpolarizabilities, averaged over all their molecular orientations.[41] The ligands on the AuNPs used in this study do not produce measurable SFG signals at experimentally relevant concentrations indicating they are likely to be highly disordered under the aqueous solution conditions employed in these experiments. The concentration of PAH relevant to the PAH-AuNP experiments (i.e. approximately 10 nM) does not cause a loss of the characteristic peaks of the bilayer formed from a mixture of 9:1 DMPC/DMPG lipids. This result of no observable change in the SFG signal of the bilayer after interaction with an experimentally-relevant concentration of free PAH is also true for the MPA ligand and is shown in the Supporting Information of Troiano et al.[29]

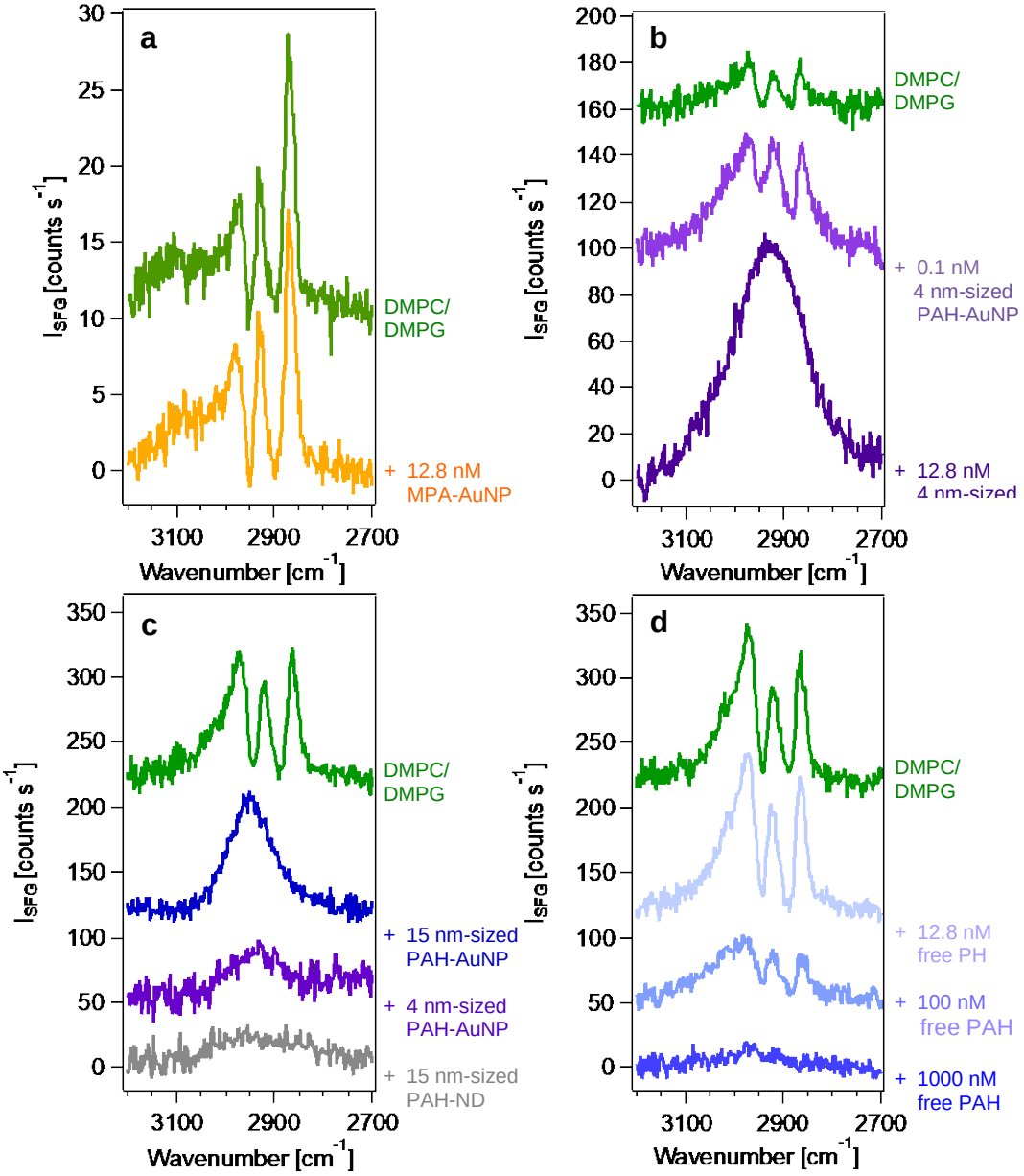

Figure 4.1. (**a**) *ssp*-Polarized SFG spectra obtained from supported lipid bilayers prepared from a 9:1 mixture of DMPC/DMPG held at 100 mM NaCl and pH 7.4 (10 mM Tris buffer) before (top) and after (bottom) introduction of MPA-coated 4 nm-sized gold metal nanoparticles. (**b**) SFG responses obtained from supported lipid bilayers prepared from a 9:1 mixture of DMPC/DMPG at 100 mM NaCl and pH 7.4 (10 mM Tris buffer) following exposure to 4 nm-sized PAH-wrapped particles at concentrations indicated. (**c**) SFG responses obtained from supported lipid bilayers prepared from a 9:1 mixture of DMPC/DMPG at 100 mM NaCl and pH 7.4 (10 mM Tris buffer) following exposure to PAH-wrapped gold and nanodiamond particles having the indicated core diameters. (**d**) SFG responses obtained from supported lipid bilayers prepared from a 9:1 mixture of DMPC/DMPG at 100 mM NaCl and pH 7.4 (10 mM Tris buffer) following exposure to free ligand at concentrations indicated.

In contrast, the SFG spectra of the supported lipid bilayers used in this chapter show strong signals from the lipid alkyl tails[42-43] (Fig. 4.1a) near 2870, 2920, and 2970 cm^{-1}, which are reliable reporters of structure and order within the bilayer itself. Following exposure of the bilayer to 10 nM solutions of 4 nm-sized spherical gold metal nanoparticles functionalized with the anionic MPA ligand, this research finds only negligible changes in the lineshapes and intensities of the SFG response at 100 mM added NaCl. Given that the QCM-D experiments completed in collaboration with the Pedersen group and SHG experiments carried out by fellow graduate student Dr. Julianne Troiano, indicate the particles are indeed present (*vide infra*) under these experimental conditions, this study concludes that the negatively charged AuNPs are interacting with the supported lipid bilayer without causing structural changes to its alkyl tails, at least as probed by SFG spectroscopy.

Exposure of the supported lipid bilayers to the positively charged 4 nm-sized PAH-AuNPs leads to a different result: the sharp molecular vibrational SFG features of the lipid tails vanish (Fig. 3.1b) and are replaced by a broad signal similar to the non-resonant SFG response of thin gold films,[44] albeit with much smaller intensities. Indeed, this chapter finds that particle concentrations as low as 1 nM PAH-AuNPs coincide with decreased SFG signal intensities. PAH-wrapped 15 nm-sized gold and nanodiamond particles show the same effect (Fig. 4.1c), even though the nonresonant SFG signal intensity following particle addition is smaller than for the 4 nm-sized AuNPs. Unlike the DMPC-based bilayer studied here, bilayers rich in DOPC do not show disruptions of the SFG signals when they are exposed to either MPA- or PAH-coated particles under otherwise identical experimental conditions.[27] Likewise, the free ligands do not alter the SFG response from the bilayer unless they are present in a 100-fold excess over the nanoparticle concentrations surveyed here (Fig. 4.1d). The interaction of a supported lipid bilayer

formed from a 9:1 mixture of DMPC/DMPG with 4 nm PAH-AuNPs in a 10 mM Tris, 100 mM NaCl, pH 7.4 buffer solution cause a loss of the characteristic 3-peaks in the SFG signal of the bilayer. Figure 4.2 shows that this loss also occurs after interaction of these materials in 1 mM NaCl buffer solution.

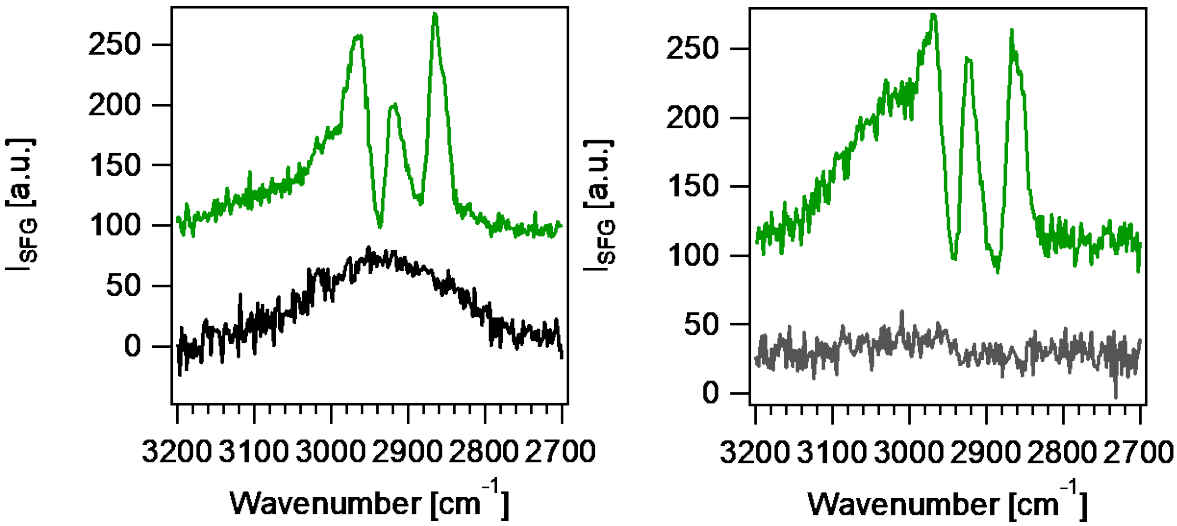

Figure 4.2. *ssp*-Polarized SFG spectra of a supported lipid bilayer formed from a 9:1 mixture of DMPC/DMPG in 1 mM NaCl and 10 mM Tris buffer before (top) and after (bottom) introduction of a 12.8 nM solution of PAH-AuNP with core diameter of 4 nm (left) and 15 nm (right).

Control experiments shown in the Supplementary Information of Olenick et al.[38] indicate that neither the positively charged particles, nor the free PAH polyelectrolyte, attach to the bare supporting substrate in our SHG and SFG flow cells (no bilayer present). Earlier collaborative work within the CSN shows that the MPA-AuNPs and PAH-AuNPs are not surface active at the silica/buffer interface in the absence of a bilayer.[29] In addition, control experiments explored the silica/buffer solution interface after addition of PAH-ND at varying concentrations. Figure 4.3 shows minimal adsorption of PAH-ND to bare fused silica in SHG experiments conducted at 300 +/- 3 nm.

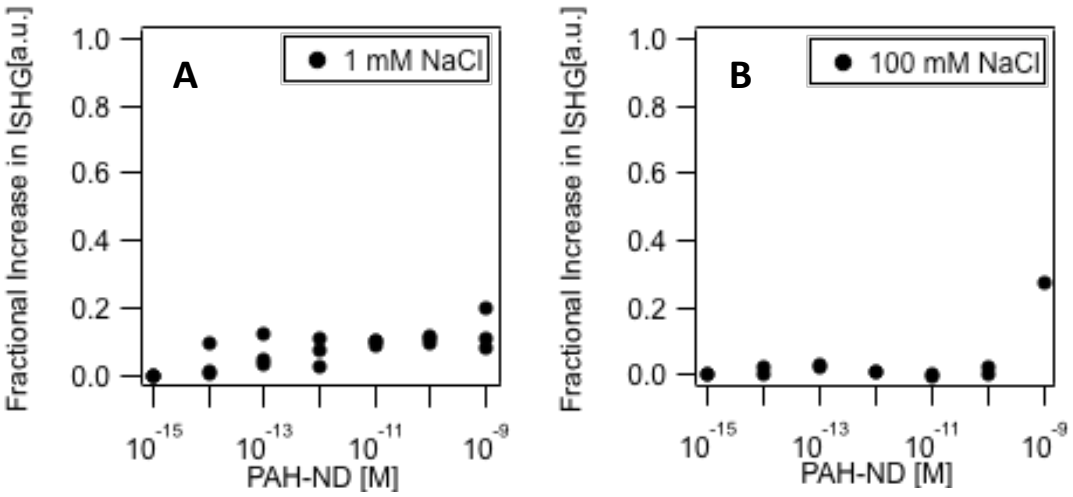

Figure 4.3. SHG adsorption isotherms indicate that PAH-ND with core diameter of 15 nm does not adsorb to bare fused silica (no bilayer present) at either 1 mM (**A**) or 100 mM NaCl (**B**).

4.2.2 High coverage of nanoparticles wrapped in cationic polyelectrolyte (in collaboration with the Pedersen group)

To quantify the amount of AuNPs on the membranes, this research applied QCM-D and SHG measurements (Fig. 4.4a and 4.4b).

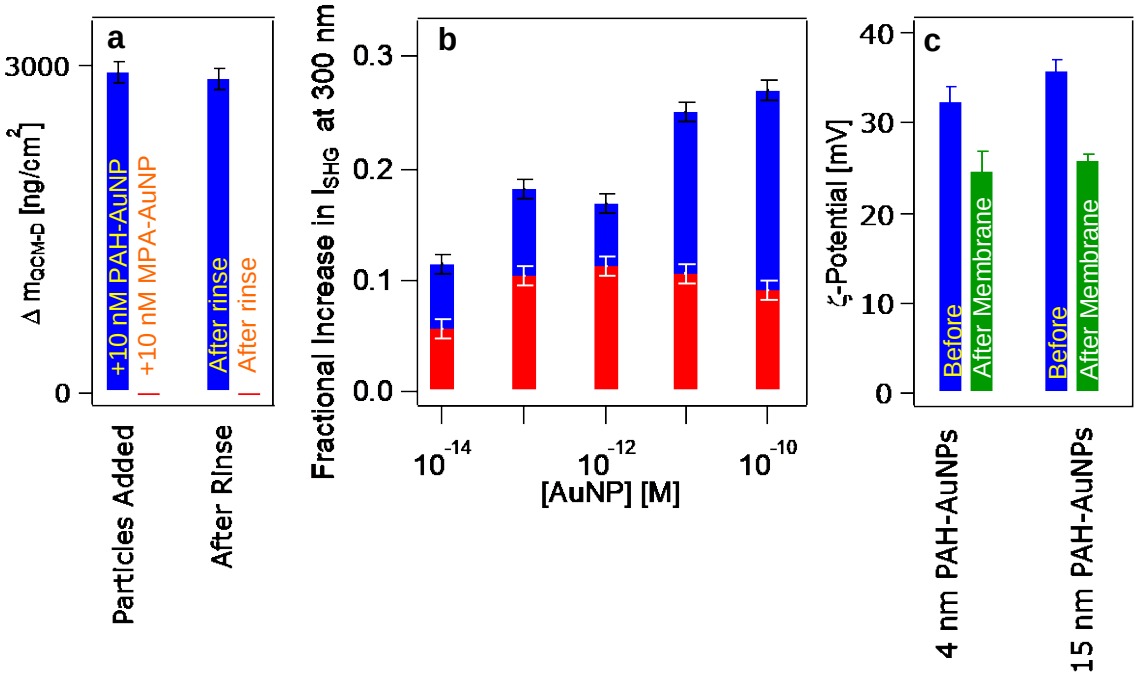

Figure 4.4. **(a)** Acoustic mass gains, determined from QCM-D measurements, of 10 nM solutions of PAH-(blue) and MPA-(red) coated 4-nm AuNPs before, during (20 min), and after contact with supported lipid bilayers composed of 9:1 DMPC/DMPG maintained at pH 7.4, 10 mM Tris buffer, and 100 mM salt. **(b**) Fractional SHG signal gain as a function of concentration of PAH-(blue) and MPA-(red) coated 4-nm AuNPs referenced to the SHG signal intensity obtained from supported lipid bilayer composed of 9:1 DMPC/DMPG maintained at pH 7.4, 10 mM Tris buffer, and 100 mM salt**.** (**c**) ζ Potentials of PAH-AuNPs prior to contact with and after rinsing from 9:1 DMPC/DMPG bilayers. Solutions were pH 7.4 (10 mM Tris) and contained 100 mM NaCl.

In collaboration with Dr. Thomas Kuech and Dr. Eric Melby in the Pedersen laboratory, QCM-D experiments revealed considerable acoustic mass gains of 920 ± 90 ng·cm^{-2} when the bilayers were exposed to 10 nM number concentrations of 4 nm-diameter PAH-AuNPs for 20 minutes at 0.1 M NaCl buffered to pH 7.4 with 0.01 M Tris. Attributing the surface mass gain solely to the AuNPs, this roughly corresponds to 1.9 (± 0.2) × 10^{12} particles·cm^{-2}. Because the acoustic mass includes hydrodynamically coupled solvent, the number of particles per cm^2 may be less. As shown in the Supplementary Information of Olenick et al.,[38] the 15 nm-diameter particles led to mass gains

corresponding to 5.0 (± 0.4) × 10^{11} particles·cm^{-2}, if the acoustic mass were attributed solely to the nanoparticles. Rinsing the supported lipid bilayers with nanoparticle-free solution after attachment of PAH-AuNPs resulted in decreases in energy dissipation and small increases in frequency, corresponding to decreases in mass, which may indicate the release of PAH-AuNPs, a small fraction of the bilayer, or some combination of the two, from the surface.

While mass gains were not detectable above the ~3 ng·cm^{-2} limit of detection of the QCM-D instrument for the negatively charged MPA-coated particles, SHG measurements recorded by fellow graduate student Dr. Julianne Troiano, provided evidence for the presence of MPA-AuNPs through SHG resonance enhancement,[45] albeit presumably at much smaller surface coverages than what is observed for the cationic PAH-wrapped particles (Fig. 4.4b). These results, together with the SFG results presented earlier in this chapter, point towards an interaction mechanism that is specific to the combination of bilayer membranes containing lipids having transition temperatures close to room temperature with nm-sized nanoparticles wrapped with polycations, as opposed to the free polymer wrapping without the nanoparticle. As illustrated in chapter 3, the transition temperature of the lipid components of an SLB in relation to the experimental temperature greatly affects the SFG spectrum of the SLB.

4.2.3 Nanoparticles leaving membrane carry lower ζ-potential (in collaboration with the Pedersen group)

Motivated by the evidence pointing to the association of membrane lipids with the PAH-coated nanoparticles, the Pedersen laboratory proceeded to collect 4 and 15 nm core PAH-AuNPs. After exposure to the supported lipid bilayers prepared from a 9:1 mix of DMPC/DMPG, Dr. Thomas Kuech measured their electrophoretic mobilities, and calculated their apparent ζ-potentials using the Smoluchowski approximation. PAH-AuNPs that had passed over bare SiO_2-

coated sensors were used as controls. Fig. 3.4c shows that the ζ-potentials of the 4 and 15 nm PAH-AuNPs measured in the eluent of the QCM-D flow cell (100 mM salt, pH 7.4, 10 mM Tris buffer) decreased from +32 ± 2 mV and +36 ± 1 mV, respectively, in the absence of lipids, to +24 ± 2 mV and +26 ± 1 mV, respectively, upon rinsing from the supported lipid bilayers. These results are consistent with the hypothesis that the nanoparticles collected following interaction with the supported lipid bilayer acquired negatively charged species, likely DMPG phospholipids, as further supported by calculations (*vide infra*).

4.2.4 Nanoparticles increase bilayer fluidity 3-4 fold (in collaboration with the Orr and Pedersen groups)

Single molecule fluorescence microscopy, which Dr. Eric Melby, Dehong Hu, and fellow graduate student Dr. Julianne Troiano used to track the trajectories of individual phospholipid molecules (Fig. 3.5a-b), showed a significant increase in the local diffusion coefficient of individual lipids, from an average of 0.0095 ± 0.0062 to 0.035 ± 0.011 $\mu m^2 s^{-1}$, after interaction with PAH-AuNPs.

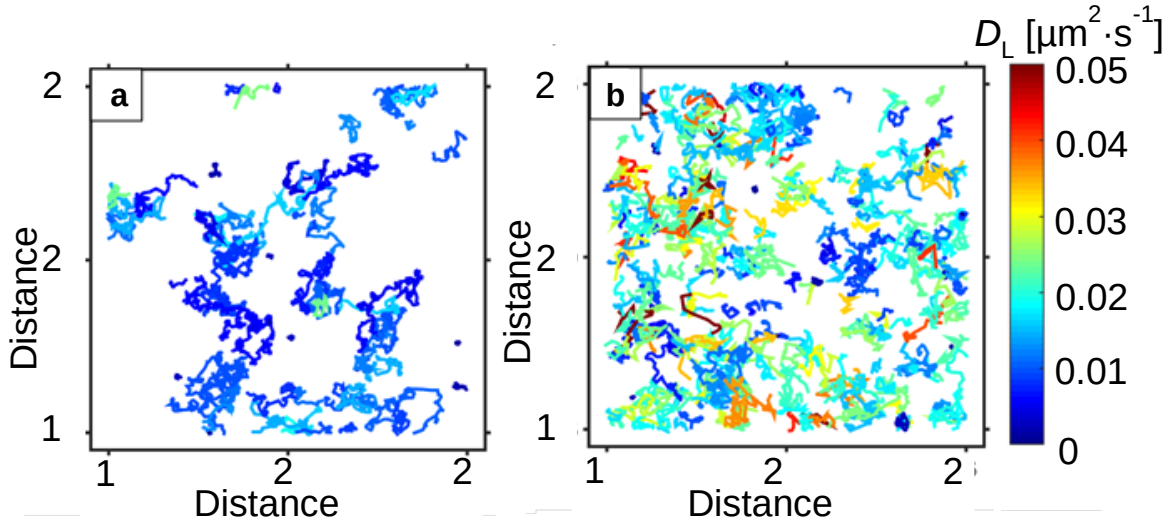

Figure 4.5. Trajectories of individual Atto 647N DOPE lipid molecules in a 9:1 DMPC/DMPG bilayer. Reconstructed lipid trajectories before (**a**) and after (**b**) the addition of 1 nM PAH-AuNPs. Colors indicate lateral diffusion coefficients [D_L, μm^{2}s^{-1}] for individual lipid molecules. Lateral diffusion coefficients of all labeled lipid molecules (three spots on each bilayer and three bilayer replicates) were averaged to determine the mean lateral diffusion coefficients presented in the main text.

Measurements by the Orr and Pedersen groups show that the average diffusion coefficients increase substantially because the distribution becomes appreciably more bimodal. The observed increase in the molecular diffusion coefficients indicates an increase in the fluidity of the gel-phase 9:1 DMPC/DMPG bilayer. This outcome is explained by the change in the tilt angle of the electric dipole of the choline headgroup induced by interaction with a cationic amine in the coating,[46] increasing the area per lipid head and thereby decreasing lipid packing density. This interaction represents an initial step in the process of lipid extraction. Removal of lipids from the bilayer would increase the free area per lipid in the remaining bilayer,[47] consistent with the observed increase in diffusivity.

4.2.5 Computer simulations show stable bilayers on nanoparticles wrapped in cationic polyelectrolytes (in collaboration with the Hernandez and Cui groups)

Molecular dynamics simulations using coarse-grained models resulted in the formation of a lipid corona (Fig. 4.6a) and provided molecular-level information regarding its formation (Fig. 4.6b). The structure of the coarse-grained PAH-AuNP was validated using atomistic simulations (Fig. 4.6c).

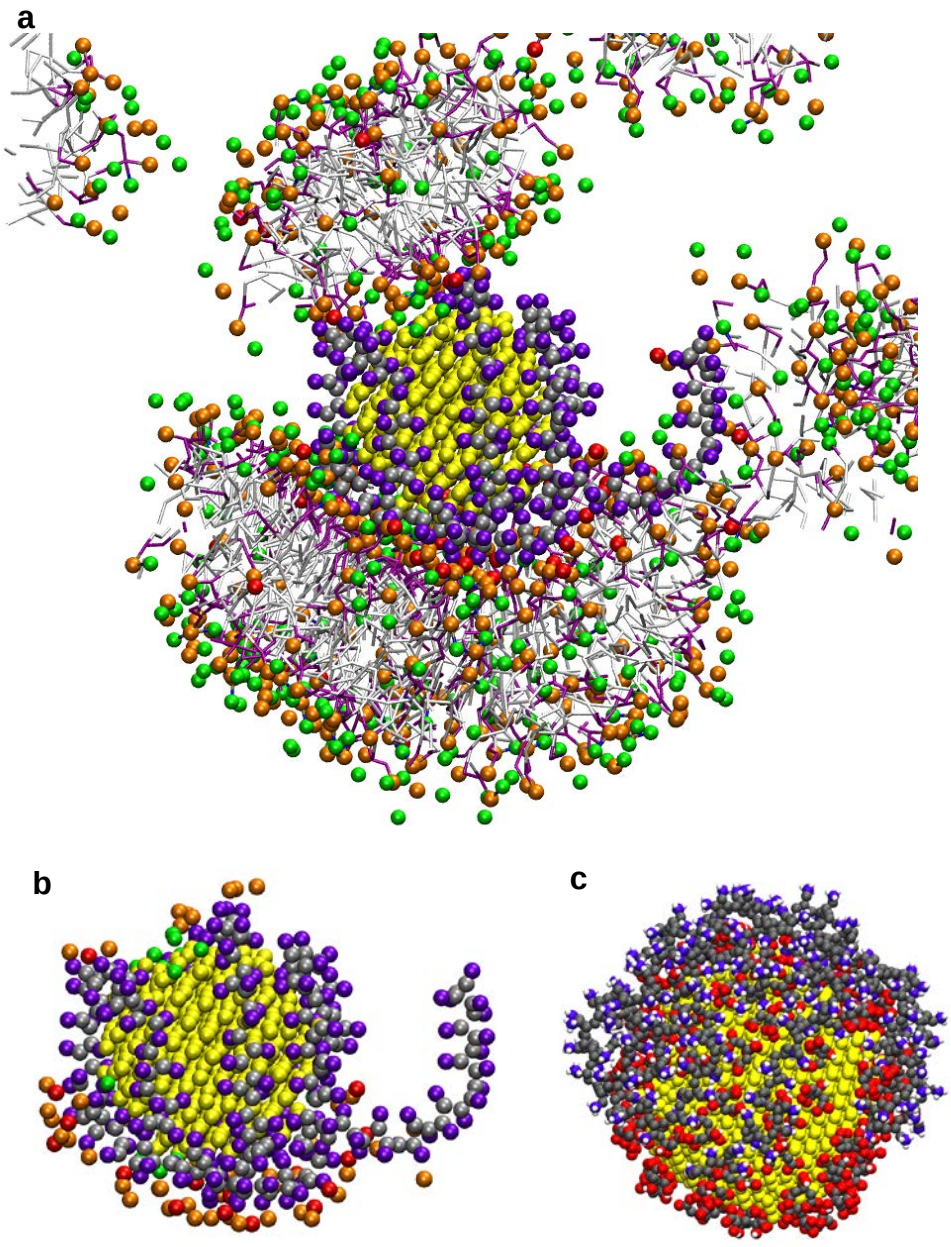

Figure 4.6. The final snapshot after 400 ns of simulations using the POL-MARTINI coarse-grained model from a self-assembly simulation of lipids corona formation around a gold metal nanoparticle wrapped in a single PAH polymer having 160 monomers (**a**) and zoomed in view of just the phosphate (orange), PG head group glycerol (red) and choline (green) groups within 6 Å of the cationic side chain of PAH (ice blue/gray) or Au (yellow) (**b**). Phosphates are colored in dark blue, lipid tails are shown as while/purple lines. Smaller yellow and light blue spheres indicate sodium and chloride ions (0.1 M). Coarse-grained water molecules omitted for clarity. (**c**) Final snapshot after 52.5 ns of an all-atom simulation of PAH deposition on a citrate-AuNP. Counterions are omitted for clarity.

Starting from a random distribution around the PAH wrapped gold nanoparticle, the lipid molecules quickly self-assemble into ribbons and micelles, which then attach to the nanoparticle during ~100 ns (see Supplementary Information in Olenick et al.[38]). An analysis of ion/lipid distributions around the nanoparticle indicates that the cationic PAH polymer plays the key role of attracting lipids by contact ion pairing between the ammonium groups with phosphate and glycerol groups (see Supplementary Information in Olenick et al.[38]). The positive charges also preferentially recruit anionic lipids (DMPG), leading to a higher fraction of DMPG (32% and 43% for the two simulated systems, respectively) in the lipid corona compared to the bulk concentration (10%). The dimensionality of the lipid corona model is consistent with observations from the electron microscopy analysis and the measured changes in the hydrodynamic radii of the PAH-wrapped nanoparticles following corona formation described below.

4.2.6 Nanoparticle-vesicle suspensions form aggregated superstructures featuring lipid headgroup association with particle wrapping moieties (in collaboration with the Murphy group and fellow graduate student Dr. Julianne Troiano)

To investigate whether the PAH-wrapped AuNPs also interact with suspended, as opposed to supported, lipid bilayers, Dr. Ariane Vartanian exposed suspended vesicles formed from a 9:1 mix of DMPC/DMPG lipids to PAH-AuNPs and the free PAH alone, followed by NMR measurements. ^{1}H spectra of vesicles formed from a 9:1 mixture of DMPC and DMPG show that the ammonium headgroup protons (−N−CH$_3$, 3.16 ppm) disappear upon addition of 4 nm PAH-AuNPs (Fig. 4.7a). Fellow graduate student, Dr. Julianne Troiano exposed suspended vesicles formed from a 9:1 mix of DMPC/DMPG lipids containing 0.1% TopFluor-labeled PC to PAH-AuNPs and recorded images using a confocal fluorescence microscope (Fig. 4.7b-c).

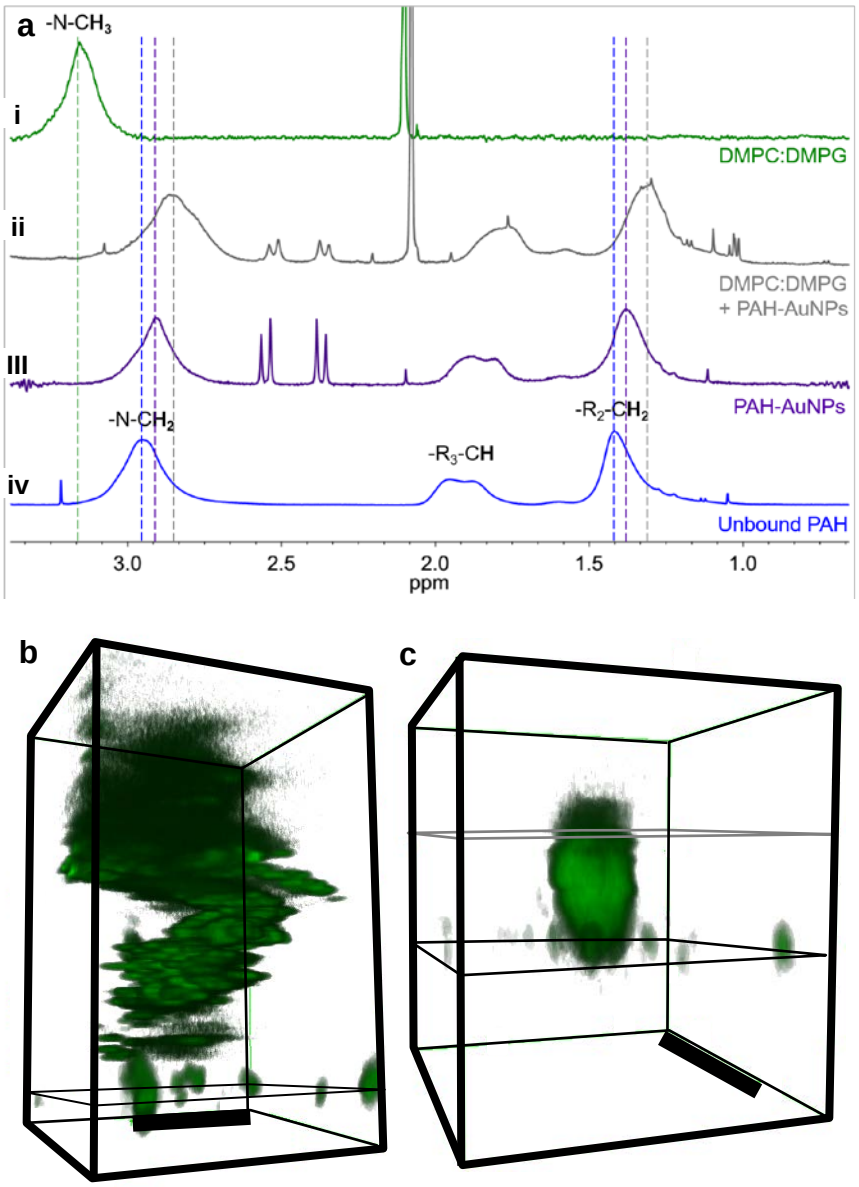

Figure 4.7. (**a**) Normalized proton NMR spectra of (**i**) vesicles formed from a 9:1 mixture of DMPC/DMPG, (**ii**) PAH-AuNPs interacting with 9:1 DMPC/DMPG vesicles, (**iii**) PAH-AuNPs alone, and (**iv**) unbound PAH. The green dotted line tracks the chemical shift of the lipid headgroup protons; the blue, purple, and grey dotted lines track the chemical shifts of the PAH protons. All measurements made at 20 °C and in 0.1 M NaCl and at pH 7.4 (0.01 M Tris) in D_2O, for 12 nM vesicles and 10 nM particles after 2 h of incubation. z-Stack fluorescence image obtained from a glass surface in contact with a solution formed from mixing a 5 nM solution of PAH-wrapped 15 nm-sized gold metal nanoparticles under conditions of 100 mM NaCl and 10 mM Tris buffer with a solution containing (**b**) 0.0625 mg/mL and (c) 0.00625 mg/mL vesicles (100 nm diameter) formed from a 9:1 mixture of DMPC/DMPG and 0.1% TopFluor-labeled PC. The liquid/solid boundary is visualized by the presence of micron-sized features and marked by the black rectangle in each image. Scale bars are 5 μm.

The hydrocarbon proton resonances broaden beyond detection because the lipids exist in the lipid ordered phase at the laboratory temperature at which the experiment was run (20 °C, below the transition temperatures of DMPC (24 °C) and DMPG (23 °C)). The disappearance of the headgroup proton resonance can best be explained by the attachment of the headgroup to another species, presumably PAH, which would immobilize the protons and broaden the resonance into the baseline. Indeed, the PAH-AuNP protons shift significantly upfield after interaction with the lipid vesicles, suggesting that the PAH layer is now sandwiched between the gold surface and an additional species. Taken together, the NMR spectra support the conclusions from the supported lipid bilayer studies that lipids strongly associate with the surface of the PAH-AuNPs.

The mixing experiments described here have two consequences: first, mixing of plain lipid vesicles with the PAH-wrapped nanoparticles at 100 mM salt, 10 mM Tris buffer, and pH 7.4 immediately doubles their hydrodynamic diameters (200 ± 10 nm), which further increase in the subsequent two hours to more than 1 μm. Second, spinning disk confocal fluorescence microscopy experiments carried out following the combination of vesicle suspensions with PAH-wrapped nanoparticles show the rapid build-up of sub- and super-μm-sized agglomerates at solution/glass interfaces, indicating that the newly formed structures are considerably stickier than the PAH-wrapped nanoparticles or the lipid vesicles themselves.

Indeed, Fig. 4.7b shows that the lipid bilayer-PAH-AuNP assemblies form sub- and supermicron-sized three-dimensional structures that can be immobilized on surfaces due to apparent strong interaction with microscope glass slides. These spinning microscopy images also show that the particles that produce fluorescence signals have the labels far enough from the gold core that the fluorescence is not quenched. Yet, many of the fluorescent features are seemingly co-localized with similarly sized features observed in the bright field (Figure 4.8), which visualizes

particles that are agglomerated to μm-sized structures.

This effect is seen for many of the sub-micron sized features. These features are not formed when PAH-wrapped nanoparticles are brought in contact with vesicles rich in DOPC (Fig. 3.8) or when 9:1 DMPC/DMPG vesicles are exposed to 10 nM free PAH.

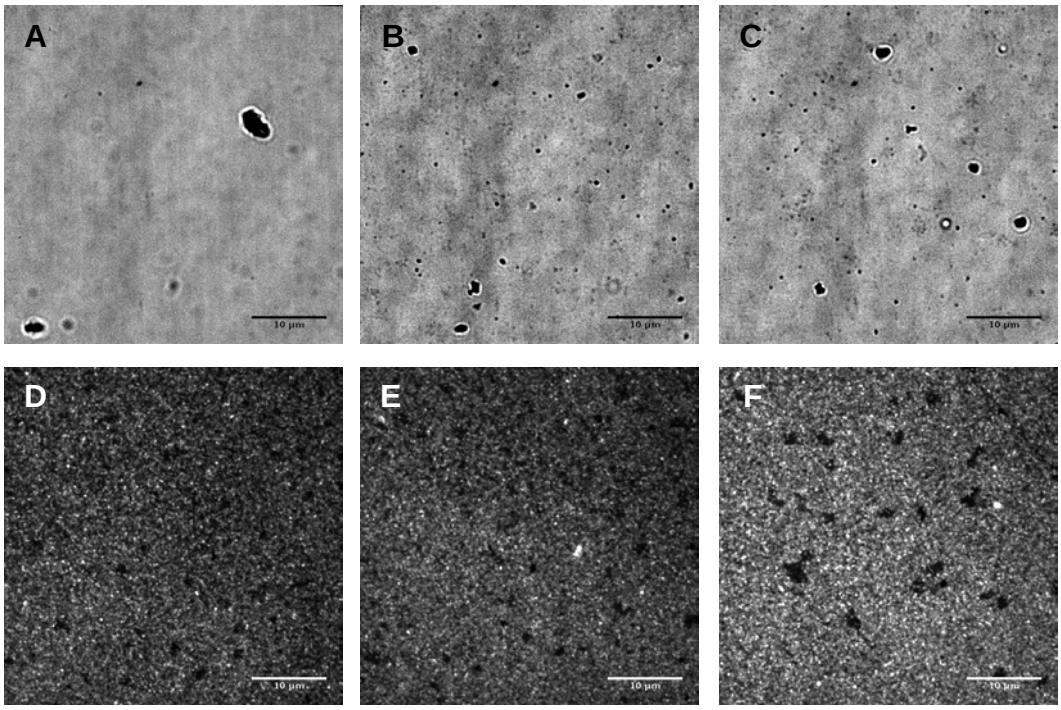

Figure 4.8. Bright field (A-C) and corresponding fluorescence (D-F) images of vesicles formed from a 9:1 mixture of DOPC and DOTAP with 0.1 mol% TopFluorPC and 5 nM 15 nm PAH-AuNPs after interaction for 2 hours.

4.2.7 Molecular connections to decreased bacterial survival and respiration rates and to changes in ribosomal gene expression in eukaryotes (in collaboration with the Haynes, Feng and Klaper groups)

To evaluate biological consequences of lipid corona formation, the Haynes, Feng, and Klaper groups considered the major motifs in cell surface chemistry presented by different types of organisms. Specifically, the Haynes and Feng groups exposed single cell organisms, namely

the gram-negative bacteria *Shewanella oneidensis* and the Klaper group exposed the aquatic multicellular organism *Daphnia magna*, to PAH-AuNPs. For the former, TEM micrographs show clear evidence of cell lysis (Fig. 4.9) and PAH-AuNPs clustering near spilled, membrane-free cytoplasmic content from cells with deformed cell walls. Closer inspection of these nanoparticle clusters at higher magnification reveals multiple segments of lipid bilayer-like structures (Fig 4.9b-c) that are 4~10 nm thick, consistent with the expected thickness of two pieces of lipid bilayer stuck back to back.

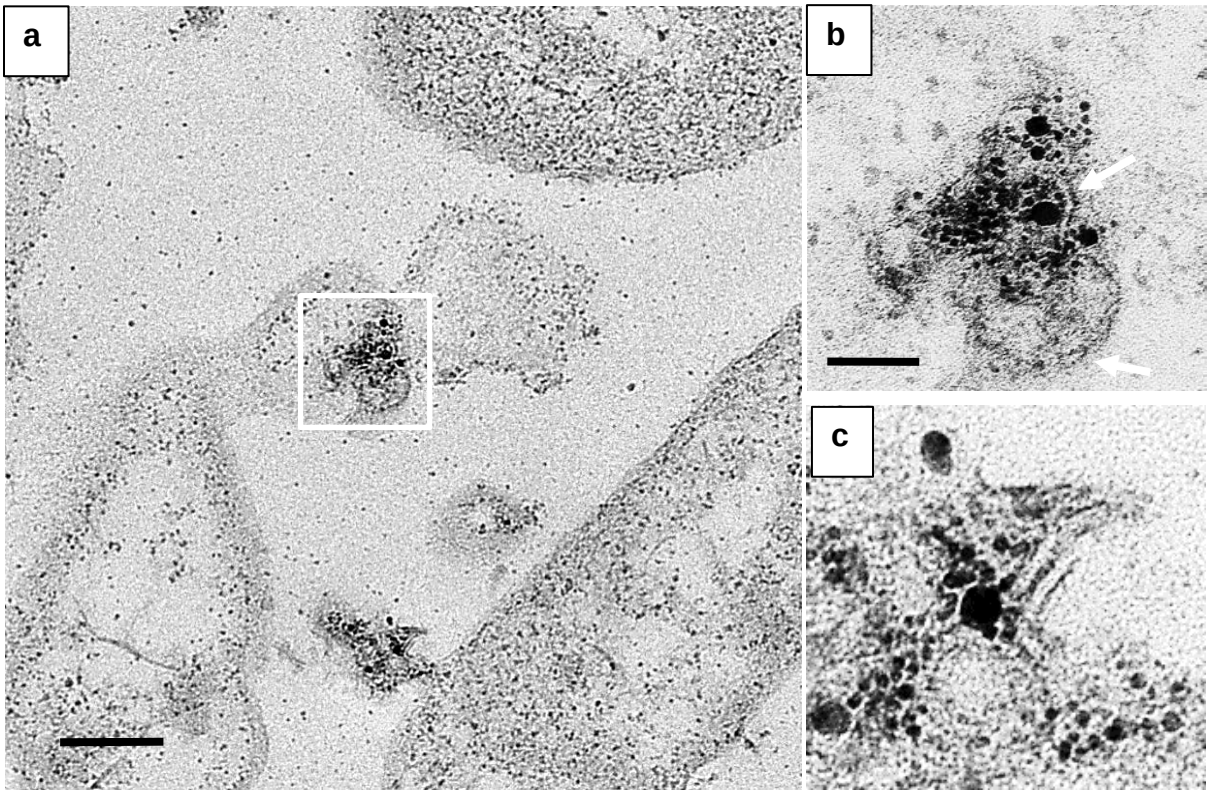

Figure 4.9. (**a**) Transmission electron micrographs of sectioned *Shewanella oneidensis* cells incubated with 0.5 mg L^{-1} PAH-AuNPs for 10 min. Magnified boxed areas, top in (**b**) and bottom in (**c**) show PAH-AuNP clusters associated with cell debris and lipid bilayer-like structures, indicated by red arrows. Scale bars are 200 nm in (**a**), and 50 nm in (**b**) and (**c**).

These TEM images provide compelling visual evidence that PAH-AuNPs interact with

lipid bilayers in a single-cell organism and acquire fragmented bilayer structures, akin to the lipid corona results obtained in the coarse-grain simulations (Fig. 4.6). This chapter hypothesizes that these results may be related to the observed dose-dependent decreases in the viability of *Shewanella*[48] that cannot be accounted for using just the PAH free ligand at particle-equivalent concentrations.

This description of lipid corona formation around PAH-wrapped nanoparticles should also be viewed in light of previously reported work from within the CSN[49] on the consequences of exposing *Daphnia magna* to the same MPA- and PAH-coated nanoparticle formulations used in the supported lipid bilayer model studies. *Daphnia* have been shown to be affected by PAH-AuNPs, while there is no impact of the PAH polymer alone even at concentrations 100 times higher, indicating a nanoparticle specific effect.[28] Even at concentrations as low as 1 μg/L daphnids have a reduced survival rate and reproduction whereas the PAH alone or MPA-coated nanoparticles do not cause a similar impact. These same nanoparticle polymer combinations have been shown to physiologically cause oxidative stress in daphnid tissues[50] and alter the expression of individual genes, in the form of RNA production, specifically those associated with metabolism, reproduction, and growth.[49]

To further explore whether the interaction between the nanoparticles and organism cell membranes, as seen in the lipid bilayer experiments, is one possible cause for a decrease in daphnid reproduction, graduate students in the Klaper laboratory analyzed Daphnia chronically exposed to PAH-AuNPs for 21 days using third-generation Pacific Biosciences RSII sequencing. Upon determining global gene expression patterns, the uptake of PAH-AuNPs is found to result in the up regulation of a number of pathways that differed significantly from those of just the PAH polymer alone. This finding indicates particle-membrane interactions specific to *Daphnia*'s

mitochondria, including its transmembrane proteins, electron transport, and cytochrome C proteins/components. PAH ligand controls, in contrast, show up regulation of different genes associated more with ion balance and energy metabolism, namely triglyceride storage, ribosomal proteins, and muscle function, further emphasizing the importance of studying not just the particle, but also the free ligands and wrappings surrounding them.

4.3 Conclusion

This chapter presents unprecedented views of lipid coronas forming spontaneously over a broad spectrum of biological membrane systems that range from idealized lipid bilayer models, to bacterial cell envelopes, to eukaryotic cytoplasmic membranes. In this investigation, the lipid corona formation is examined from atomistic information derived from nonlinear optical spectroscopy, super-resolution imaging, and computer simulations, which indicate contact ion pair formation as a key lipid corona formation mechanism, all the way to biological outcomes obtained from third-generation sequencing. Lipid coronas were shown to form spontaneously when polycation-wrapped 4 and 15 nm diameter nanoparticles, be their cores made of gold or nanodiamond, interact with a variety of bilayer membranes, be they immobilized, suspended, or biologic in nature. Connections between laboratory observations of decreased survival and respiration rates and changes in ribosomal gene expression were made, while paying careful attention to free ligand studies to identify the particle-specific effects.

Taken together, the results described in this chapter provide several concrete lines of evidence regarding nanoparticle-lipid interactions that may help us understand and predict, from a molecular level, why some nanomaterial/ligand combinations are detrimental to cellular organisms while others are not. The implications of these reported results are limited to the nanoparticle formulations and lipid compositions surveyed here. Yet, initial experiments with two

environmentally relevant organisms support the finding that this lipid corona formation may also be critically important even in more complex biological systems. This approach, which is carefully explained in this chapter, and which considers both the nanomaterial and the biological membrane equally, will increase our ability to predict the impact that the increasingly widespread use of engineered nanomaterials in industrial applications and consumer products has on these materials once they enter the environment[51-54] and the food chain, which many of them may eventually do.[55]

Chapter 5

Sum Frequency Scattering Spectroscopy of the Interactions of Cationic Polymers and Phospholipid Monolayers on Oil Nanodroplets

Portions of this chapter are part of the following pending manuscript:

Olenick, L. L.; Troiano, J. M.; Smolentsev, N; Ohno, P. E.; Roke, S.; Geiger, F. M., Sum Frequency Scattering Spectroscopy of the Interactions of Cationic Polymers and Phospholipid Monolayers on Oil Nanodroplets. **2017.** *In Prep.*

5.1 Introduction

The discovery of the formation of a lipid corona upon interaction of nanomaterials with the biointerface raises many questions. Explored in this chapter are the ways in which poly(allylamine hydrochloride) interacts with a monolayer of DMPC lipids on the surface of an oil droplet. This research adds to the information gained from the studies of the lipid corona formation discussed in Chapter 4. By examining the conditions under which PAH alone interacts with DMPC, this chapter finds that the concentration of NaCl added to solution, as well as the concentration of PAH, affect the pathways in which these interactions take place. All research discussed in this chapter was performed in collaboration with Professor Sylvie Roke and Roke group member Nikolay Smolentsev from École Polytechnique Fédérale de Lausanne (EPFL), along with fellow graduate students Dr. Julianne Troiano and Paul Ohno.

Polycations are an important component of many modern materials, where they are used as ligands for engineered nanomaterials,[1] in drug delivery systems,[2] as anti-microbials,[3] and as additives in polymer resins used in consumer products, for instance.[4] While the benefits of polycations are numerous, these compounds also have the potential to be harmful once they enter the environment, as they may interact strongly with bacterial membranes even at relatively modest concentrations, as reported for the common polycation poly(allylamine hydrochloride) (PAH).[5] The interaction between another cationic polymer, polyethylenimine, and mouse fibroblast cells has been shown to induce necrotic cell death.[6] Similarly, polycation-DNA polyplexes have been reported to adhere to cells by interacting with the negatively charged phospholipids in cell membranes,[7] while the polycationic bioadhesive chitosan has been reported to disturb the protective boundary of the outer membrane of Gram-negative bacteria.[8] In addition, cationic molecules coupled with complexes of adenovirus can modify the efficiency of gene transfer,[9]

while the incorporation of hydrophilic spacers into polycations has been shown to improve gene delivery into targeted cells.[7] Understanding polycation-lipid interaction on the molecular level therefore provides an opportunity to chemically modify polycations so that potentially negative biological outcomes may be avoided while technological benefits are maintained, or perhaps even improved.

While several approaches are being used to determine polycation-membrane interaction mechanisms on a molecular level, ascertaining the contribution of various characteristics of polymer classes to cell toxicity has been difficult, in part due to the broad molecular weight distributions of many polymers.[3] The elucidation of interaction mechanisms has been further complicated by variations in the degree of polymerization, lipid composition, lipid phase state, solution conditions, temperature, etc. Yet, important insight has been gained by the scientific community. For instance, Banaszak-Holl and co-workers combined atomic force microscopy (AFM) and NMR spectroscopy to determine that polymer class and fluid phase state govern the interaction mechanism between polycationic polymer nanoparticles and lipid bilayers formed from the zwitterionic lipid 1,2-dimyristoyl-*sn*-glycero-3-phosphocholine (DMPC).[10] Likewise, Hong et al. used AFM and confocal laser scanning microscopy to identify the importance of polymer charge state in the formation of nanoscale holes within supported lipid bilayers exposed to polycations but not neutral polymers.[11] Standard fluorescence techniques have also been used in permeability assays, quantifying leakage of fluorescent materials out of, or into, suspended vesicles exposed to cationic polymers,[8] and identifying that polycationic dendrimers bend anionic membranes, thus inducing stress and increasing vesicle leakage.[12] Davydov et al. reported phase transition temperatures measured using differential scanning calorimetry that indicated structural changes within membranes exposed to polycations depend on lipid composition.[13] Finally, recent

work within the CSN combined nonlinear optical spectroscopy with molecular dynamics simulations to probe supported lipid bilayers interacting with PAH. This work identified considerable shifts in the pK_a values of the PAH ammonium groups, along with counterion condensation, as a means for building up significant PAH surface coverages while mitigating charge-charge repulsion in the crowded interfacial environment.[14] Direct ammonium-phosphate interactions were shown to be important as well in that study.

Despite the abundance of research into biointerfaces, much remains to be discovered about the molecular changes that occur in response to various stressors, and under conditions of varying ionic strength. Research in this chapter combines dynamic light scattering (DLS) measurements and infrared (IR) spectroscopy with the interface- and bond-specificity of vibrational sum frequency generation (SFG) spectroscopy to probe several aspects of the molecular structure of lipid monolayers from DMPC suspended in a liquid system composed on the surface of oil/water droplets. These droplets are exposed to varying concentrations of PAH in the presence of low and high salt concentration and studied using sum frequency scattering (SFS) spectroscopy,[15] which is uniquely suited for probing lipid membranes in suspensions rather than for supported lipid bilayers, for which SFG spectroscopy in a reflection geometry is amenable.[16-25] This chapter illustrates that polycationic polymer interactions with zwitterionic lipid bilayers generally result in two distinct outcomes that depend upon salt concentration, explained below as Scenario 1 and Scenario 2.

5.2 Results and Discussion

5.2.1 PAH modifies SFS spectral intensity of DMPC/d-hexadecane nanodroplets depending on NaCl concentration.

SFS spectra in the CH stretching region were obtained from DMPC/oil nanodroplets dispersed in D_2O. The *ssp*-polarized spectra in the absence of salt (Fig. 5.1A) include the symmetric methylene stretch (s-CH_2) near 2850 cm^{-1}, the symmetric methyl stretch (s-CH_3) near 2879 cm^{-1}, the antisymmetric methyl stretch (as-CH_3) near 2865 cm^{-1}, the antisymmetric methylene stretch (as-CH_2) near 2919 cm^{-1}, as well as the symmetric methylene Fermi resonance near 2905 cm^{-1} and the symmetric methyl Fermi resonance near 2937 cm^{-1}.[26-28]

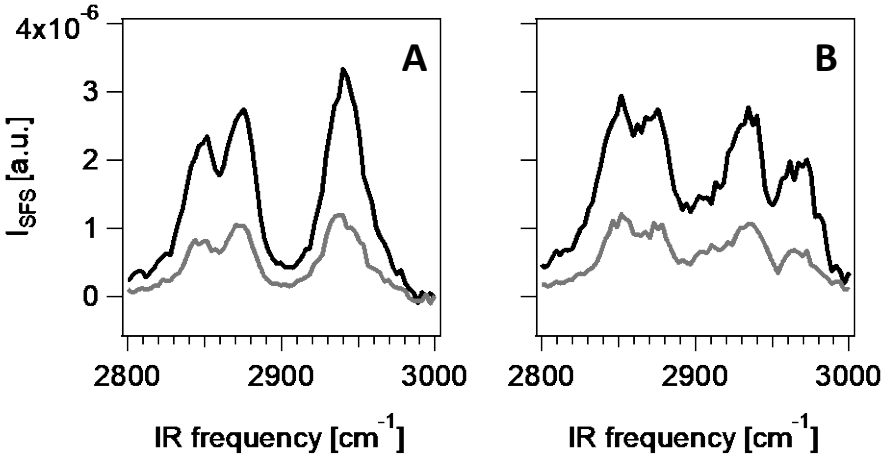

Figure 5.1. *ssp*- (A) and *ppp*- (B) polarized sum frequency scattering spectra of DMPC at the d-hexadecane/D_2O interface before (black) and after (gray) interaction with 140 μM PAH at 0 mM NaCl in D_2O.

Upon interaction with a 140 μM solution of PAH with no added NaCl, the SFS signal intensity of DMPC/oil nanodroplets decreases by approximately 60% in the *ssp* and *ppp* polarizations (Fig. 5.1). The relative peak intensities remain the same, demonstrating that the orientation of the lipids with respect to the interface does not change in response to the presence of PAH.

Unlike the SFS spectra from DMPC/oil nanodroplets interacting with PAH under conditions of no added salt, the addition of PAH to the droplets in the presence of 100 mM NaCl

concentration results in increases in the intensity of the SFS spectra (Fig. 5.2). This signal intensity increase may be attributed to either an increase in the number of oscillators at the droplet surface, or to increased lipid ordering of the surface (the PAH methylene groups themselves do not provide SFS signal intensity in PAH only control experiments in D_2O, shown in Figure S1 of Olenick et al.)[29]

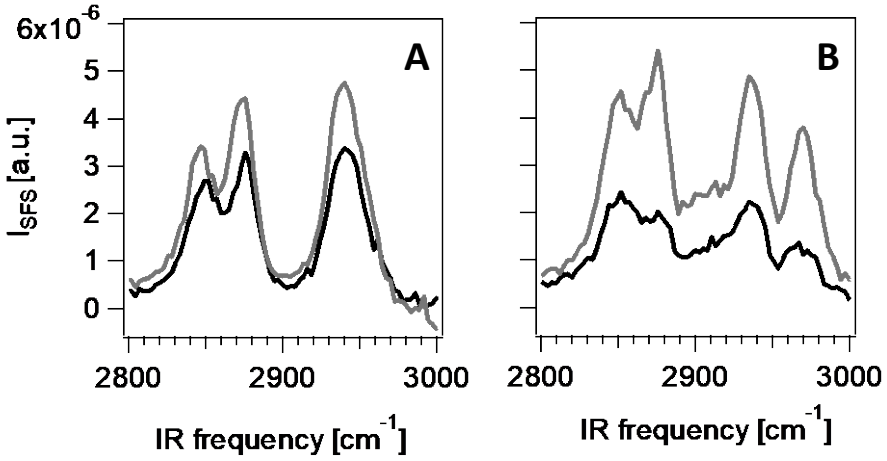

Figure 5.2. *ssp*- (A) and *ppp*- (B) polarized sum frequency scattering spectra of DMPC at the d-hexadecane/D_2O interface before (black) and after (gray) interaction with 140 μM PAH at 100 mM NaCl in D_2O.

Addition of PAH at 100 mM salt concentration also leads to a reversal in the intensity ratio between the peaks at 2875 cm^{-1} and 2850 cm^{-1} in the *ppp*-polarized SFS spectra. This outcome indicates a change in lipid orientation at the surface, as a simple increase or decrease in the number of oscillators, without a corresponding change in the ordering, would leave the peak intensity ratios the same. This effect is similar to what Okur et al. observed earlier when comparing oil droplets coated by lipids of varying alkyl tail lengths.[28] The conformation of PAH in no added salt and 100 mM NaCl solutions may also play a role in this interaction. According to a study of polyelectrolyte

multilayers (PEMUs) which included PAH, PAH became more coiled in solution in response to the presence of various salt solutions.[30] Without salt, the PAH layer swelled, indicating a more extended conformation in aqueous solutions.[30] Other researchers of PAH-containing polyelectrolyte systems have also documented this swelling response to solutions without salt as well as structural changes of thin films in response to rinsing with no salt present.[31-32]

Complementary DLS experiments illustrate an increase in droplet size for the case of 100 mM NaCl. In Figure 5.3, the similarities between droplet sizes in the absence of added salt and the size of droplets in a salt concentration of 100 mM NaCl are apparent. Both size distributions are bimodal, with one population centered at approximately 150 nm and one at either 350 nm or 500 nm.

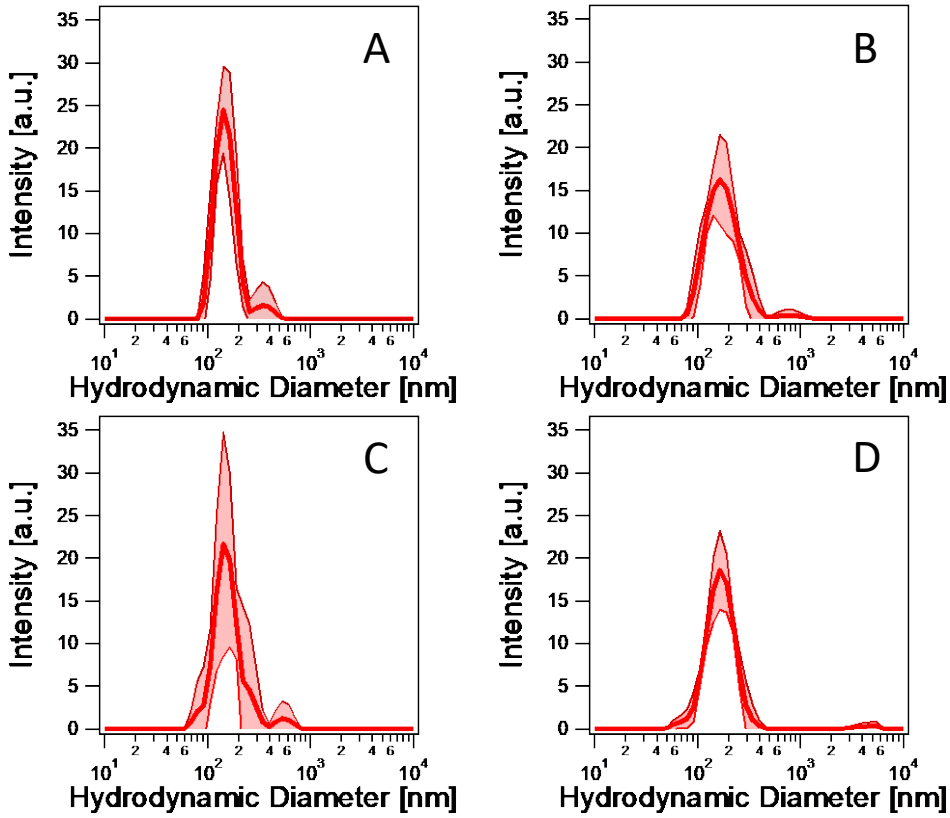

Figure 5.3. Hydrodynamic diameter measurements of DMPC/oil nanodroplets dispersed in water before (A, C) and after (B, D) interaction with 140 μM PAH under no added NaCl (top) and 100 mM NaCl (bottom) conditions.

While there is some uncertainty in the exact size of the large particles due to the way the DLS data is fit within the Malvern Zetasizer software, the trend is clear. After interaction with a 140 μM PAH solution, the population of smaller droplets remains relatively unchanged, whereas the population of larger droplets increases in size to around 700 nm and around 4000 nm in the case of zero added NaCl and 100 mM NaCl, respectively. Thus, the growth of a population of large objects occurs under high salt conditions, which also occurs to a lesser extent in low salt conditions. This data points towards two competing scenarios that can take place, determined by the NaCl and PAH concentrations present in the solution, as discussed next.

According to the theory of SFS spectroscopy and sum frequency generation (SFG) spectroscopy,[15, 33] a decrease in peak intensity indicates either a loss in the number of oscillators, a randomization in the orientation of oscillators, or an ordering of the oscillators in such a way that they destructively interfere with each other (as commonly seen in all-*trans*-configured methylene groups). Discussed first is the scenario where the observed increase in intensity results from a loss of oscillators (Scenario 1).

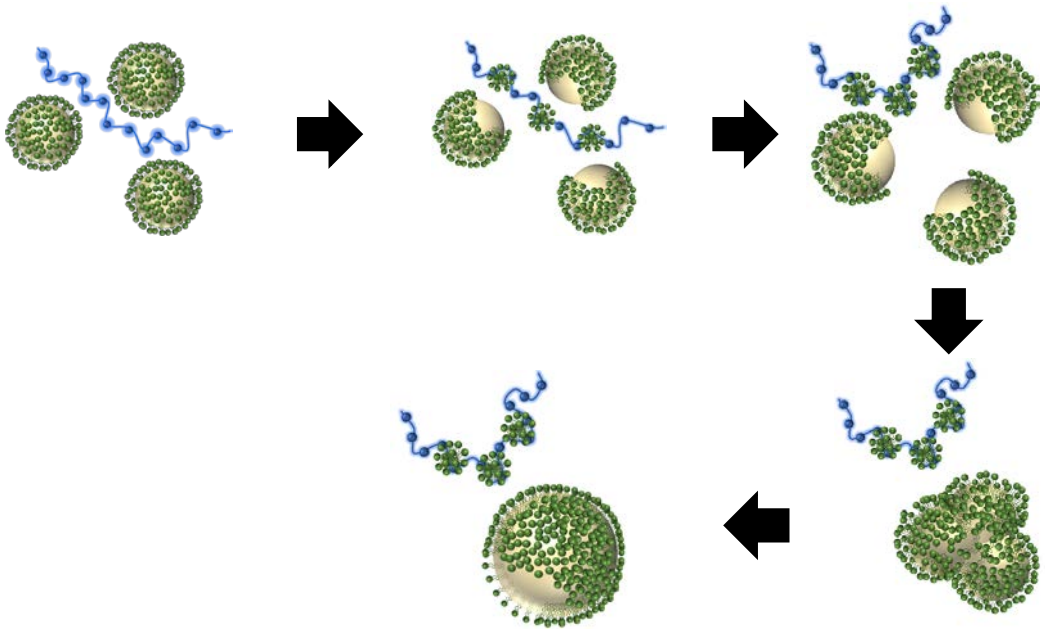

Scenario 1. One possible mechanistic pathway for interaction between PAH and DMPC oil nanodroplets. In this scenario, droplets increase in size and become more disordered at the surface. Gold spheres represent oil droplets. Green shapes represent lipids. Blue shapes represent PAH. Counterions were omitted for clarity.

In Scenario 1, PAH removes lipids from the nanodroplets. The decrease in the number of oscillators at the surface of the oil droplet due to lipid removal leads to a greater amount of disorder at the interface, a decrease in SFS signal cancellation and a corresponding increase in *ssp*- and *ppp*-polarized SFS intensity. In addition, the increase in *spp*-polarized SFS intensity results from uneven lipid dispersion on the oil droplet. Droplet size also increases, as shown by DLS data.

Charge plays a large role in the stability of oil-in-water macroemulsions, with monovalent cations preventing aggregation of droplets better than di- or tri-valent cations when the counter-ion is kept consistent.[34] Indeed, Kundu et al. reported that coalescence and Ostwald ripening occur as mechanisms for destabilization and droplet growth in oil-in-water macroemulsions with anionic surfactants.[34] In the experiments presented in this chapter, PAH may promote the coalescence of droplets by removing the surfactant. The removal of the surfactant provides a destabilizing force by increasing the interfacial tension. The DLS data presented here supports this interpretation of the resulting droplet size increase. Also of note is that hexadecane has a low, but non-zero, solubility in water. During DMPC removal by PAH, hexadecane could dissolve into the bulk phase and droplets may grow in a process similar to Ostwald ripening.[35-36]

In the second scenario (Scenario 2), PAH is bound to the surface of the lipid droplet and does not remove lipids, but instead it orders the lipids at the interface, resulting in a decrease in SFS intensity in *spp*, *ssp*, and *ppp* polarizations.

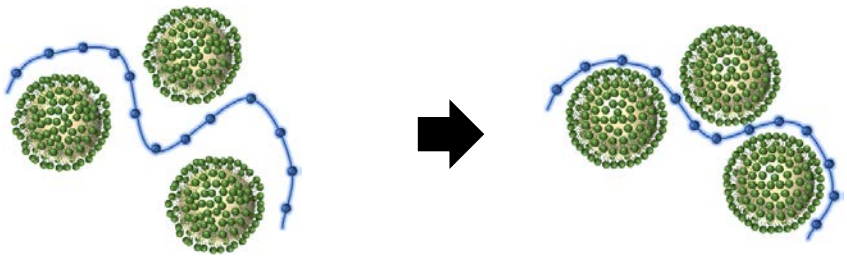

Scenario 2. Another possible mechanistic pathway for interaction between PAH and DMPC oil nanodroplets. In this scenario, droplet size remains steady, but PAH causes an increase in ordering of the lipids at the surface due to the proximity of the polymer and electrostatic attraction. Gold spheres represent oil droplets. Green shapes represent lipids. Blue shapes represent PAH. Counterions were omitted for clarity.

This scenario is reminiscent of work reported by Kabalnov et al., who describe a nonionic surfactant-water-decane system whereby the adsorption of a hydrophobically modified naturally

occurring polymer causes a change in the curvature of the surfactant leading to an increased rigidity in the system upon polymer addition.[37]

The experimental conditions employed in this study determine which scenario is more likely to occur. From the DLS data as well as the *ssp*-, *ppp*-, and *spp*-polarized SFS data, Scenario 1 is considered to be most plausible under high salt conditions, whereas Scenario 2 is more plausible at low salt conditions. The salt concentration dependence of the observations is consistent with increased charge screening under high salt conditions, which decreases the electrical double layer thickness between the polymer and the oil nanodroplet, allowing the PAH to approach the droplet and remove the lipids from the surface.[38-39]

5.2.2 PAH modifies SFS signal intensity of DMPC/d-hexadecane nanodroplets depending on PAH concentration

In various surfactant polymer systems, changing the polymer concentration is known to change the interfacial tension, thus affecting the critical micelle concentration.[40] Therefore, the PAH concentration was lowered from 140 μM, discussed in the previous section, to 15 μM at no added salt conditions. Figure 5.4 shows an increase in *ssp*-polarized SFS intensity at low salt conditions, reminiscent of Scenario 1.

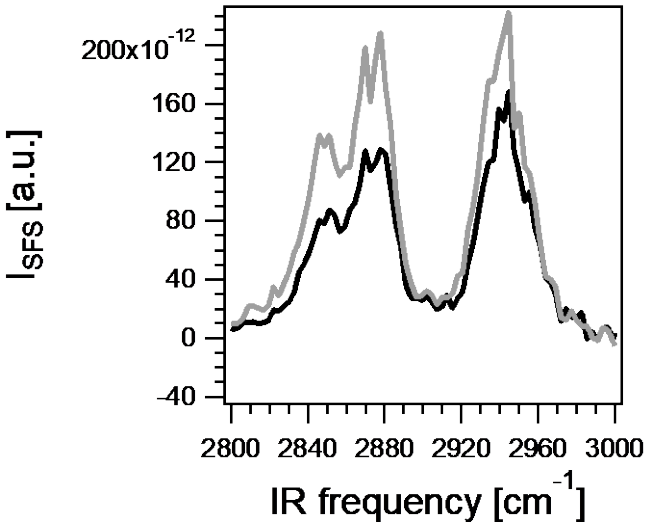

Figure 5.4. *ssp*-polarized sum frequency scattering spectra of DMPC at the d-hexadecane/D_2O interface before (black) and after (gray) interaction with 15 μM PAH in D_2O with no added salt.

This increase is potentially due to an abundance of oil droplets compared to the concentration of PAH. The *spp*-polarized SFS spectra, which show a decrease in SFS intensity after PAH addition (Figure 5.5), support this explanation.

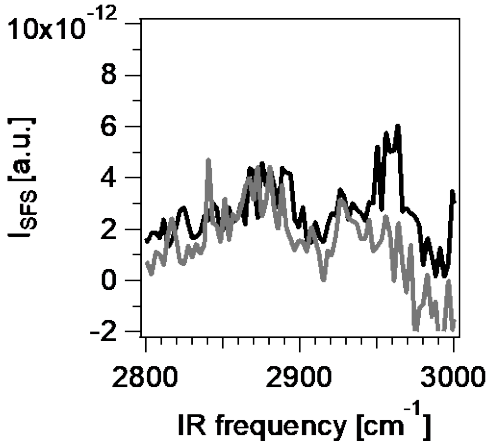

Figure 5.5. *spp*-polarized sum frequency scattering spectra of DMPC at the d-hexadecane/D_2O interface before (black) and after (gray) interaction with 15 μM PAH in D_2O with no added salt.

The *spp* polarization combination is sensitive to the changes in dispersion of lipids on the surface of the oil droplet. If all the lipids were evenly separated at the surface, and in the presence of uniform lipid coverage, *spp* signal intensity would not be observable.[41-42] If the lipids were distributed non-uniformly, considerable *spp*-polarized SFS signal intensity should be observed.[41-42] Therefore, the observed decrease in the *spp*-polarized SFS signal intensity provides some evidence that the lipids are more evenly dispersed under low vs high PAH concentrations, pointing towards Scenario 2.

In addition, a PAH concentration of 40 μM causes an SFS signal decrease of DMPC/oil droplets in the PO stretching region. As shown in Figure 5.6, the observable features in this spectral region occur near 1070 cm^{-1} (the s-CO-O-C stretch) and near 1100 cm^{-1} (the s-PO_2^- stretch).[28]

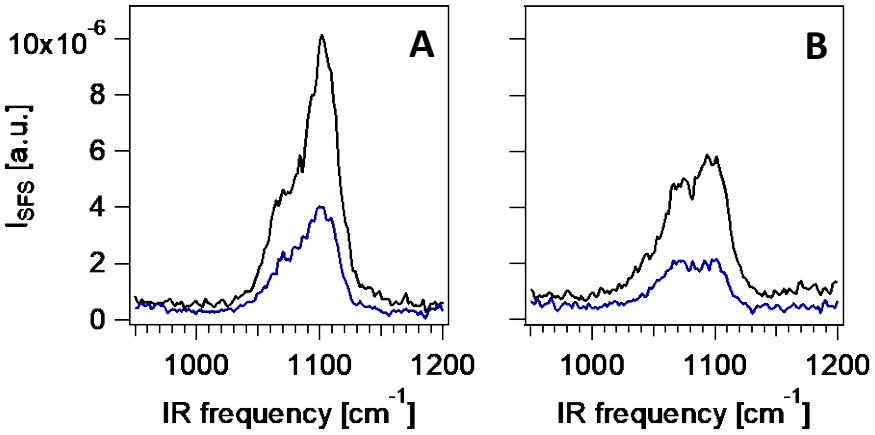

Figure 5.6. *ssp*- (A) and *ppp*- (B) polarized SFS spectra in the PO stretching region of DMPC/d-hexadecane droplets dispersed in D_2O before (black) and after (blue) addition of 40 μM PAH in D_2O under no added salt conditions.

As in the case of the CH stretching region for DMPC, the change in the ratio of the SFS intensity at 1070 cm^{-1} and 1100 cm^{-1} indicates lipid reordering, specifically in the choline headgroup of DMPC. These observations in low salt conditions further support the Scenario 2 hypothesis.

5.3 Conclusion

Two scenarios for the interactions of PAH with DMPC/oil nanodroplets dispersed in D_2O were examined. In Scenario 1, droplets increase in size and become more disordered at the surface in response to lipid removal by PAH. In Scenario 2, droplet size remains steady, but PAH causes an increase in ordering of the lipids at the surface due to the proximity of the polymer and electrostatic attraction. This chapter found that under 100 mM NaCl and 140 μM PAH, Scenario 1 prevailed which involved lipid removal by PAH followed by droplet coalescence. Under conditions of no added NaCl and 140 μM PAH, Scenario 2 dominated, which involved PAH surrounding several droplets, thereby changing the lipid orientation, but keeping the droplet size constant. Under conditions of no added NaCl and 15 μM PAH, Scenario 1 flourished, indicating an interplay between NaCl and PAH concentration in determining which scenario is most likely. Further investigation is necessary to probe an expanded set of experimental conditions in order to determine the extent of the application of these two scenarios.

These results illustrate that cationic polymers do not always interact in inherently destructive ways with a lipid bilayer. Under certain experimental conditions, polymers could simply cause the formation of lipid rafts or areas of more densely packed lipids. The way in which the lipids partition across the surface of the oil droplet in response might be enough to cause apoptosis of a cell, but could also encourage transmembrane protein activity, depending on the type of lipid encouraged to move by the polymer.

Chapter 6

Conclusions and Future Outlook

6.1 Conclusion

As decried in chapter 1, nanomaterials are becoming the "go-to" technology for challenging problems which include energy storage,[1] cancer therapy,[2] food preservation[3] and food production[4] among many others. Their presence in a large and growing number of consumer products[5] such as car batteries,[6] food packaging,[7] cosmetics,[8] and clothing[9] indicates an increasing potential for environmental release. With much left unknown about these materials, science needs to catch up to production and better understand their toxic effects to control the possible negative impact on the environment. The Center for Sustainable Nanotechnology (CSN) has answered the call for more fundamental research on the nano-biointerface. The work presented in this thesis is part of this Center.

In this thesis, the concept of the nano-biointerface was introduced in Chapter 1 and various techniques to probe this complex boundary layer were examined, such as Atomic Force Microscopy, Fluorescence Imaging, and Electrophysiology. Sum Frequency Generation (SFG) Spectroscopy was discussed as a promising tool to investigate the nano-biointerface because of the specificity of the technique for regions that are non-centrosymmetric and that have some inherent order. Supported lipid bilayers (SLBs) predominantly composed of zwitterionic phosphatidylcholine lipids were used as model systems for eukaryotic cell membranes. The simplicity of the SLBs and the ease of interpretation of experimental results, while remaining focused on the fundamental forces which govern the interactions at the nano-biointerface, make SLBs good model systems for a cell membrane. Coupling this model system with SFG spectroscopy and connecting this research to other studies within the CSN creates a compelling framework on which to understand interactions at the nano-biointerface.

SFG spectroscopy, an important technique in the study of the nano-biointerface, was explained in detail in Chapter 2. The key reasons why this technique is useful with respect to this interface include the requirement for a break in centrosymmetry (which is generally true of interfaces), and its applicability to study supported lipid bilayers *in situ*, without labels, and under biologically relevant conditions without destruction of the sample. Limitations of this spectroscopic technique were discussed, as well as the necessity for complementary techniques to help analyze the SFG spectra.

SFG spectroscopy probed the differences in order and orientation of lipids in a supported lipid bilayer (SLB) composed of lipids that have various transition temperatures. This research explored in Chapter 3 found that the SFG spectra of the SLBs studied fell into two distinct groups: those with transition temperatures below the experimental temperature, and those with transition temperatures above the experimental temperature. This result opens the door for probing nanomaterial interactions with SLBs whereby the nanomaterial alters the phase state of the bilayer.

The description of the formation of a lipid corona surrounding a nanomaterial (Chapter 4) utilized many of the techniques within the CSN. The chapter described work showing that nanoparticles coated with a polycationic ligand, poly(allylamine hydrochloride), (PAH-AuNPs), removed lipids from SLBs formed from a mixture of 9:1 DMPC/DMPG lipids. This effect was not observed with the PAH ligand alone, i.e. without the gold nanoparticle core, indicating a nanoparticle-specific effect. Given the loss of SFG signal intensity observed in this thesis for several cases of SLBs exposed to certain bulk solution conditions, considering the various possible molecular origins for the observations is important. Since SFG spectroscopy is sensitive to order and orientation, loss of spectral features could be due to loss of oscillators, complete randomization of the order of the oscillators, or complete ordering of the oscillators, creating centrosymmetry.

Therefore, a loss of signal does not indicate which of these possibilities is occurring. To determine the reasons behind loss of spectral features, a variety of complementary techniques have been employed through collaborative work within the CSN, including second harmonic generation (SHG) spectroscopy, AFM, confocal fluorescence imaging, Fluorescence Recovery After Photobleaching (FRAP), and Quartz Crystal Microbalance with Dissipation Monitoring (QCM-D). Single molecule fluorescence microscopy and fluorescence imaging with particle analysis (Orr and Pedersen groups) determined that bilayer fluidity increased after interaction with PAH-AuNPs. With information from studies on *Shewanella oneidensis*, (Haynes and Feng groups) we found evidence that points towards lipid corona formation at the cell membrane of a model bacterium. With information from multi-generational research on *Daphnia magna*, (Klaper group) we found that there exists a long-term effect of these materials on the offspring of a model multi-cellular organism. Additional calculations (Cui and Hernandez groups) suggested that the key mechanism in this interaction was the contact ion pairing of the amine groups of the PAH with the phosphate present in both PC and PG lipids and glycerol groups present in the PG lipids. The detailed analysis of the lipid corona formation mechanism lays the foundation for scientists exploring this complex interface to understand other mechanisms of interaction and connect fundamental studies with larger-scale biological assays.

To probe the effect of PAH on lipid membranes further, we examined the interaction of PAH with a monolayer of PC lipids at the surface of an oil droplet with sum frequency scattering (SFS) spectroscopy (Chapter 5). In studying a monolayer in place of a bilayer, this research removed the need for a support. We concluded that it is likely that PAH interacts with a monolayer of lipids in two main ways. In Scenario 1, PAH removes some lipids from the surface of several droplets, and the droplets then aggregate to form one larger droplet potentially through a

mechanism similar to Ostwald ripening. In Scenario 2, PAH approaches the surface of the oil droplet and causes an increase in ordering of the lipids on that surface. These two Scenarios depend heavily on the concentration of added NaCl in the solution as well as the concentration of the PAH. This research shows that PAH, without nanoparticles present, can modify the order and orientation of lipids in a monolayer with or without removal of the lipids from a monolayer. It also illustrates that SFS spectroscopy can give insight on more complex systems than this type of spectroscopy typically probes.

6.2 Future Work

The research presented in this thesis provides a foundation on which to build an understanding of the nano-biointerface using SFG spectroscopy. The thesis demonstrates that SFG spectroscopy, when combined with complementary techniques, is quite powerful for providing molecular insights into interfaces as complex as the nano-bio interface. Future research should extend SFG spectroscopy to the carbonyl and PO stretching regions. The CO and PO stretching regions will give insights into the order and orientation of lipids that may otherwise not yield signal in the CH stretching region. Probing this additional spectroscopic space will open the research field to other classes of lipids. Access to information regarding a wider variety of lipids will allow for more lipid/nanomaterial pairings to be studied to better understand the extent of lipid corona formation, the effects of changing the transition temperature of a lipid on the interactions of lipids with nanomaterials, and to probe fully the vast number of ways in which a nanomaterial may interact with a lipid bilayer. This spectroscopic expansion is already underway in the Geiger group by fellow graduate student, Merve Doğangün.

One of the ways in which a nanomaterial may interact with a lipid bilayer is by passing through the bilayer, or “puncturing” the bilayer. This pathway is inhibited by the presence of a

support in a SLB. Future work should include research on suspended lipid bilayers. These free-standing lipid bilayers are formed within a small hole in a thin Teflon partition and are frequently studied using microscopy. Research utilizing fluorescence microscopy on suspended lipid bilayers has been reported before, but not within the context of the Center. Effort should also be made in exploring interactions with these suspended bilayers using SHG imaging. In SHG imaging, we have the opportunity to study changes to nonlinear optical properties of the bilayer and nanomaterial with excellent spatial and time resolution. The spatial resolution could allow us to probe differences in local interactions in bilayers containing lipid rafts and connect the interactions at these locations with information from AFM and fluorescence studies to draw conclusions based upon these differences. The time resolution could yield important kinetic information about "penetration time," which could vary between types of nanomaterials and nanomaterial/bilayer combinations.

More fundamental studies are also necessary to tease out all of the information regarding the interactions at the nano-biointerface contained within the SFG spectra. One suggested experiment is to cross-link the phospholipid tails within the bilayer to differentiate between nanoparticle/bilayer interactions in which the nanomaterial removes the lipids and those in which the nanomaterial adsorbs to the surface of the bilayer and changes the order, but does not remove the lipids from the bilayer. Crosslinking can be performed using engineered lipids.[10-12] Another useful experiment would be to covalently bond the lipid tails to the silica window using silanol chemistry. This experiment would differentiate between SFG spectral changes occurring as a result of a change in curvature of the bilayer and those occurring as a result of a change in headgroup tilt.

In addition to gaining more information regarding interactions at the nano-biointerface, future work should center around a better understanding of features present in the SFG spectra of these interactions. These experiments can be carried out in two ways: 1. using deuterium oxide in place of water and 2. using selectively deuterated lipids. A strength of the work presented in this thesis is certainly that the conditions are biologically relevant. However, for spectral interpretation of certain experiments whereby the spectral features are not well-understood, these suggested experiments can clarify what features are peaks stemming from lipids or the nanomaterials, and what features are dips from interference with the OH stretches in the CH stretching region.

Finally, future work should take advantage of the expertise of the skilled scientists within the CSN. Effort should be focused on improving communication within groups to ensure standardized methods at the start of a research project for better comparison across techniques. Communication could be improved in two main ways. One way is for advisors to introduce students into the Center in a more focused way at the start of their PhD. Reinforcing the fact that collaboration and communication with Center scientists is paramount in a research project will give students the best framework on which to build a project at the start of their PhD programs. Incoming students will pay closer attention to an advisor than any other academic they encounter, and rightfully so. Another way to improve communication is through constant communication during projects. These smaller subgroup meetings should be scheduled in advance and take place regularly during the entire length of the project. Even if no new research conclusions are drawn, keeping these lines of communication open is essential. Communication infrastructure is imperative for the knowledge to flow easily between groups within the Center to improve the science.

Chapter 1 References

1. Murphy, C. J., et al., Biological Responses to Engineered Nanomaterials: Needs for the Next Decade. *ACS Central Science* **2015**, *1*, 117-123.

2. All Products: Consumer Products Inventory from the Project on Emerging Nanotechnologies. http://www.nanotechproject.org/cpi/products/page3?sort=-datestamp (accessed April 14, 2014).

3. Lee, S. S., et al., Sulfated Glycopeptide Nanostructures for Multipotent Protein Activation. *Nature Nanotechnology* **2017**, *12*, 821-829.

4. Pumera, M., Graphene-Based Nanomaterials for Energy Storage. *Energy & Environmental Science* **2011**, *4*, 668-674.

5. Deng, Y.; Ediriwickrema, A.; Yang, F.; Lewis, J.; Girardi, M.; Saltzman, W. M., A Sunblock Based on Bioadhesive Nanoparticles. *Nature Materials* **2015**, *14*, 1278-1285.

6. Demir, H. V.; Nizamoglu, S.; Erdem, T.; Mutlugun, E.; Gaponik, N.; Eychmüller, A., Quantum Dot Integrated Leds Using Photonic and Excitonic Color Conversion. *Nano Today* **2011**, *6*, 632-647.

7. Hubbell, J. A.; Chilkoti, A., Nanomaterials for Drug Delivery. *Science* **2012**, *337*, 303.

8. PRNewswire Nanomaterials Market, 2027. http://www.prnewswire.com/news-releases/nanomaterials-market-2027-300483189.html (accessed July 12, 2017).

9. National Science Foundation Media Advisory 14-004 http://www.nsf.gov/news/news_summ.jsp?org=NSF&cntn_id=130586&preview=false (accessed April 14, 2014).

10. National Nanotechnology Initiative. http://www.nano.gov/about-nni/what/funding (accessed December 28, 2015).

11. Dodaro, G. L.; Persons, T. M., United States Government Accountability Office Report to Congressional Requesters. Nanomanufacturing, Emergence and Implications for U.S. Competitiveness, the Environment, and Human Health. 2014; Vol. January 2014, p 125.

12. Nanomaterials and the Environment: The Chemistry and Materials Perspective. A Report from a National Science Foundation Supported Workshop Held June 28th and June 29th, 2011 in Arlington, Va. . http://nsfenv-nano.chem.wisc.edu (accessed June 11, 2013).

13. Plant, A. L., Supported Hybrid Bilayer Membranes as Rugged Cell Membrane Mimics. *Langmuir* **1999**, *15*, 5128-5135.

14. Simons, K.; Vaz, W. L. C., Model Systems, Lipid Rafts, and Cell Membranes. *Annual Review of Biophysics and Biomolecular Structure* **2004**, *33*, 269-295.

15. Kam, L. C., Capturing the Nanoscale Complexity of Cellular Membranes in Supported Lipid Bilayers. *Journal of Structural Biology* **2009**, *168*, 3-10.

16. Kasemo, B., Biological Surface Science. *Surface Science Reports* **2002**, *500*, 656-677.

17. Chen, H.; Hu, Q.-Y.; Yue-Zheng; Jiang, J.-H.; Shen, G.-L.; Yu, R.-Q., Construction of Supported Lipid Membrane Modified Piezoelectric Biosensor for Sensitive Assay of Cholera Toxin Based on Surface-Agglutination of Ganglioside-Bearing Liposomes. *Analytica Chimica Acta* **2010**, *657*, 204-209.

18. Phillips, K. S.; Cheng, Q., Microfluidic Immunoassay for Bacterial Toxins with Supported Phospholipid Bilayer Membranes on Poly(Dimethylsiloxane). *Analytical Chemistry* **2004**, *77*, 327-334.

19. Liu, J.; Jiang, X.; Ashley, C.; Brinker, C. J., Electrostatically Mediated Liposome Fusion and Lipid Exchange with a Nanoparticle-Supported Bilayer for Control of Surface Charge, Drug Containment, and Delivery. *Journal of the American Chemical Society* **2009**, *131*, 7567-7569.

20. Nair, P. M.; Salaita, K.; Petit, R. S.; Groves, J. T., Using Patterned Supported Lipid Membranes to Investigate the Role of Receptor Organization in Intercellular Signaling. *Nature Protocols* **2011**, *6*, 523-539.

21. Groves, J. T.; Dustin, M. L., Supported Planar Bilayers in Studies on Immune Cell Adhesion and Communication. *Journal of Immunological Methods* **2003**, *278*, 19-32.

22. Perez, T. D.; Nelson, W. J.; Boxer, S. G.; Kam, L., E-Cadherin Tethered to Micropatterned Supported Lipid Bilayers as a Model for Cell Adhesion. *Langmuir* **2005**, *21*, 11963-11968.

23. Jonsson, M. P.; Jönsson, P.; Dahlin, A. B.; Höök, F., Supported Lipid Bilayer Formation and Lipid-Membrane-Mediated Biorecognition Reactions Studied with a New Nanoplasmonic Sensor Template. *Nano Letters* **2007**, *7*, 3462-3468.

24. Bayley, H.; Cremer, P. S., Stochastic Sensors Inspired by Biology. *Nature* **2001**, *413*, 226-230.

25. Nicolson, G. L., The Fluid—Mosaic Model of Membrane Structure: Still Relevant to Understanding the Structure, Function and Dynamics of Biological Membranes after More Than 40 Years. *Biochimica et Biophysica Acta (BBA) - Biomembranes* **2014**, *1838*, 1451-1466.

26. Singer, S. J.; Nicolson, G. L., The Fluid Mosaic Model of the Structure of Cell Membranes. *Science* **1972**, *175*, 720-731.

27. Vereb, G.; Szöllősi, J.; Matkó, J.; Nagy, P.; Farkas, T.; Vígh, L.; Mátyus, L.; Waldmann, T. A.; Damjanovich, S., Dynamic, yet Structured: The Cell Membrane Three Decades after the Singer–Nicolson Model. *Proceedings of the National Academy of Sciences* **2003**, *100*, 8053-8058.

28. Munro, S., Lipid Rafts: Elusive or Illusive? *Cell* **2003**, *115*, 377-388.

29. Bain, C. D., Sum-Frequency Vibrational Spectroscopy of the Solid/Liquid Interface. *Journal of the Chemical Society, Faraday Transactions* **1995**, *91*, 1281-1296.

30. Humbert, C.; Busson, B., Sum-Frequency Generation Spectroscopy of Biointerfaces. In *Biointerface Characterization by Advanced Ir Spectroscopy*, Pradier, C. M.; Chabal, Y. J., Eds. Academic Press: New York, NY, 2011; pp 279-321.

31. Zhu, M.; Nie, G.; Meng, H.; Xia, T.; Nel, A.; Zhao, Y., Physicochemical Properties Determine Nanomaterial Cellular Uptake, Transport, and Fate. *Accounts of Chemical Research* **2013**, *46*, 622-631.

32. Muller, D. A., Structure and Bonding at the Atomic Scale by Scanning Transmission Electron Microscopy. *Nature Materials* **2009**, *8*, 263-270.

33. Winey, M.; Meehl, J. B.; O'Toole, E. T.; Giddings, T. H., Conventional Transmission Electron Microscopy. *Molecular Biology of the Cell* **2014**, *25*, 319-323.

34. Shimoda, K.; Park, J.-S.; Hinoki, T.; Kohyama, A., Influence of Surface Structure of Sic Nano-Sized Powder Analyzed by X-Ray Photoelectron Spectroscopy on Basic Powder Characteristics. *Applied Surface Science* **2007**, *253*, 9450-9456.

35. Danino, D., Cryo-Tem of Soft Molecular Assemblies. *Current Opinion in Colloid & Interface Science* **2012**, *17*, 316-329.

36. Leonenko, Z. V.; Finot, E.; Ma, H.; Dahms, T. E. S.; Cramb, D. T., Investigation of Temperature-Induced Phase Transitions in Dopc and Dppc Phospholipid Bilayers Using Temperature-Controlled Scanning Force Microscopy. *Biophysical Journal* **2004**, *86*, 3783-3793.

37. Kent, R. D.; Vikesland, P. J., Controlled Evaluation of Silver Nanoparticle Dissolution Using Atomic Force Microscopy. *Environmental Science & Technology* **2012**, *46*, 6977-6984.

38. Udpa, L.; Ayres, V. M.; Yuan, F.; Qian, C.; Kumar, S. A., Deconvolution of Atomic Force Microscopy Data for Cellular and Molecular Imaging. *IEEE Signal Processing Magazine* **2006**, *23*, 73-83.

39. Kahya, N.; Scherfeld, D.; Bacia, K.; Schwille, P., Lipid Domain Formation and Dynamics in Giant Unilamellar Vesicles Explored by Fluorescence Correlation Spectroscopy. *Journal of Structural Biology* **2004**, *147*, 77-89.

40. Anglin, T. C.; Conboy, J. C., Kinetics and Thermodynamics of Flip-Flop in Binary Phospholipid Membranes Measured by Sum-Frequency Vibrational Spectroscopy. *Biochemistry* **2009**, *48*, 10220-10234.

41. Bartsch, P.; Walter, C.; Selenschik, P.; Honigmann, A.; Wagner, R., Horizontal Bilayer for Electrical and Optical Recordings. *Materials* **2012**, *5*, 2705-2730.

42. Ide, T.; Ichikawa, T., A Novel Method for Artificial Lipid-Bilayer Formation. *Biosensors and Bioelectronics* **2005**, *21*, 672-677.

43. Zhu, X. D.; Suhr, H.; Shen, Y. R., Surface Vibrational Spectroscopy by Infrared-Visible Sum Frequency Generation. *Physical Review B* **1987**, *35*, 3047-3050.

44. Williams, C. T.; Beattie, D. A., Probing Buried Interfaces with Non-Linear Optical Spectroscopy. *Surface Science* **2002**, *500*, 545-576.

45. Boyd, R. W., *Nonlinear Optics*, Third ed.; Academic Press: New York, NY, 2008.

46. Shen, Y. R., Surface Properties Probed by Second-Harmonic and Sum-Frequency Generation. *Nature* **1989**, *337*, 519-525.

47. Yang, P.; Ramamoorthy, A.; Chen, Z., Membrane Orientation of Msi-78 Measured by Sum Frequency Generation Vibrational Spectroscopy. *Langmuir* **2011**, *27*, 7760-7767.

48. Karpierz, M. A.; Stegeman, G. I., Nonlinear Optics: A Vibrant Field. *Photonics Letters of Poland* **2009**, *1*, 145-147.

49. Bloembergen, N., Surface Nonlinear Optics: A Historical Review. *Applied Physics B: Lasers and Optics* **1999**, *68*, 289-293.

50. Liu, J.; Conboy, J. C., Structure of a Gel Phase Lipid Bilayer Prepared by the Langmuir−Blodgett/Langmuir-Schaefer Method Characterized by Sum-Frequency Vibrational Spectroscopy. *Langmuir* **2005**, *21*, 9091-9097.

51. Bordi, F.; Cametti, C.; De Luca, F.; Gili, T.; Gaudino, D.; Sennato, S., Charged Lipid Monolayers at the Air–Solution Interface: Coupling to Polyelectrolytes. *Colloids and Surfaces B: Biointerfaces* **2003**, *29*, 149-157.

52. Ma, G.; Allen, H. C., Condensing Effect of Palmitic Acid on Dppc in Mixed Langmuir Monolayers. *Langmuir* **2006**, *23*, 589-597.

53. Smits, M.; Sovago, M.; Wurpel, G. W. H.; Kim, D.; Müller, M.; Bonn, M., Polarization-Resolved Broad-Bandwidth Sum-Frequency Generation Spectroscopy of Monolayer Relaxation. *The Journal of Physical Chemistry C* **2007**, *111*, 8878-8883.

54. Liu, J.; Conboy, J. C., Phase Transition of a Single Lipid Bilayer Measured by Sum-Frequency Vibrational Spectroscopy. *Journal of the American Chemical Society* **2004**, *126*, 8894-8895.

55. Liu, J.; Conboy, J. C., 1,2-Diacyl-Phosphatidylcholine Flip-Flop Measured Directly by Sum-Frequency Vibrational Spectroscopy. *Biophysical Journal* **2005**, *89*, 2522-2532.

56. Liu, J.; Conboy, J. C., Direct Measurement of the Transbilayer Movement of Phospholipids by Sum-Frequency Vibrational Spectroscopy. *Journal of the American Chemical Society* **2004**, *126*, 8376-8377.

57. Anglin, T. C.; Cooper, M. P.; Li, H.; Chandler, K.; Conboy, J. C., Free Energy and Entropy of Activation for Phospholipid Flip-Flop in Planar Supported Lipid Bilayers. *The Journal of Physical Chemistry B* **2010**, *114*, 1903-1914.

58. Xiaoyun Chen, J. W., Cornelius B. Kristalyn, Zhan Chen, Real-Time Structural Investigation of a Lipid Bilayer During Its Interaction with Melittin Using Sum Frequency Generation Vibrational Spectroscopy. *Biophysical Journal* **2007**, *93*, 866-875.

59. Liu, J.; Conboy, J. C., Phase Behavior of Planar Supported Lipid Membranes Composed of Cholesterol and 1,2-Distearoyl-Sn-Glycerol-3-Phosphocholine Examined by Sum-Frequency Vibrational Spectroscopy. *Vibrational Spectroscopy* **2009**, *50*, 106-115.

60. Brown, K. L.; Conboy, J. C., Electrostatic Induction of Lipid Asymmetry. *Journal of the American Chemical Society* **2011**, *133*, 8794-8797.

61. Roke, S.; Schins, J.; Müller, M.; Bonn, M., Vibrational Spectroscopic Investigation of the Phase Diagram of a Biomimetic Lipid Monolayer. *Physical Review Letters* **2003**, *90*, 128101.

62. Sung, W.; Seok, S.; Kim, D.; Tian, C. S.; Shen, Y. R., Sum-Frequency Spectroscopic Study of Langmuir Monolayers of Lipids Having Oppositely Charged Headgroups. *Langmuir* **2010**, *26*, 18266-18272.

63. Walker, R. A.; Gruetzmacher, J. A.; Richmond, G. L., Phosphatidylcholine Monolayer Structure at a Liquid−Liquid Interface. *Journal of the American Chemical Society* **1998**, *120*, 6991-7003.

64. Watry, M. R.; Tarbuck, T. L.; Richmond, G. L., Vibrational Sum-Frequency Studies of a Series of Phospholipid Monolayers and the Associated Water Structure at the Vapor/Water Interface. *The Journal of Physical Chemistry B* **2002**, *107*, 512-518.

65. Brown, M. G.; Raymond, E. A.; Allen, H. C.; Scatena, L. F.; Richmond, G. L., The Analysis of Interference Effects in the Sum Frequency Spectra of Water Interfaces. *The Journal of Physical Chemistry A* **2000**, *104*, 10220-10226.

Chapter 2 References

1. Boyd, R. W., *Nonlinear Optics*, Third ed.; Academic Press: New York, NY, 2008.

2. Shen, Y. R., *The Principles of Nonlinear Optics*; John Wiley & Sons, Inc.: Hoboken, NJ, 1984, p 575.

3. Lambert, A. G.; Davies, P. B.; Neivandt, D. J., Implementing the Theory of Sum Frequency Generation Vibrational Spectroscopy: A Tutorial Review. *Applied Spectroscopy Reviews* **2005**, *40*, 103-145.

4. Kelley, A. M., *Condensed-Phase Molecular Spectroscopy and Photophysics*; John Wiley & Sons, Inc.: Hoboken, NJ, 2013, p 330.

5. Karpierz, M. A.; Stegeman, G. I., Nonlinear Optics: A Vibrant Field. *Photonics Letters of Poland* **2009**, *1*, 145-147.

6. P. A. Franken, A. E. H., C. W. Peters, G. Weinreich, Generation of Optical Harmonics. *Physical Review Letters* **1961**, *7*, 118-120.

7. Armstrong, J. A.; Bloembergen, N.; Ducuing, J.; Pershan, P. S., Interactions between Light Waves in a Nonlinear Dielectric. *Physical Review* **1962**, *127*, 1918-1939.

8. Bloembergen, N.; Pershan, P. S., Light Waves at the Boundary of Nonlinear Media. *Physical Review* **1962**, *128*, 606-622.

9. Bain, C. D., Sum-Frequency Vibrational Spectroscopy of the Solid/Liquid Interface. *Journal of the Chemical Society, Faraday Transactions* **1995**, *91*, 1281-1296.

10. Bloembergen, N., Surface Nonlinear Optics: A Historical Review. *Applied Physics B: Lasers and Optics* **1999**, *68*, 289-293.

11. Nobelprize.org The Nobel Prize in Physics 1981. http://www.nobelprize.org/nobel_prizes/physics/laureates/1981/.

12. AmericanInstituteofPhysics Y. R. Shen. https://history.aip.org/phn/11602032.html (accessed August 11, 2017).

13. Zhu, X. D.; Suhr, H.; Shen, Y. R., Surface Vibrational Spectroscopy by Infrared-Visible Sum Frequency Generation. *Physical Review B* **1987**, *35*, 3047-3050.

14. Halliday, D.; Resnick, R.; Walker, J., *Fundamentals of Physics*; Wiley, 2002.

15. Lambert, A. G. Resonantly Enhanced Sum Frequency Spectroscopy of Adsorption on Hydrophilic Mica Substrates. University of Cambridge, 2001

16. K. Kemnitz, K. B., J. M. Hicks, G. R. Pinto, K. B. Eisenthal, T. F. Heinz, The Phase of Second-Harmonic Light Generated at an Interface and Its Relation to Absolute Molecular Orientation. *Chemical Physical Letters* **1986**, *131*, 285-290.

17. Eisenthal, K. B., Liquid Interfaces Probed by Seond-Harmonic and Sum-Frequency Spectroscopy. *Chemical Reviews* **1996**, *96*, 1343-1360.

18. Ward, R. N.; Davies, P. B.; Bain, C. D., Orientation of Surfactants Adsorbed on a Hydrophobic Surface. *The Journal of Physical Chemistry* **1993**, *97*, 7141-7143.

19. Humbert, C.; Busson, B., Sum-Frequency Generation Spectroscopy of Biointerfaces. In *Biointerface Characterization by Advanced Ir Spectroscopy*, Pradier, C. M.; Chabal, Y. J., Eds. Academic Press: New York, NY, 2011; pp 279-321.

20. Shiratori, K.; Morita, A., Theory of Quadrupole Contributions from Interface and Bulk in Second-Order Optical Processes. *Bulletin of the Chemical Society of Japan* **2012**, *85*, 1061-1076.

21. Ishiyama, T.; Morita, A., Computational Analysis of Vibrational Sum Frequency Generation Spectroscopy. *Annual Review of Physical Chemistry* **2017**, *68*, 355-377.

22. Kundu, A.; Tanaka, S.; Ishiyama, T.; Ahmed, M.; Inoue, K.-i.; Nihonyanagi, S.; Sawai, H.; Yamaguchi, S.; Morita, A.; Tahara, T., Bend Vibration of Surface Water Investigated by Heterodyne-Detected Sum Frequency Generation and Theoretical Study: Dominant Role of Quadrupole. *The Journal of Physical Chemistry Letters* **2016**, *7*, 2597-2601.

23. Gonella, G.; Lütgebaucks, C.; de Beer, A. G. F.; Roke, S., Second Harmonic and Sum-Frequency Generation from Aqueous Interfaces Is Modulated by Interference. *The Journal of Physical Chemistry C* **2016**, *120*, 9165-9173.

24. Jena, K. C.; Covert, P. A.; Hore, D. K., The Effect of Salt on the Water Structure at a Charged Solid Surface: Differentiating Second- and Third-Order Nonlinear Contributions. *The Journal of Physical Chemistry Letters* **2011**, *2*, 1056-1061.

25. Geiger, F. M., Second Harmonic Generation, Sum Frequency Generation and X^3: Dissecting Environmental Interfaces with a Nonlinear Optical Swiss Army Knife. *Annual Review of Physical Chemistry* **2009**, *60*, 61-83.

26. Hayes, P. L.; Malin, J. N.; Jordan, D. S.; Geiger, F. M., Get Charged Up: Nonlinear Optical Voltammetry for Quantifying the Thermodynamics and Electrostatics of Metal Cations at Aqueous/Oxide Interfaces. *Chemical Physics Letters* **2010**, *499*, 183-192.

27. Hayes, P. L.; Chen, E. H.; Achtyl, J. L.; Geiger, F. M., An Optical Voltmeter for Studying Cetyltrimethylammonium Interacting with Fused Silica/Aqueous Interfaces at High Ionic Strength. *The Journal of Physical Chemistry A* **2009**, *113*, 4269-4280.

28. Reviakine, I.; Brisson, A., Formation of Supported Phospholipid Bilayers from Unilamellar Vesicles Investigated by Atomic Force Microscopy. *Langmuir* **2000**, *16*, 1806-1815.

29. Schönherr, H.; Johnson, J. M.; Lenz, P.; Frank, C. W.; Boxer, S. G., Vesicle Adsorption and Lipid Bilayer Formation on Glass Studied by Atomic Force Microscopy. *Langmuir* **2004**, *20*, 11600-11606.

30. Mingeot-Leclercq, M.-P.; Deleu, M.; Brasseur, R.; Dufrene, Y. F., Atomic Force Microscopy of Supported Lipid Bilayers. *Nature Protocols* **2008**, *3*, 1654-1659.

31. Bartsch, P.; Walter, C.; Selenschik, P.; Honigmann, A.; Wagner, R., Horizontal Bilayer for Electrical and Optical Recordings. *Materials* **2012**, *5*, 2705-2730.

32. Ide, T.; Ichikawa, T., A Novel Method for Artificial Lipid-Bilayer Formation. *Biosensors and Bioelectronics* **2005**, *21*, 672-677.

33. Rodahl, M.; Höök, F.; Krozer, A.; Brzezinski, P.; Kasemo, B., Quartz Crystal Microbalance Setup for Frequency and Q-Factor Measurements in Gaseous and Liquid Environments. *Review of Scientific Instruments* **1995**, *66*, 3924-3930.

34. Rodahl, M.; Hook, F.; Fredriksson, C.; A. Keller, C.; Krozer, A.; Brzezinski, P.; Voinova, M.; Kasemo, B., Simultaneous Frequency and Dissipation Factor Qcm Measurements of Biomolecular Adsorption and Cell Adhesion. *Faraday Discussions* **1997**, *107*, 229-246.

35. Korlach, J.; Schwille, P.; Webb, W. W.; Feigenson, G. W., Characterization of Lipid Bilayer Phases by Confocal Microscopy and Fluorescence Correlation Spectroscopy. *Proc. Natl. Acad. Sci. U. S. A.* **1999**, *96*, 8461-8466.

36. Andrecka, J.; Spillane, K. M.; Ortega-Arroyo, J.; Kukura, P., Direct Observation and Control of Supported Lipid Bilayer Formation with Interferometric Scattering Microscopy. *ACS Nano* **2013**, *7*, 10662-10670.

37. Liedberg, B.; Nylander, C.; Lunström, I., Surface Plasmon Resonance for Gas Detection and Biosensing. *Sensors and Actuators* **1983**, *4*, 299-304.

38. Liu, J.; Conboy, J. C., 1,2-Diacyl-Phosphatidylcholine Flip-Flop Measured Directly by Sum-Frequency Vibrational Spectroscopy. *Biophysical Journal* **2005**, *89*, 2522-2532.

39. Anglin, T. C.; Conboy, J. C., Kinetics and Thermodynamics of Flip-Flop in Binary Phospholipid Membranes Measured by Sum-Frequency Vibrational Spectroscopy. *Biochemistry* **2009**, *48*, 10220-10234.

40. Anglin, T. C.; Cooper, M. P.; Li, H.; Chandler, K.; Conboy, J. C., Free Energy and Entropy of Activation for Phospholipid Flip-Flop in Planar Supported Lipid Bilayers. *The Journal of Physical Chemistry B* **2010**, *114*, 1903-1914.

41. Wu, H.-L.; Tong, Y.; Peng, Q.; Li, N.; Ye, S., Phase Transition Behaviors of the Supported Dppc Bilayer Investigated by Sum Frequency Generation (Sfg) Vibrational Spectroscopy and Atomic Force Microscopy (Afm). *Physical Chemistry Chemical Physics* **2016**, *18*, 1411-1421.

42. Chen, X.; Chen, Z., Sfg Studies on Interactions between Antimicrobial Peptides and Supported Lipid Bilayers. *Biochimica et Biophysica Acta (BBA) - Biomembranes* **2006**, *1758*, 1257-1273.

43. Chen, X.; Wang, J.; Boughton, A. P.; Kristalyn, C. B.; Chen, Z., Multiple Orientation of Melittin inside a Single Lipid Bilayer Determined by Combined Vibrational Spectroscopic Studies. *Journal of the American Chemical Society* **2007**, *129*, 1420-1427.

44. Xiaoyun Chen, J. W., Cornelius B. Kristalyn, Zhan Chen, Real-Time Structural Investigation of a Lipid Bilayer During Its Interaction with Melittin Using Sum Frequency Generation Vibrational Spectroscopy. *Biophysical Journal* **2007**, *93*, 866-875.

45. Ye, S.; Li, H.; Wei, F.; Jasensky, J.; Boughton, A. P.; Yang, P.; Chen, Z., Observing a Model Ion Channel Gating Action in Model Cell Membranes in Real Time in Situ: Membrane Potential Change Induced Alamethicin Orientation Change. *Journal of the American Chemical Society* **2012**, *134*, 6237-6243.

46. Nguyen, K. T.; Soong, R.; lm, S.-C.; Waskell, L.; Ramamoorthy, A.; Chen, Z., Probing the Spontaneous Membrane Insertion of a Tail-Anchored Membrane Protein by Sum Frequency Generation Spectroscopy. *Journal of the American Chemical Society* **2010**, *132*, 15112-15115.

47. Liu, J.; Conboy, J. C., Phase Behavior of Planar Supported Lipid Membranes Composed of Cholesterol and 1,2-Distearoyl-Sn-Glycerol-3-Phosphocholine Examined by Sum-Frequency Vibrational Spectroscopy. *Vibrational Spectroscopy* **2009**, *50*, 106-115.

48. Liu, J.; Conboy, J. C., Phase Transition of a Single Lipid Bilayer Measured by Sum-Frequency Vibrational Spectroscopy. *Journal of the American Chemical Society* **2004**, *126*, 8894-8895.

49. Troiano, J. M., et al., Direct Probes of 4 Nm Diameter Gold Nanoparticles Interacting with Supported Lipid Bilayers. *The Journal of Physical Chemistry C* **2015**, *119*, 534-546.

50. Liu, Y.; Yan, E. C. Y.; Zhao, X.; Eisenthal, K. B., Surface Potential of Charged Liposomes Determined by Second Harmonic Generation. *Langmuir* **2001**, *17*, 2063-2066.

51. Eisenthal, K. B., Second Harmonic Spectroscopy of Aqueous Nano- and Microparticle Interfaces. *Chemical Reviews* **2006**, *106*, 1462-1477.

52. Srivastava, A.; Eisenthal, K. B., Kinetics of Molecular Transport across a Liposome Bilayer. *Chemical Physics Letters* **1998**, *292*, 345-351.

53. Salafsky, J. S.; Eisenthal, K. B., Second Harmonic Spectroscopy: Detection and Orientation of Molecules at a Biomembrane Interface. *Chem. Phys. Lett.* **2000**, *319*, 435-439.

54. Salafsky, J. S.; Eisenthal, K. B., Protein Adsorption at Interfaces Detected by Second Harmonic Generation. *J. Phys. Chem. B* **2000**, *104*, 7752-7755.

55. Fu, L.; Ma, G.; Yan, E. C. Y., In Situ Misfolding of Human Islet Amyloid Polypeptide at Interfaces Probed by Vibrational Sum Frequency Generation. *Journal of the American Chemical Society* **2010**, *132*, 5405-5412.

56. Ries, R. S.; Choi, H.; Blunck, R.; Bezanilla, F.; Heath, J. R., Black Lipid Membranes: Visualizing the Structure, Dynamics, and Substrate Dependence of Membranes. *J. Phys. Chem. B* **2004**, *41*, 16040-16049.

57. Wurpel, G. W. H.; Sovago, M.; Bonn, M., Sensitive Probing of DNA Binding to a Cationic Lipid Monolayer. *J. Am. Chem. Soc.* **2007**, *129*, 8420-8421.

58. Pavinatto, F. J.; Caseli, L.; Pavinatto, A.; dos Santos, D. S.; Nobre, T. M.; Zaniquelli, M. E. D.; Silva, H. S.; Miranda, P. B.; de Oliveira, O. N., Probing Chitosan and Phospholipid Interactions Using Langmuir and Langmuir−Blodgett Films as Cell Membrane Models. *Langmuir* **2007**, *23*, 7666-7671.

59. Troiano, J. M.; Kuech, T. R.; Vartanian, A. M.; Torelli, M. D.; Sen, A.; Jacob, L. M.; Hamers, R. J.; Murphy, C. J.; Pedersen, J. A.; Geiger, F. M., On Electronic and Charge Interference in Second Harmonic Generation Responses from Gold Metal Nanoparticles at Supported Lipid Bilayers. *The Journal of Physical Chemistry C* **2016**.

60. Troiano, J. M., et al., Direct Probes of 4 Nm Diameter Gold Nanoparticles Interacting with Supported Lipid Bilayers. *The Journal of Physical Chemistry C* **2014**, *119*, 534-546.

61. McGeachy, A. C.; Olenick, L. L.; Troiano, J. M.; Lankone, R. S.; Melby, E. S.; Kuech, T. R.; Ehimiaghe, E.; Fairbrother, D. H.; Pedersen, J. A.; Geiger, F. M., Resonantly Enhanced Nonlinear Optical Probes of Oxidized Multiwalled Carbon Nanotubes at Supported Lipid Bilayers. *J. Phys. Chem. B* **2017**, *121*, 1321-1329.

62. Dogangun, M.; Hang, M. N.; Troiano, J. M.; McGeachy, A. C.; Melby, E. S.; Pedersen, J. A.; Hamers, R. J.; Geiger, F. M., Alteration of Membrane Compositional Asymmetry by Licoo2 Nanosheets. *ACS Nano* **2015**, *9*, 8755-8765.

63. Jacobson, K. H., et al., Lipopolysaccharide Density and Structure Govern the Extent and Distance of Nanoparticle Interaction with Actual and Model Bacterial Outer Membranes. *Env. Sci. & Technol.* **2015**, *49*, 10642-10650.

64. Boyd, R. W., *Nonlinear Optics, 3rd Edition*; Elsevier Academic Press Inc: San Diego, 2008, p 1-613.

65. Roke, S.; Schins, J.; Müller, M.; Bonn, M., Vibrational Spectroscopic Investigation of the Phase Diagram of a Biomimetic Lipid Monolayer. *Physical Review Letters* **2003**, *90*, 128101.

66. Liu, J.; Conboy, J. C., Direct Measurement of the Transbilayer Movement of Phospholipids by Sum-Frequency Vibrational Spectroscopy. *Journal of the American Chemical Society* **2004**, *126*, 8376-8377.

67. Zhang, C.; Wu, F.-G.; Hu, P.; Chen, Z., Interaction of Polyethylenimine with Model Cell Membranes Studied by Linear and Nonlinear Spectroscopic Techniques. *The Journal of Physical Chemistry C* **2014**, *118*, 12195-12205.

68. Kundu, A.; Yamaguchi, S.; Tahara, T., Evaluation of Ph at Charged Lipid/Water Interfaces by Heterodyne-Detected Electronic Sum Frequency Generation. *The Journal of Physical Chemistry Letters* **2014**, *5*, 762-766.

69. Tan, J.; Ye, S.; Luo, Y., Observing Peptide-Induced Lipid Accumulation in a Single-Component Zwitterionic Lipid Bilayer. *The Journal of Physical Chemistry C* **2015**, *119*, 28523-28529.

70. Wei, F.; Ye, S.; Li, H.; Luo, Y., Phosphate Ions Promoting Association between Peptide and Modeling Cell Membrane Revealed by Sum Frequency Generation Vibrational Spectroscopy. *The Journal of Physical Chemistry C* **2013**, *117*, 11095-11103.

71. Ye, S.; Li, H.; Yang, W.; Luo, Y., Accurate Determination of Interfacial Protein Secondary Structure by Combining Interfacial-Sensitive Amide I and Amide Iii Spectral Signals. *Journal of the American Chemical Society* **2014**, *136*, 1206-1209.

72. Yang, P.; Wu, F.-G.; Chen, Z., Dependence of Alamethicin Membrane Orientation on the Solution Concentration. *The Journal of Physical Chemistry C* **2013**, *117*, 3358-3365.

73. Richmond, G. L., Molecular Bonding and Interactions at Aqueous Surfaces as Probed by Vibrational Sum Frequency Spectroscopy. *Chem. Rev.* **2002**, *102*, 2693-2724.

74. Yan, E. C. Y.; Fu, L.; Wang, Z.; Liu, W., Biological Macromolecules at Interfaces Probed by Chiral Vibrational Sum Frequency Generation Spectroscopy. *Chem. Rev.* **2014**, *114*, 8471-8498.

75. Marrapu, P.; Cheng, Y.; Carmichael, G.; Beig, G.; Spak, S. In *Local and Regional Interactions between Air Quality and Climate in New Delhi - a Sector Based Analysis*, AGU Annual Meeting, Dec. 2011.

76. Liu, J.; Conboy, J. C., Structure of a Gel Phase Lipid Bilayer Prepared by the Langmuir−Blodgett/Langmuir-Schaefer Method Characterized by Sum-Frequency Vibrational Spectroscopy. *Langmuir* **2005**, *21*, 9091-9097.

77. Brown, K. L.; Conboy, J. C., Electrostatic Induction of Lipid Asymmetry. *Journal of the American Chemical Society* **2011**, *133*, 8794-8797.

78. Chen, Y.; Jena, K. C.; Luetgebaucks, C.; Okur, H. I.; Roke, S., Three Dimensional Nano "Langmuir Trough" for Lipid Studies. *Nano Lett.* **2015**, *15*, 5558-5563.

79. Smolentsev, N.; Luetgebaucks, C.; Okur, H. I.; de Beer, A. G. F.; Roke, S., Intermolecular Headgroup Interaction and Hydration as Driving Forces for Lipid Transmembrane Asymmetry. *J. Am. Chem. Soc.* **2016**, *138*, 4053-4060.

80. Anderson, N. A.; Richter, L. J.; Stephenson, J. C.; Briggman, K. A., Characterization and Control of Lipid Layer Fluidity in Hybrid Bilayer Membranes. *J. Am. Chem. Soc.* **2007**, *129*, 2094-2100.

81. Doyle, A. W.; Fick, J.; Himmelhaus, M.; Eck, W.; Graziani, I.; Prudovsky, I.; Grunze, M.; Maciag, T.; Neivandt, D. J., Protein Deformation of Lipid Hybrid Bilayer Membranes Studied by Sum Frequency Generation Vibrational Spectroscopy. *Langmuir* **2004**, *20*, 8961-8965.

82. Chen, X.; Hua, W.; Huang, Z.; Allen, H. C., Interfacial Water Structure Associated with Phospholipid Membranes Studied by Phase-Sensitive Vibrational Sum Frequency Generation Spectroscopy. *J. Am. Chem. Soc.* **2010**, *132*, 11336-11342.

83. Fu, L.; Liu, J.; Yan, E. C. Y., Chiral Sum Frequency Generation Spectroscopy for Characterizing Protein Secondary Structures at Interfaces. *Journal of the American Chemical Society* **2011**, *133*, 8094-8097.

84. Smits, M.; Sovago, M.; Wurpel, G. W. H.; Kim, D.; Müller, M.; Bonn, M., Polarization-Resolved Broad-Bandwidth Sum-Frequency Generation Spectroscopy of Monolayer Relaxation. *The Journal of Physical Chemistry C* **2007**, *111*, 8878-8883.

85. Sung, W.; Seok, S.; Kim, D.; Tian, C. S.; Shen, Y. R., Sum-Frequency Spectroscopic Study of Langmuir Monolayers of Lipids Having Oppositely Charged Headgroups. *Langmuir* **2010**, *26*, 18266-18272.

86. Walker, R. A.; Gruetzmacher, J. A.; Richmond, G. L., Phosphatidylcholine Monolayer Structure at a Liquid−Liquid Interface. *Journal of the American Chemical Society* **1998**, *120*, 6991-7003.

87. Allgeyer, E. D.; Sterling, S. M.; Gunewardene, M. S.; Hess, S. T.; Neivandt, D. J.; Mason, M. D., Combining Total Internal Reflection Sum Frequency Spectroscopy Spectral Imaging and Confocal Fluorescence Microscopy. *Langmuir* **2015**, *31*, 987-994.

88. Kim, G.; Gurau, M. C.; Lim, S.-M.; Cremer, P. S., Investigations of the Orientation of a Membrane Peptide by Sum Frequency Spectroscopy. *J. Phys. Chem. B* **2003**, *107*, 1403-1409.

89. Nojima, Y.; Suzuki, Y.; Yamaguchi, S., Weakly Hydrogen-Bonded Water inside Charged Lipid Monolayer Observed with Heterodyne-Detected Vibrational Sum Frequency Generation Spectroscopy. *J. Phys. Chem. C* **2017**, *121*, 2173-2180.

90. Livingston, R. A.; Zhang, Z.; Piatkowski, L.; Bakker, H. J.; Hunger, J.; Bonn, M.; Backus, E. H., Water in Contact with a Cationic Lipid Exhibits Bulklike Vibrational Dynamics. *J. Phys. Chem. B* **2016**, *120*, 10069-1008.

91. Casper, C. B.; Verreault, D.; Adams, E. M.; Hua, W.; Allen, H. C., Surface Potential of Dppc Monolayers on Concentrated Aqueous Salt Solutions. *Journal of Physical Chemistry B* **2016**, *120*, 2043-2052.

92. Watry, M. R.; Tarbuck, T. L.; Richmond, G. L., Vibrational Sum-Frequency Studies of a Series of Phospholipid Monolayers and the Associated Water Structure at the Vapor/Water Interface. *The Journal of Physical Chemistry B* **2002**, *107*, 512-518.

93. Brown, M. G.; Raymond, E. A.; Allen, H. C.; Scatena, L. F.; Richmond, G. L., The Analysis of Interference Effects in the Sum Frequency Spectra of Water Interfaces. *The Journal of Physical Chemistry A* **2000**, *104*, 10220-10226.

94. Anglin, T. C.; Brown, K. L.; Conboy, J. C., Phospholipid Flip-Flop Modulated by Transmembrane Peptides Walp and Melittin. *Journal of Structural Biology* **2009**, *168*, 37-52.

95. Liu, W.; Wang, Z.; Fu, L.; Leblanc, R. M.; Yan, E. C. Y., Lipid Compositions Modulate Fluidity and Stability of Bilayers: Characterization by Surface Pressure and Sum Frequency Generation Spectroscopy. *Langmuir* **2013**, *29*, 15022-15031.

96. Li, B.; Lu, X.; Han, X.; Wu, F.-G.; Myers, J. N.; Chen, Z., Interfacial Fresnel Coefficients and Molecular Structures of Model Cell Membranes: From a Lipid Monolayer to a Lipid Bilayer. *The Journal of Physical Chemistry C* **2014**, *118*, 28631-28639.

97. Li, B.; Wang, H.-Y.; Feng, P.; Han, X.; Chen, Z.; Lu, X.; Wu, F.-G., Qualitative and Quantitative Analyses of the Molecular-Level Interaction between Memantine and Model Cell Membranes. *The Journal of Physical Chemistry C* **2015**, *119*, 17074-17083.

98. Keszthelyi, T.; Hollo, G.; Nyitrai, G.; Kardos, J.; Heja, L., Bilayer Charge Reversal and Modification of Lipid Organization by Dendrimers as Observed by Sum-Frequency Vibrational Spectroscopy. *Langmuir* **2015**, *31*, 7815-7825.

99. Esenturk, O.; Walker, R. A., Surface Structure at Hexadecane and Halo-Hexadecane Liquid/Vapor Interfaces. *The Journal of Physical Chemistry B* **2004**, *108*, 10631-10635.

100. Stokes, G. Y.; Buchbinder, A. M.; Gibbs-Davis, J. M.; Scheidt, K. A.; Geiger, F. M., Heterogeneous Ozone Oxidation Reactions of 1-Pentene, Cyclopentene, Cyclohexene, and a Menthenol Derivative Studied by Sum Frequency Generation. *The Journal of Physical Chemistry A* **2008**, *112*, 11688-11698.

101. Stokes, G. Y.; Buchbinder, A. M.; Gibbs-Davis, J. M.; Scheidt, K. A.; Geiger, F. M., Chemically Diverse Environmental Interfaces and Their Reactions with Ozone Studied by Sum Frequency Generation. *Vibrational Spectroscopy* **2009**, *50*, 86-98.

102. Voges, A. B.; Al-Abadleh, H. A.; Musorrafiti, M. J.; Bertin, P. A.; Nguyen, S. T.; Geiger, F. M., Carboxylic Acid- and Ester-Functionalized Siloxane Scaffolds on Glass Studied by Broadband Sum Frequency Generation. *The Journal of Physical Chemistry B* **2004**, *108*, 18675-18682.

103. Zhuang, X.; Miranda, P. B.; Kim, D.; Shen, Y. R., Mapping Molecular Orientation and Conformation at Interfaces by Surface Nonlinear Optics. *Physical Review B* **1999**, *59*, 12632-12640.

104. Szoka, F.; Papahadjopoulos, D., Comparative Properties and Methods of Preparation of Lipid Vesicles (Liposomes). *Annual Review of Biophysics and Bioengineering* **1980**, *9*, 467-508.

105. Avanti Polar Lipids, Inc. Extrusion Method. https://www.avantilipids.com/index.php?option=com_content&view=article&id=533&Itemid=297 (accessed April 15, 2014).

106. Kalb, E.; Frey, S.; Tamm, L. K., Formation of Supported Planar Bilayers by Fusion of Vesicles to Supported Phospholipid Monolayers. *Biochimica et Biophysica Acta (BBA) - Biomembranes* **1992**, *1103*, 307-316.

107. Van Meer, G.; Voelker, D. R.; Feigenson, G. W., Membrane Lipids: Where They Are and How They Behave. *Nature Reviews Molecular Cell Biology* **2008**, *9*, 112-124.

108. Spector, A. A.; Yorek, M. A., Membrane Lipid Composition and Cellular Function. *Journal of Lipid Research* **1985**, *26*, 1015-35.

109. Perez-Gil, J.; Weaver, T. E., Pulmonary Surfactant Pathophysiology: Current Models and Open Questions. *Physiology* **2010**, *25*, 132-141.

110. Ridgway, N. D., The Role of Phosphatidylcholine and Choline Metabolites to Cell Proliferation and Survival. *Critical Reviews in Biochemistry and Molecular Biology* **2013**, *48*, 20-38.

111. Leventis, P. A.; Grinstein, S., The Distribution and Function of Phosphatidylserine in Cellular Membranes. *Annual Review of Biophysics* **2010**, *39*, 407-427.

112. Cui, Z.; Houweling, M., Phosphatidylcholine and Cell Death. *Biochimica et Biophysica Acta (BBA) - Molecular and Cell Biology of Lipids* **2002**, *1585*, 87-96.

113. Geiger, O.; López-Lara, I. M.; Sohlenkamp, C., Phosphatidylcholine Biosynthesis and Function in Bacteria. *Biochimica et Biophysica Acta (BBA) - Molecular and Cell Biology of Lipids* **2013**, *1831*, 503-513.

114. Szoka, F.; Papahadjopoulos, D., Comparative Properties and Methods of Preparation of Lipid Vesicles (Liposomes). *Annual Review of Biophysics and Bioengineering* **1980**, *9*, 467-508.

115. Hamai, C.; Cremer, P. S.; Musser, S. M., Single Giant Vesicle Rupture Events Reveal Multiple Mechanisms of Glass-Supported Bilayer Formation. *Biophysical Journal* **2007**, *92*, 1988-1999.

116. Mifflin, A. L., et al., Accurate Line Shapes from Sub-1 Cm–1 Resolution Sum Frequency Generation Vibrational Spectroscopy of A-Pinene at Room Temperature. *The Journal of Physical Chemistry A* **2015**, *119*, 1292-1302.

117. Lu, Z.; Karakoti, A.; Velarde, L.; Wang, W.; Yang, P.; Thevuthasan, S.; Wang, H.-f., Dissociative Binding of Carboxylic Acid Ligand on Nanoceria Surface in Aqueous Solution: A Joint in Situ Spectroscopic Characterization and First-Principles Study. *J. Phys. Chem. C* **2013**, *117*, 24329-24338.

118. Wang, H.-F.; Gan, W.; Lu, R.; Rao, Y.; Wu, B.-H., Quantitative Spectral and Orientational Analysis in Surface Sum Frequency Generation Vibrational Spectroscopy (Sfg-Vs). *International Reviews in Physical Chemistry* **2005**, *24*, 191-256.

119. Blumenthal, D.; Goldstien, L.; Edidin, M.; Gheber, L. A., Universal Approach to Frap Analysis of Arbitrary Bleaching Patterns. *Scientific Reports* **2015**, *5*, 11655.

120. Olenick, L. L.; Chase, H. M.; Fu, L.; Zhang, Y.; McGeachy, A. C.; Dogangun, M.; Walter, S. R.; Wang, H.-f.; Geiger, F. M., Single-Component Supported Lipid Bilayers Probed Using Broadband Nonlinear Optics. *Physical Chemistry Chemical Physics* **2017**.

121. Bozich, J. S.; Lohse, S. E.; Torelli, M. D.; Murphy, C. J.; Hamers, R. J.; Klaper, R. D., Surface Chemistry, Charge and Ligand Type Impact the Toxicity of Gold Nanoparticles to Daphnia Magna. *Environmental Science: Nano* **2014**, *1*, 260-270.

122. Troiano, J. M., et al., Direct Probes of 4 Nm Diameter Gold Nanoparticles Interacting with Supported Lipid Bilayers. *J. Phys. Chem. C* **2015**, *119*, 534-546.

123. Qiu, T. A.; Torelli, M. D.; Vartanian, A. M.; Rackstraw, N. B.; Jacob, L. M.; Buchman, J. T.; Murphy, C. J.; Hamers, R. J.; Haynes, C. L., Quantification of Free Ligands Present in Colloidal Suspension Reveals Source of Toxic Responses for Polyelectrolyte-Wrapped 4-Nm-Diameter Gold Nanoparticles. *Analytical Chemistry* **2017**, *89*, 1823-1830.

124. Marrink, S. J.; Risselada, H. J.; Yefimov, S.; Tieleman, D. P.; Vries, A. H. d., The Martini Force Field: Coarse Grained Model for Biomolecular Simulations. *J. Phys. Chem. B* **2007**, *111*, 7812-7824.

125. Yesylevskyy, S. O.; Schafer, L. V.; Sengupta, D.; Marrink, S. J., Polarizable Water Model for the Coarse-Grained Martini Force Field. *PLoS Comp. Biol.* **2010**, *6*, e1000810.

126. Lehn, R. C. V.; Alexander-Katz, A., Penetration of Lipid Bilayers by Nanoparticles with Environmentally-Responsive Surfaces: Simulations and Theory. *Soft Matt.* **2011**, *7*, 11392-11404.

127. Rossi, G.; Monticelli, L.; Puisto, S. R.; Vattulainen, I.; Ala-Nissila, T., Coarse-Graining Polymers with the Martini Force Field: Polysteyrene as a Benchmark Case. *Soft Matt.* **2011**, *7*, 698-708.

128. Troiano, J. M., et al., Quantifying the Electrostatics of Polycation–Lipid Bilayer Interactions. *J. Am. Chem. Soc.* **2017**, *in press*.

129. Troiano, J., et al., Direct Probes of 4-Nm Diameter Gold Nanoparticles Interacting with Supported Lipid Bilayers. *J. Phys. Chem C* **2014**, *119*, 534-546.

130. Olenick, L. L., et al., Lipid Corona Formation from Nanoparticle Interactions with Bilayers and Membrane-Specific Biological Outcomes. **2017**, In Revision.

131. Frenkel, D.; Smit, B., *Understanding Molecular Simulation: From Algorithms to Applications*; Academic Press, 2001.

132. Berendsen, H. J. C.; Postma, J. P. M.; van Gunsteren, W. F.; Di Nola, A.; Haak, J. R., Molecular Dynamics with Coupling to an External Bath. *J. Chem. Phys.* **1984**, *81*, 3684-3690.

133. Rand, D.; Ortiz, V.; Liu, Y.; Derdak, Z.; Wands, J. R.; Tatíček, M.; Rose-Petruck, C., Nanomaterials for X-Ray Imaging: Gold Nanoparticle-Enhancement of X-Ray Scatter Imaging of Hepatocellular Carcinoma. *Nano letters* **2011**, *11*, 2678-2683.

134. Lohse, S. E.; Eller, J. R.; Sivapalan, S. T.; Plews, M. R.; Murphy, C. J., A Simple Millifluidic Benchtop Reactor System for the High-Throughput Synthesis and Functionalization of Gold Nanoparticles with Different Sizes and Shapes. *ACS Nano* **2013**, *7*, 4135-4150.

135. Chen, Y.; Jena, K. C.; Roke, S., From Hydrophobic to Hydrophilic: The Structure and Density of the Hexadecane Droplet/Alkanol/Water Interface. *The Journal of Physical Chemistry C* **2015**, *119*, 17725-17734.

136. Scheu, R.; Rankin, B. M.; Chen, Y.; Jena, K. C.; Ben-Amotz, D.; Roke, S., Charge Asymmetry at Aqueous Hydrophobic Interfaces and Hydration Shells. *Angewandte Chemie International Edition* **2014**, *53*, 9560-9563.

137. Mabrey, S.; Sturtevant, J. M., Investigation of Phase Transitions of Lipids and Lipid Mixtures by Sensitivity Differential Scanning Calorimetry. *Proceedings of the National Academy of Sciences* **1976**, *73*, 3862-3866.

138. de Aguiar, H. B.; Strader, M. L.; de Beer, A. G. F.; Roke, S., Surface Structure of Sodium Dodecyl Sulfate Surfactant and Oil at the Oil-in-Water Droplet Liquid/Liquid Interface. A Manifestation of a Nonequilibrium Surface State. *The Journal of Physical Chemistry B* **2011**, *115*, 2970-2978.

139. de Aguiar, H. B.; Scheu, R.; Jena, K. C.; de Beer, A. G. F.; Roke, S., Comparison of Scattering and Reflection Sfg: A Question of Phase-Matching. *Physical Chemistry Chemical Physics* **2012**, *14*, 6826-6832.

140. Scheu, R.; Chen, Y.; Subinya, M.; Roke, S., Stern Layer Formation Induced by Hydrophobic Interactions: A Molecular Level Study. *Journal of the American Chemical Society* **2013**, *135*, 19330-19335.

141. Roke, S.; Gonella, G., Nonlinear Light Scattering and Spectroscopy of Particles and Droplets in Liquids. *Annual Review of Physical Chemistry* **2012**, *63*, 353-378.

Chapter 3 References

1. Chan, Y.-H. M.; Boxer, S. G., Model Membrane Systems and Their Applications. *Current Opinion in Chemical Biology* **2007**, *11*, 581-587.

2. Plant, A. L., Supported Hybrid Bilayer Membranes as Rugged Cell Membrane Mimics. *Langmuir* **1999**, *15*, 5128-5135.

3. Kasemo, B., Biological Surface Science. *Surface Science Reports* **2002**, *500*, 656-677.

4. Groves, J. T.; Dustin, M. L., Supported Planar Bilayers in Studies on Immune Cell Adhesion and Communication. *Journal of Immunological Methods* **2003**, *278*, 19-32.

5. Nel, A. E.; Madler, L.; Velegol, D.; Xia, T.; Hoek, E. M. V.; Somasundaran, P.; Klaessig, F.; Castranova, V.; Thompson, M., Understanding Biophysicochemical Interactions at the Nano-Bio Interface. *Nature Materials* **2009**, *8*, 543-557.

6. Milhaud, J., New Insights into Water–Phospholipid Model Membrane Interactions. *Biochimica et Biophysica Acta (BBA) - Biomembranes* **2004**, *1663*, 19-51.

7. Tristram-Nagle, S.; Nagle, J. F., Lipid Bilayers: Thermodynamics, Structure, Fluctuations, and Interactions. *Chemistry and Physics of Lipids* **2004**, *127*, 3-14.

8. Liu, W.; Wang, Z.; Fu, L.; Leblanc, R. M.; Yan, E. C. Y., Lipid Compositions Modulate Fluidity and Stability of Bilayers: Characterization by Surface Pressure and Sum Frequency Generation Spectroscopy. *Langmuir* **2013**, *29*, 15022-15031.

9. Troiano, J. M., et al., Direct Probes of 4 Nm Diameter Gold Nanoparticles Interacting with Supported Lipid Bilayers. *The Journal of Physical Chemistry C* **2015**, *119*, 534-546.

10. Liu, J.; Conboy, J. C., 1,2-Diacyl-Phosphatidylcholine Flip-Flop Measured Directly by Sum-Frequency Vibrational Spectroscopy. *Biophys. J.* **2005**, *89*, 2522-2532.

11. Liu, J.; Conboy, J. C., Phase Transition of a Single Lipid Bilayer Measured by Sum-Frequency Vibrational Spectroscopy. *Journal of the American Chemical Society* **2004**, *126*, 8894-8895.

12. Hu, P.; Quian, W.; Liu, B.; Pichan, C.; Chen, Z., Molecular Interactions between Gold Nanoparticles and Model Cell Membranes: A Study of Nanoparticle Surface Charge Effect. *J. Phys. Chem. C* **2016**, *120*, 22718-22729.

13. Buchbinder, A. M.; al, e., Method for Evaluating Vibrational Mode Assignments in Surface-Bound Cyclic Hydrocarbons Using Sum-Frequency Generation. *J. Phys. Chem. C* **2011**, *115*, 18284-18294.

14. Ebben, C. J.; Strick, B. F.; Upshur, M. A.; Chase, H. M.; Achtyl, J. L.; Thomson, R. J.; Geiger, F. M., Towards the Identification of Molecular Constituents Associated with the Surfaces of Isoprene-Derived Secondary Organic Aerosol (Soa) Particles. *Atmospheric Chemistry and Physics* **2014**, *14*, 2303-2314.

15. Moad, A. J.; Simpson, G. J., A Unified Treatment of Selection Rules and Symmetry Relations for Sum-Frequency and Second Harmonic Spectroscopies. *J. Phys. Chem. B* **2004**, *108*, 3548-3562.

16. Wang, H.-F.; Gan, W.; Lu, R.; Rao, Y.; Wu, B.-H., Quantitative Spectral and Orientational Analysis in Surface Sum Frequency Generation Vibrational Spectroscopy (Sfg-Vs). *International Reviews in Physical Chemistry* **2005**, *24*, 191-256.

17. Xu, M.; Liu, D.; Allen, H. C., Ethylenediamine at Air/Liquid and Air/Silica Interfaces: Protonation Versus Hydrogen Bonding Investigated by Sum Frequency Generation Spectroscopy. *Environ. Sci. Technol.* **2006**, *40*, 1566-1572.

18. Olenick, L. L.; Chase, H. M.; Fu, L.; Zhang, Y.; McGeachy, A. C.; Dogangun, M.; Walter, S. R.; Wang, H.-f.; Geiger, F. M., Single-Component Supported Lipid Bilayers Probed Using Broadband Nonlinear Optics. *Physical Chemistry Chemical Physics* **2017**.

19. Simpson, G. J.; Rowlen, K. L., An Shg Magic Angle: Dependence of Second Harmonic Generation Orientation Measurements on the Width of the Orientation Distribution. *J. Am. Chem. Soc.* **1999**, *121*, 2635-2636.

20. Liu, J.; Conboy, J. C., Structure of a Gel Phase Lipid Bilayer Prepared by the Langmuir-Blodgett/Langmuir-Schaefer Method Characterized by Sum-Frequency Vibrational Spectroscopy. *Langmuir* **2005**, *21*, 9091-9097.

21. Reviakine, I.; Brisson, A., Formation of Supported Phospholipid Bilayers from Unilamellar Vesicles Investigated by Atomic Force Microscopy. *Langmuir* **2000**, *16*, 1806-1815.

22. Richter, R.; Mukhopadhyay, A.; Brisson, A., Pathways of Lipid Vesicle Deposition on Solid Surfaces: A Combined Qcm-D and Afm Study. *Biophysical Journal* **2003**, *85*, 3035-3047.

23. Scomparin, C.; Lecuyer, S.; Ferreira, M.; Charitat, T.; Tinland, B., Diffusion in Supported Lipid Bilayers: Influence of Substrate and Preparation Technique on the Internal Dynamics. *The European Physical Journal E* **2009**, *28*, 211-220.

24. Tamm, L. K.; McConnell, H. M., Supported Phospholipid Bilayers. *Biophysical Journal* **1985**, *47*, 105-113.

25. Ratto, T. V.; Longo, M. L., Obstructed Diffusion in Phase-Separated Supported Lipid Bilayers: A Combined Atomic Force Microscopy and Fluorescence Recovery after Photobleaching Approach. *Biophysical Journal* **2002**, *83*, 3380-3392.

26. Almeida, P. F.; Vaz, W. L., Lateral Diffusion in Membranes. *Handbook of biological physics* **1995**, *1*, 305-357.

27. Chen, L.; Yu, Z.; Quinn, P. J., The Partition of Cholesterol between Ordered and Fluid Bilayers of Phosphatidylcholine: A Synchrotron X-Ray Diffraction Study. *Biochimica et Biophysica Acta (BBA) - Biomembranes* **2007**, *1768*, 2873-2881.

28. Hac, A. E.; Seeger, H. M.; Fidorra, M.; Heimburg, T., Diffusion in Two-Component Lipid Membranes—a Fluorescence Correlation Spectroscopy and Monte Carlo Simulation Study. *Biophysical Journal* **2005**, *88*, 317-333.

29. Harb, F.; Simon, A.; Tinland, B., Ripple Formation in Unilamellar-Supported Lipid Bilayer Revealed by Frapp. *The European Physical Journal E* **2013**, *36*, 140.

30. Zhang, L.; Granick, S., Dynamical Heterogeneity in Supported Lipid Bilayers. *MRS Bulletin* **2011**, *31*, 527-531.

31. Zhu, Y.; Moran-Mirabal, J., Micropatterning of Phase-Segregated Supported Lipid Bilayers and Binary Lipid Phases through Polymer Stencil Lift-Off. *Langmuir* **2016**, *32*, 11021-11028.

32. Madrid, W.; Horswell, S. L., Effect of Deuteration on Phase Behavior of Supported Phospholipid Bilayers: A Spectroelectrochemical Study. *Langmuir* **2015**, *31*, 12544-12551.

33. Yamaji-Hasegawa, A.; Tsujimoto, M., Asymmetric Distribution of Phospholipids in Biomembranes. *Biol. Pharm. Bull.* **2006**, *29*, 1547-1553.

34. Leventis, P. A.; Grinstein, S., The Distribution and Function of Phosphatidylserine in Cellular Membranes. *Annual Review of Biophysics* **2010**, *39*, 407-427.

35. Dowhan, W., Molecular Basis for Membrane Phospholipid Diversity:Why Are There So Many Lipids? *Annual Review of Biochemistry* **1997**, *66*, 199-232.

36. Trandum, C.; Westh, P.; Jørgensen, K.; Mouritsen, O. G., A Thermodynamic Study of the Effects of Cholesterol on the Interaction between Liposomes and Ethanol. *Biophysical Journal*, *78*, 2486-2492.

37. Petralli-Mallow, T. P.; Plant, A. L.; Lewis, M. L.; Hicks, J. M., Cytochrome C at Model Membrane Surfaces: Exploration Via Second Harmonic Generation-Circular Dichroism and Surface-Enhanced Resonance Raman Spectroscopy. *Langmuir* **2000**, *16*, 5960-5966.

38. Salafsky, J. S.; Eisenthal, K. B., Protein Adsorption at Interfaces Detected by Second Harmonic Generation. *J. Phys. Chem. B* **2000**, *104*, 7752-7755.

39. Liu, J.; Subir, M.; Nguyen, K.; Eisenthal, K. B., Second Harmonic Studies of Ions Crossing Liposome Membranes in Real Time. *J. Phys. Chem. B* **2008**, *112*, 15263-15266.

40. Anglin, T. C.; Liu, J.; Conboy, J. C., Facile Lipid Flip-Flop in a Phospholipid Bilayer Induced by Gramicidin a Measured by Sum-Frequency Vibrational Spectroscopy. *Biophysical Journal* **2007**, *92*, L1-L3.

41. Kim, G.; Gurau, M. C.; Lim, S.-M.; Cremer, P. S., Investigations of the Orientation of a Membrane Peptide by Sum Frequency Spectroscopy. *J. Phys. Chem. B* **2003**, *107*, 1403-1409.

Chapter 4 References

1. Cedervall, T.; Lynch, I.; Lindman, S.; Berggard, T.; Thulin, E.; Nilsson, H.; Dawson, K. A.; Linse, S., Understanding the Nanoparticle-Protein Corona Using Methods to Quantify Exchange Rates and Affinities of Proteins for Nanoparticles. *Proc. Natl. Acad. Sci.* **2007**, *104*, 2050-2055.

2. Liu, J. Q.; Zhang, Q.; Remsen, E. E.; Wooley, K. L., Nanostructured Materials Designed for Cell Binding and Transduction. *Biomacromolecules* **2001**, *2*, 362-368.

3. Docter, D.; Westmeier, D.; Markiewicz, M.; Stolte, S.; Knauer, S. K.; Staubert, R. H., The Nanoparticle Biomolecule Corona: Lessons Learned – Challenge Accepted? *Chem. Soc. Rev.* **2015**, *44*, 6096-6121.

4. Westmeier, D.; Stauber, R. H.; Docter, D., The Concept of Bio-Corona in Modulating the Toxicity of Engineered Nanomaterials (Enm). *Toxicology and Applied Pharmacology* **2016**, *299*, 53-57.

5. Salvati, A.; Pitek, A. S.; Monopoli, M. P.; Prapainop, K.; Bombelli, F. B.; Hristov, D. R.; Kelly, P. M.; Aberg, C.; Mahon, E.; Dawson, K. A., Transferrin-Functionalized Nanoparticles Lose Their Targeting Capabilities When a Biomolecular Corona Adsorbs on the Surface. *Nature Nanotechnology* **2013**, *8*, 137-143.

6. Lesniak, A.; Fenaroli, F.; Monopoli, M. P.; Aberg, C.; Dawson, K. A.; Salvati, A., Effects of Presence or Absence of a Protein Corona on Silica Nanoparticle Uptake and Impact on Cells. *ACS Nano* **2012**, *6*, 5845-57.

7. Hellstrand, E.; Lynch, I.; Andersson, A.; Drakenberg, T.; Dahlback, B.; Dawson, K. A.; Linse, S.; Cedervall, T., Complete High-Density Lipoproteins in Nanoparticle Corona. *FEBS* **2009**, *276*, 3372-81.

8. Guo, Y.; Terrazzi, E.; Seemann, R.; Fleury, J. B.; Baulin, V. A., Direct Proof of Spontaneous Translocation of Lipid-Covered Hydrophobic Nanoparticles through a Phospholipid Bilayer. *Science Advances* **2016**, *2*, e1600261.

9. Xu, F. D.; Reiser, M.; Yu, X. W.; Gummuluru, S.; Wetzler, L.; Reinhard, B. M., Lipid-Mediated Targeting with Membrane Wrapped Nanoparticles in the Presence of Corona Formation. *ACS Nano* **2016**, *10*, 1189-1200.

10. Bahrami, A. H.; Raatz, M.; Agudo-Canalejo, J.; Michel, R.; Curtis, E. M.; Hall, C. K.; Gradzielski, M.; Lipowsky, R.; Weikl, T. R., Wrapping of Nanoparticles by Membranes. *Adv. Colloid Interface Sci.* **2014**, *208*, 214-224.

11. Zhang, S. L.; Gao, H.; Bao, G., Physical Principles of Nanoparticle Cellular Endocytosis. *ACS Nano* **2015**, *9*, 8655-8671.

12. Milani, S.; Bombelli, F. B., Reversible Versus Irreversible Binding of Transferrin to Polystyrene Nanoparticles: Soft and Hard Corona. **2012**.

13. Sachan, A. K.; Harishchandra, R. K.; Bantz, C.; Maskos, M.; Reichelt, R.; Galla, H.-J., High-Resolution Investigation of Nanoparticle Interaction with a Model Pulmonary Surfactant Monolayer. *ACS Nano* **2012**, *2*, 1677-1687.

14. Raesch, S. S.; Tenzer, S.; Storck, W.; Rurainski, A.; Selzer, D.; Ruge, C. A.; Perez-Gil, J.; Schaefer, U. F.; Lehr, C.-M., Proteomic and Lipidomic Analysis of Nanoparticle Corona Upon Contact with Lung Surfactant Reveals Differences in Protein, but Not Lipid Composition. *ACS Nano* **2015**, *12*, 11872-11885.

15. Kapralov, A. A., et al., Adsorption of Surfactant Lipids by Single-Walled Carbon Nanotubes in Mouse Lung Upon Pharyngeal Aspiration. *ACS Nano* **2012**, *6*, 4147-4156.

16. Casper, C. B.; Verreault, D.; Adams, E. M.; Hua, W.; Allen, H. C., Surface Potential of Dppc Monolayers on Concentrated Aqueous Salt Solutions. *Journal of Physical Chemistry B* **2016**, *120*, 2043-2052.

17. Bornholdt, Z. A.; Noda, T.; Abelson, D. M.; Halfmann, P.; Wood, M. R.; Kawaoka, Y.; Saphire, E. O., Structural Rearrangement of Ebola Virus Vp40 Begets Multiple Functions in the Virus Life Cycle. *Cell* **2013**, *154*, 763-774.

18. Dessen, A.; Volchkov, V.; Dolnik, O.; Klenk, H.-D.; Weissenhorn, W., Crystal Structure of the Matrix Protein Vp40 from Ebola Virus. *EMBO* **2000**, *19*, 4228.

19. Hu, M.; Stanzione, F.; Sum, A. K.; Faller, R.; Deserno, M., Design Principles for Nanoparticles Enveloped by a Polymer-Tethered Lipid Membrane. *ACS Nano* **2015**, *9*, 9942-9954.

20. Spangler, E. J.; Upreti, S.; Laradji, M., Partial Wrapping and Spontaneous Endocytosis of Spherical Nanoparticles by Tensionless Lipid Membranes. *J. Chem. Phys.* **2016**, *144*, 044901.

21. Van Lehn, R. C.; Ricci, M.; Silva, P. H. J.; Andreozzi, P.; Reguera, J.; Voïtchovsky, K.; Stellacci, F.; Alexander-Katz, A., Lipid Tail Protrusions Mediate the Insertion of Nanoparticles into Model Cell Membranes. **2014**, *5*, 4482.

22. Cui, Q.; Hernandez, R.; Mason, S. E.; Fraunheim, T.; Pedersen, J. A.; Geiger, F. M., Sustainable Nanotechnology: Opportunities and Challenges for Theoretical/Computational Studies. *J. Phys. Chem. B* **2016**, *120*, 7297-7306.

23. Dreaden, E. C.; Alkilany, A. M.; Huang, X. H.; Murphy, C. J.; El-Sayed, M. A., The Golden Age: Gold Nanoparticles for Biomedicine. *Chem. Soc. Rev.* **2012**, *41*, 2740-2779.

24. Qiu, T. A.; Torelli, M. D.; Vartanian, A. M.; Rackstraw, N. B.; Jacob, L. M.; Buchman, J. T.; Murphy, C. J.; Hamers, R. J.; Haynes, C. L., Quantification of Free Ligands Present in Colloidal Suspension Reveals Source of Toxic Responses for Polyelectrolyte-Wrapped 4-Nm-Diameter Gold Nanoparticles. *Analytical Chemistry* **2017**, *89*, 1823-1830.

25. Martinez-Morales, F.; Schobert, M.; Lopez-Lara, I. M.; Geiger, O., Pathways for Phosphatidylcholine Biosynthesis in Bacteria. *Microbiology* **2003**, *149*, 3461-3471.

26. Geiger, O.; López-Lara, I. M.; Sohlenkamp, C., Phosphatidylcholine Biosynthesis and Function in Bacteria. *Biochimica et Biophysica Acta (BBA) - Molecular and Cell Biology of Lipids* **2013**, *1831*, 503-513.

27. Troiano, J. M., et al., Direct Probes of 4 Nm Diameter Gold Nanoparticles Interacting with Supported Lipid Bilayers. *The Journal of Physical Chemistry C* **2015**, *119*, 534-546.

28. Bozich, J. S.; Lohse, S. E.; Torelli, M. D.; Murphy, C. J.; Hamers, R. J.; Klaper, R. D., Surface Chemistry, Charge and Ligand Type Impact the Toxicity of Gold Nanoparticles to Daphnia Magna. *Environmental Science: Nano* **2014**, *1*, 260-270.

29. Troiano, J. M., et al., Direct Probes of 4 Nm Diameter Gold Nanoparticles Interacting with Supported Lipid Bilayers. *J. Phys. Chem. C* **2015**, *119*, 534-546.

30. Kalb, E.; Frey, S.; Tamm, L. K., Formation of Supported Planar Bilayers by Fusion of Vesicles to Supported Phospholipid Monolayers. *Biochimica et Biophysica Acta (BBA) - Biomembranes* **1992**, *1103*, 307-316.

31. Schönherr, H.; Johnson, J. M.; Lenz, P.; Frank, C. W.; Boxer, S. G., Vesicle Adsorption and Lipid Bilayer Formation on Glass Studied by Atomic Force Microscopy. *Langmuir* **2004**, *20*, 11600-11606.

32. Marrink, S. J.; Risselada, H. J.; Yefimov, S.; Tieleman, D. P.; Vries, A. H. d., The Martini Force Field: Coarse Grained Model for Biomolecular Simulations. *J. Phys. Chem. B* **2007**, *111*, 7812-7824.

33. Yesylevskyy, S. O.; Schafer, L. V.; Sengupta, D.; Marrink, S. J., Polarizable Water Model for the Coarse-Grained Martini Force Field. *PLoS Comp. Biol.* **2010**, *6*, e1000810.

34. Lehn, R. C. V.; Alexander-Katz, A., Penetration of Lipid Bilayers by Nanoparticles with Environmentally-Responsive Surfaces: Simulations and Theory. *Soft Matt.* **2011**, *7*, 11392-11404.

35. Rossi, G.; Monticelli, L.; Puisto, S. R.; Vattulainen, I.; Ala-Nissila, T., Coarse-Graining Polymers with the Martini Force Field: Polysteyrene as a Benchmark Case. *Soft Matt.* **2011**, *7*, 698-708.

36. Troiano, J. M., et al., Quantifying the Electrostatics of Polycation–Lipid Bilayer Interactions. *J. Am. Chem. Soc.* **2017**, *in press*.

37. Troiano, J., et al., Direct Probes of 4-Nm Diameter Gold Nanoparticles Interacting with Supported Lipid Bilayers. *J. Phys. Chem C* **2014**, *119*, 534-546.

38. Olenick, L. L., et al., Lipid Corona Formation from Nanoparticle Interactions with Bilayers and Membrane-Specific Biological Outcomes. **2017**, Under Review.

39. Frenkel, D.; Smit, B., *Understanding Molecular Simulation: From Algorithms to Applications*; Academic Press, 2001.

40. Berendsen, H. J. C.; Postma, J. P. M.; van Gunsteren, W. F.; Di Nola, A.; Haak, J. R., Molecular Dynamics with Coupling to an External Bath. *J. Chem. Phys.* **1984**, *81*, 3684-3690.

41. Zhu, X. D.; Suhr, H. J.; Shen, Y. R., Surface Vibrational Spectroscopy by Infrared-Visible Sum-Frequency Generation. *J. Opt. Soc. America B-Optical Physics* **1986**, *3*, P252.

42. Walker, R. A.; Conboy, J. C.; Richmond, G. L., Molecular Structure and Ordering of Phospholipids at a Liquid−Liquid Interface. *Langmuir* **1997**, *13*, 3070-3073.

43. Liu, J.; Conboy, J. C., Direct Measurement of the Transbilayer Movement of Phospholipids by Sum-Frequency Vibrational Spectroscopy. *J. Am. Chem. Soc.* **2004**, *126*, 8376-8377.

44. Richter, L. J.; Petralli-Mallow, T. P.; Stephenson, J. C., Vibrationally Resolved Sum-Frequency Generation with Broad-Bandwidth Infrared Pulses. *Opt. Lett.* **1998**, *23*, 1594-1596.

45. Troiano, J. M.; Kuech, T. R.; Vartanian, A. M.; Torelli, M. D.; Sen, A.; Jacob, L. M.; Hamers, R. J.; Murphy, C. J.; Pedersen, J. A.; Geiger, F. M., On Electronic and Charge Interference in Second Harmonic Generation Responses from Gold Metal Nanoparticles at Supported Lipid Bilayers. *The Journal of Physical Chemistry C* **2016**.

46. Wang, B.; Zhang, L.; Bae, S. C.; Granick, S., Nanoparticle-Induced Surface Reconstruction of Phospholipid Membranes. In *Proceedings of the National Academy of Sciences*, 1345043428 ed.; National Acad Sciences: 2008; Vol. 105, pp 18171-18175.

47. Vaz, W. L. C.; Goodsaid-Zalduondo, F.; Jacobson, K., Lateral Diffusion of Lipids and Proteins in Bilayer Membranes. *Federation of European Biochemical Societies* **1984**, *174*, 199-207.

48. Feng, Z. V., et al., Impacts of Gold Nanoparticle Charge and Ligand Type on Surface Binding and Toxicity to Gram-Negative and Gram-Positive Bacteria. *Chemical Science* **2015**, *6*, 5186-5196.

49. Qiu, T. A., et al., Gene Expression as an Indicator of the Molecular Response and Toxicity in the Bacterium Shewanella Oneidensis and the Water Flea Daphnia Magna Exposed to Functionalized Gold Nanoparticles. *Environmental Science: Nano* **2015**, *2*, 615-629.

50. Dominguez, G. A.; Lohse, S. E.; Torelli, M. D.; Murphy, C. J.; Hamers, R. J.; Orr, G.; Klaper, R. D., Effects of Charge and Surface Ligand Properties of Nanoparticles on Oxidative Stress and Gene Expression within the Gut of Daphnia Magna. *Aquatic Toxicology* **2015**, *162*, 1-9.

51. Nel, A.; Xia, T.; Mädler, L.; Li, N., Toxic Potential of Materials at the Nanolevel. *Science* **2006**, *311*, 622-627.

52. Maynard, A. D., et al., Safe Handling of Nanotechnology. *Nature* **2006**, *444*, 267-269.

53. Lead, J. R.; Smith, E., *Envrionmental and Human Health Impacts of Nanotechnology*. John Wiley & Sons: United Kingdom, 2009.

54. Westerhoff, P.; B., N., Searching for Global Descriptors of Engineered Nanomaterial Fate and Transport in the Environment. *Acc. Chem. Res.* **2013**, *46*, 844-853.

55. Ferry, J. L., et al., Transfer of Gold Nanoparticles from the Water Column to the Estuarine Food Web. *Nature Nanotechnology* **2009**, *4*, 441-444.

Chapter 5 References

1. Gole, A.; Murphy, C. J., Polyelectrolyte-Coated Gold Nanorods: Synthesis, Characterization and Immobilization. *Chemistry of Materials* **2005**, *17*, 1325-1330.

2. Schmaljohann, D., Thermo- and Ph-Responsive Polymers in Drug Delivery. *Advanced Drug Delivery Reviews* **2006**, *58*, 1655-1670.

3. Carmona-Ribeiro, A.; de Melo Carrasco, L., Cationic Antimicrobial Polymers and Their Assemblies. *International Journal of Molecular Sciences* **2013**, *14*, 9906.

4. Bruno, M. M.; Cotella, N. G.; Miras, M. C.; Barbero, C. A., A Novel Way to Maintain Resorcinol–Formaldehyde Porosity During Drying: Stabilization of the Sol–Gel Nanostructure Using a Cationic Polyelectrolyte. *Colloids and Surfaces A: Physicochemical and Engineering Aspects* **2010**, *362*, 28-32.

5. Qiu, T. A.; Torelli, M. D.; Vartanian, A. M.; Rackstraw, N. B.; Jacob, L. M.; Buchman, J. T.; Murphy, C. J.; Hamers, R. J.; Haynes, C. L., Quantification of Free Ligands Present in Colloidal Suspension Reveals Source of Toxic Responses for Polyelectrolyte-Wrapped 4-Nm-Diameter Gold Nanoparticles. *Analytical Chemistry* **2017**, *89*, 1823-1830.

6. Fischer, D.; Li, Y.; Ahlemeyer, B.; Krieglstein, J.; Kissel, T., In Vitro Cytotoxicity Testing of Polycations: Influence of Polymer Structure on Cell Viability and Hemolysis. *Biomaterials* **2003**, *24*, 1121-1131.

7. Chew, S. A.; Hacker, M. C.; Saraf, A.; Raphael, R. M.; Kasper, F. K.; Mikos, A. G., Biodegradable Branched Polycationic Polymers with Varying Hydrophilic Spacers for Nonviral Gene Delivery. *Biomacromolecules* **2009**, *10*, 2436-2445.

8. Helander, I. M.; Nurmiaho-Lassila, E. L.; Ahvenainen, R.; Rhoades, J.; Roller, S., Chitosan Disrupts the Barrier Properties of the Outer Membrane of Gram-Negative Bacteria. *International Journal of Food Microbiology* **2001**, *71*, 235-244.

9. Fasbender, A.; Zabner, J.; Chillon, M.; Moninger, T. O.; Puga, A. P.; Davidson, B. L.; Welsh, M. J., Complexes of Adenovirus with Polycationic Polymers and Cationic Lipids Increase the Efficiency of Gene Transfer in Vitro and in Vivo. *The Journal of biological chemistry* **1997**, *272*, 6479-89.

10. Mecke, A.; Lee, D.-K.; Ramamoorthy, A.; Orr, B. G.; Banaszak Holl, M. M., Synthetic and Natural Polycationic Polymer Nanoparticles Interact Selectively with Fluid-Phase Domains of Dmpc Lipid Bilayers. *Langmuir* **2005**, *21*, 8588-8590.

11. Hong, S.; Leroueil, P. R.; Janus, E. K.; Peters, J. L.; Kober, M.-M.; Islam, M. T.; Orr, B. G.; Baker, J. R.; Banaszak Holl, M. M., Interaction of Polycationic Polymers with Supported Lipid Bilayers and Cells: Nanoscale Hole Formation and Enhanced Membrane Permeability. *Bioconjugate Chemistry* **2006**, *17*, 728-734.

12. Zhang, Z.-Y.; Smith, B. D., High-Generation Polycationic Dendrimers Are Unusually Effective at Disrupting Anionic Vesicles: Membrane Bending Model. *Bioconjugate Chemistry* **2000**, *11*, 805-814.

13. Davydov, D. A.; Romanyuk, A. V.; Rakhnyanskaya, A. A.; Semenyuk, P. I.; Orlov, V. N.; Samoshin, V. V.; Yaroslavov, A. A., Cationic Polymer Adsorption on Bilayer Membrane Containing Anionic and Cationic Lipids. *Colloid Journal* **2011**, *73*, 33-38.

14. Troiano, J. M., et al., Quantifying the Electrostatics of Polycation–Lipid Bilayer Interactions. *Journal of the American Chemical Society* **2017**, *139*, 5808-5816.

15. Roke, S.; Gonella, G., Nonlinear Light Scattering and Spectroscopy of Particles and Droplets in Liquids. *Annual Review of Physical Chemistry* **2012**, *63*, 353-378.

16. Liu, J.; Conboy, J. C., 1,2-Diacyl-Phosphatidylcholine Flip-Flop Measured Directly by Sum-Frequency Vibrational Spectroscopy. *Biophysical Journal* **2005**, *89*, 2522-2532.

17. Anglin, T. C.; Conboy, J. C., Kinetics and Thermodynamics of Flip-Flop in Binary Phospholipid Membranes Measured by Sum-Frequency Vibrational Spectroscopy. *Biochemistry* **2009**, *48*, 10220-10234.

18. Anglin, T. C.; Cooper, M. P.; Li, H.; Chandler, K.; Conboy, J. C., Free Energy and Entropy of Activation for Phospholipid Flip-Flop in Planar Supported Lipid Bilayers. *The Journal of Physical Chemistry B* **2010**, *114*, 1903-1914.

19. Wu, H.-L.; Tong, Y.; Peng, Q.; Li, N.; Ye, S., Phase Transition Behaviors of the Supported Dppc Bilayer Investigated by Sum Frequency Generation (Sfg) Vibrational Spectroscopy and Atomic Force Microscopy (Afm). *Physical Chemistry Chemical Physics* **2016**, *18*, 1411-1421.

20. Liu, J.; Conboy, J. C., Phase Behavior of Planar Supported Lipid Membranes Composed of Cholesterol and 1,2-Distearoyl-Sn-Glycerol-3-Phosphocholine Examined by Sum-Frequency Vibrational Spectroscopy. *Vibrational Spectroscopy* **2009**, *50*, 106-115.

21. Liu, J.; Conboy, J. C., Phase Transition of a Single Lipid Bilayer Measured by Sum-Frequency Vibrational Spectroscopy. *Journal of the American Chemical Society* **2004**, *126*, 8894-8895.

22. Troiano, J. M., et al., Direct Probes of 4 Nm Diameter Gold Nanoparticles Interacting with Supported Lipid Bilayers. *The Journal of Physical Chemistry C* **2014**, *119*, 534-546.

23. Liu, Y.; Yan, C. Y.; Zhao, X. L.; Eisenthal, K. B., Surface Potential of Charged Liposomes Determined by Second Harmonic Generation. *Langmuir* **2001**, *17*, 2063-2066.

24. Eisenthal, K. B., Liquid Interfaces Probed by Second-Harmonic and Sum-Frequency Spectroscopy. *Chem. Rev.* **1996**, *96*, 1343-1360.

25. Eisenthal, K. B., Second Harmonic Spectroscopy of Aqueous Nano- and Microparticle Interfaces *Chem. Rev.* **2006**, *106*, 1462-1477.

26. Chen, Y.; Jena, K. C.; Lütgebaucks, C.; Okur, H. I.; Roke, S., Three Dimensional Nano "Langmuir Trough" for Lipid Studies. *Nano Letters* **2015**, *15*, 5558-5563.

27. Smolentsev, N.; Lutgebaucks, C.; Okur, H. I.; de, B. A. G. F.; Roke, S., Intermolecular Headgroup Interaction and Hydration as Driving Forces for Lipid Transmembrane Asymmetry. *Journal of the American Chemical Society* **2016**, *138*, 4053-60.

28. Okur, H. I.; Chen, Y.; Smolentsev, N.; Zdrali, E.; Roke, S., Interfacial Structure and Hydration of 3d Lipid Monolayers in Aqueous Solution. *The Journal of Physical Chemistry B* **2017**, *121*, 2808-2813.

29. Olenick, L. L.; Troiano, J. M.; Smolentsev, N.; Ohno, P. E.; Roke, S.; Geiger, F., Sum Frequency Scattering Spectroscopy of the Interactions of Cationic Polymers and Phospholipid Monolayers on Oil Nanodroplets. **2017**, In Prep.

30. Feldötö, Z.; Varga, I.; Blomberg, E., Influence of Salt and Rinsing Protocol on the Structure of Pah/Pss Polyelectrolyte Multilayers. *Langmuir* **2010**, *26*, 17048-17057.

31. Ibarz, G.; Dähne, L.; Donath, E.; Möhwald, H., Smart Micro- and Nanocontainers for Storage, Transport, and Release. *Advanced Materials* **2001**, *13*, 1324-1327.

32. Fery, A.; Schöler, B.; Cassagneau, T.; Caruso, F., Nanoporous Thin Films Formed by Salt-Induced Structural Changes in Multilayers of Poly(Acrylic Acid) and Poly(Allylamine). *Langmuir* **2001**, *17*, 3779-3783.

33. Boyd, R. W., *Nonlinear Optics*, Third ed.; Academic Press: New York, NY, 2008.

34. Kundu, P.; Agrawal, A.; Mateen, H.; Mishra, I. M., Stability of Oil-in-Water Macro-Emulsion with Anionic Surfactant: Effect of Electrolytes and Temperature. *Chemical Engineering Science* **2013**, *102*, 176-185.

35. Taylor, P., Ostwald Ripening in Emulsions. *Advances in Colloid and Interface Science* **1998**, *75*, 107-163.

36. Thiam, A. R.; Farese, R. V.; Walther, T. C., The Biophysics and Cell Biology of Lipid Droplets. *Nature reviews. Molecular cell biology* **2013**, *14*, 775-786.

37. Kabalnov, A.; Lindman, B.; Olsson, U.; Piculell, L.; Thuresson, K.; Wennerström, H., Microemulsions in Amphiphilic and Polymer-Surfactant Systems. *Colloid Polym Sci* **1996**, *274*, 297-308.

38. Chattopadhyay, A. K.; Mittal, K. L., *Surfactants in Solution*; Taylor & Francis, 1996.

39. Butt, H. J.; Graf, K.; Kappl, M., *Physics and Chemistry of Interfaces*; Wiley, 2003.

40. Kronberg, B.; Holmberg, K.; Lindman, B., *Surface Chemistry of Surfactants and Polymers*; Wiley, 2014.

41. de Beer, A. G. F.; Roke, S.; Dadap, J. I., Theory of Optical Second-Harmonic and Sum-Frequency Scattering from Arbitrarily Shaped Particles. *J. Opt. Soc. Am. B* **2011**, *28*, 1374-1384.

42. Smit, W. J.; Smolentsev, N.; Versluis, J.; Roke, S.; Bakker, H. J., Freezing Effects of Oil-in-Water Emulsions Studied by Sum-Frequency Scattering Spectroscopy. *The Journal of Chemical Physics* **2016**, *145*, 044706.

Chapter 6 References

1. Arico, A. S.; Bruce, P.; Scrosati, B.; Tarascon, J.-M.; van Schalkwijk, W., Nanostructured Materials for Advanced Energy Conversion and Storage Devices. *Nature Materials* **2005**, *4*, 366-377.

2. Smith, T. T.; Stephan, S. B.; Moffett, H. F.; McKnight, L. E.; Ji, W.; Reiman, D.; Bonagofski, E.; Wohlfahrt, M. E.; Pillai, S. P. S.; Stephan, M. T., In Situ Programming of Leukaemia-Specific T Cells Using Synthetic DNA Nanocarriers. *Nature Nanotechnology* **2017**, *12*, 813-820.

3. Park, J., et al., Antimicrobial Spray Nanocoating of Supramolecular Fe(Iii)-Tannic Acid Metal-Organic Coordination Complex: Applications to Shoe Insoles and Fruits. *Scientific Reports* **2017**, *7*, 6980.

4. Zheng, Y., et al., Bioimaging Application and Growth-Promoting Behavior of Carbon Dots from Pollen on Hydroponically Cultivated Rome Lettuce. *ACS Omega* **2017**, *2*, 3958-3965.

5. Cho, R. The Promise and Peril of Nanotechnology. https://phys.org/news/2014-03-peril-nanotechnology.html (accessed August 16, 2017).

6. Lombardo, T. Nanomaterials Produce Better Batteries at Half the Cost. http://www.engineering.com/ElectronicsDesign/ElectronicsDesignArticles/ArticleID/14950/Nanomaterials-Produce-Better-Batteries-at-Half-the-Cost.aspx (accessed August 16, 2017).

7. Bradley, E. L.; Castle, L.; Chaudhry, Q., Applications of Nanomaterials in Food Packaging with a Consideration of Opportunities for Developing Countries. *Trends in Food Science & Technology* **2011**, *22*, 604-610.

8. Ngô, C.; Van de Voorde, M. H., Nanomaterials and Cosmetics. In *Nanotechnology in a Nutshell: From Simple to Complex Systems*, Atlantis Press: Paris, 2014; pp 311-319.

9. Marambio-Jones, C.; Hoek, E. M. V., A Review of the Antibacterial Effects of Silver Nanomaterials and Potential Implications for Human Health and the Environment. *J Nanopart Res* **2010**, *12*, 1531-1551.

10. Halter, M.; Nogata, Y.; Dannenberger, O.; Sasaki, T.; Vogel, V., Engineered Lipids That Cross-Link the Inner and Outer Leaflets of Lipid Bilayers. *Langmuir* **2004**, *20*, 2416-2423.

11. Ross, E. E.; Rozanski, L. J.; Spratt, T.; Liu, S.; O'Brie, D. F.; Saavedra, S. S., Planar Supported Lipid Bilayer Polymers Formed by Vesicle Fusion. 1. Influence of Diene Monomer Structure and Polymerization Method on Film Properties. *Langmuir* **2003**, *19*, 1752-1765.

12. Bhattacharya, S.; Bajaj, A., Recent Advances in Lipid Molecular Design. *Current Opinion in Chemical Biology* **2005**, *9*, 647-655.

LAURA L. OLENICK

lauraolenick@u.northwestern.edu

EDUCATION

Northwestern University, Evanston, IL — *expected* September 2017
Ph.D. Chemistry | GPA 3.78
Certificate, Kellogg School of Management
Program in Management for Scientists and Engineers

Cornell University, Ithaca, NY — August 2009
M.S. Chemical Engineering

Colby College, Waterville, ME — May 2004
B.A. Chemistry, | GPA 3.47, *cum laude*, Dean's List
Minor in Mathematics

School for International Training, Brattleboro, VT — Spring 2003
Ecology and Conservation Study Abroad Program in Botswana.

RESEARCH EXPERIENCE

Graduate Research Assistant, Advisor: Professor Franz Geiger — 2012-*present*
Department of Chemistry, Northwestern University, *Evanston, IL*

- Investigated the interactions of nanomaterials with supported lipid bilayers using Sum Frequency Generation Spectroscopy
- Analyzed fundamental mechanisms behind nanomaterial toxicity using a model membrane system
- Determined effect of lipid phase transition temperature on SFG spectral resolution
- Characterized nanomaterials of various shapes and sizes using UV-Vis, DLS, ζ-potential, TEM
- Collaborated with at least 6 other research groups at various institutions in various disciplines
- Participated in weekly teleconferences with 50+ attendees to update collaborators on research progress
- Engaged in several lab exchanges with collaborators to understand all aspects of joint research
- Traveled to Pacific Northwest National Labs and Ecole Polytechnique Federale de Lausanne where I used specialized laser systems to advance my research
- Contributed to grant proposal and presentation to the NSF which was awarded CCI Phase II funding for the Center for Sustainable Nanotechnology
- Managed lab maintenance, waste, and co-worker instrument schedules; organized lab clean-ups
- Trained new co-workers on several nonlinear optical systems

Research Assistant, Advisor: Professor SonBinh Nguyen — Summer 2012
Department of Chemistry, Northwestern University, *Evanston IL*

- Optimized synthesis of porous organic polymers (POPs) to increase surface area for catalytic reactions.
- Purified POPs using column chromatography and characterized with NMR, MALDI-Tof

Polymer R&D Chemist, Gelest, Inc., *Morrisville, PA* — 2010-2011

- Synthesized, characterized, and evaluated specialty silicones and developed new products and processes
  as part of a research and development team
- Prepared reactions for scale-up by evaluating reactions from the 1 L to 12 L scale
- Characterized product viscosity, color, molecular weight, purity using NMR, GPC, viscometer, rheometer, FT-IR
- Managed and taught a summer intern several reactions and analytical techniques

- Trained to use a forklift and whole-face respirator
- ISO-9001:2008 Certified Internal Auditor

Chemist, PPG Industries, *Pittsburgh, PA* 2009-2010

- Developed and synthesized paint, coating and resin formulations for durability, hardness, and cure time
- Wrote white papers for internal research evaluations
- Used an electronic lab notebook system

Graduate Research Assistant, Advisor: Professor Lynden Archer 2007-2009
School of Chemical and Biomolecular Engineering, Cornell University, *Ithaca, NY*

- Wrote a Thesis: Synthesis of Silica-Poly(Ethylene Glycol)-Poly(Hexyl Methacrylate): Novel Nanoparticle-Organic Hybrid Molecules
- Developed lab SOPs for high vacuum Schlenk lines, ATRP synthesis and glove box usage

Undergraduate Research Assistant, Advisor: Professor Rebecca Conry 2002-2004
Department of Chemistry, Colby College, *Waterville, ME*

INSTRUMENT SKILLS

NMR	TGA	MALDI-TOF	GPC/HPLC	DSC	Ultrafast Pump Lasers
Rheometer	FT-IR	GC/MS	TEM	XPS	Fluorescence Microscopy
Raman	DLS	FRAP	ICP	AFM	Thermal Evaporator

SELECTED PRESENTATIONS (6 total)

Investigating the Interactions of Engineered Nanomaterials with Supported Lipid Bilayers Using Nonlinear Optical Spectroscopy, *Biddeford, ME* August 2014
Oral Presentation given at the Gordon Research Seminar on Vibrational Spectroscopy

SELECTED PUBLICATIONS (7 total)

Olenick, L. L.; Chase, H. M.; *et al*., Single-Component Supported Lipid Bilayers Probed Using Broadband Nonlinear Optics. *Physical Chemistry Chemical Physics* **2017.** *In press.*

Olenick, L.L.; Troiano, J. M.; *et al*., Lipid Corona Formation from Nanoparticle Interactions with Bilayers and Membrane-Specific Biological Outcomes. **2017.** *In Revision.*

Olenick, L. L.; Troiano, J. M.; Smolentsev, N; Ohno, P. E.; Roke, S.; Geiger, F. M. Sum Frequency Scattering Spectroscopy of the Interactions of Cationic Polymers and Phospholipid Monolayers on Oil Nanodroplets. **2017.** *In Prep.*

Totten, R. K.; **Olenick, L. L.**; *et al*. A Dual Approach to Tuning the Porosity of Porous Organic Polymers: Controlling the Porogen Size and Supercritical CO_2 Processing. *Chem. Sci.* **2014**, *5*, 782-7.

Troiano, J. M.; **Olenick, L. L.**; *et al.* Direct Probes of 4 Nm Diameter Gold Nanoparticles Interacting with Supported Lipid Bilayers. *J. Phys. Chem. C* **2015**, *119*, 534-46.

PATENTS

Archer, L. A.; **Olenick, L. L.**; Schaefer, J. L.; Corona, A. M. E.; Kim, D. Nanoparticle organic hybrid materials (nohms) and compositions and uses of NOHMs. U. S. Patent 9,142,863, Sep 22, 2015.

AWARDS/HONORS

L. Carroll King Award for Excellence in 100-level teaching May 2014
Northwestern University
$100 award based upon faculty and student evaluations within the chemistry department

Pacific Conference on Spectroscopy and Dynamics Scholarship November 2013

Evans B. Reid Prize in Chemistry May 2004
Colby College
$500 award given to the senior student who shows the most promise for a future in chemistry

LEADERSHIP

Teaching Experience, Northwestern University, Dept. of Chemistry 2012-*present*

- Gave lecture before each chemistry lab on learning goals, experimental principles, and lab safety
- Mentored 15-25 students in individual study projects
- Trained students to use ICP, DSC, and GPC and aided in troubleshooting experimental and instrumental concerns for individual projects

Mentoring Experience, Northwestern University and Cornell University 2008, 2013-2016

- Mentored a veteran in a Research Experience for Veterans program
- Co-Mentored an undergraduate student in a Research Experience for Undergraduates program

Science in the Classroom Volunteer, Phi Lambda Upsilon 2014-2016

- Inspired 3rd and 4th grade students at a local school through hands-on demonstrations and scientific discussions in small groups

Sustainable Nano Blog Contributor, Center for Sustainable Nanotechnology 2012-*present*

- Wrote several scientific blogs to make science accessible and engaging to a general audience

AFFILIATIONS

American Chemical Society (2004-*present*)
Phi Lambda Upsilon, Alpha Gamma Chapter (2014-*present*)
Iota Sigma Pi (2016-*present*)